Rapid Online Detection of Nitrate and Quantification of Nitrate Removal via Capacitive Deionisation (CDI)

Jojo Jose

A thesis submitted in fulfilment

of the requirements for the degree of Master of Engineering

Supervisor: Dr. Peter Kovalsky

School of Engineering

The University of Waikato

New Zealand

2025

Abstract

The increasing nitrate contamination in water poses significant environmental and public health challenges. With the rapid development of Capacitive Deionization (CDI) as a low-cost point-of-use (POU) solution to the problem, there was a rapid need for an online in-situ method for nitrate detection to support emerging POU technologies.

Due to these circumstances, it was necessary to investigate a new method for detecting nitrates, optimised for CDI's requirements. Spectrophotometric based methods in small batch configuration (cuvette style) became our focus at the onset. A review of all the viable techniques reduced the design to the following common steps that needed to be converted into a viable miniature scale process: i) sample the liquid continuously, ii) pretreatment , iii) nitrate to nitrite reduction, iv) dye addition, v) colour development, vi) spectrophotometric measurement, and vii) dispense the waste.

With the aim of trialling a range of methods that had the potential of functioning as a continuous flow cell system within this design process, reverse engineering attempts were made using commercially available reagent sets from Palintest, and Hach Nitraver5 showing poor colour development. Thus, they were eliminated from further testing

Subsequent experiments employed the zinc reduction method, which offered a cost-effective means of nitrate concentration through its reduction to nitrite, followed by colorimetric analysis. Even though the zinc method demonstrated promising results, challenges such as sensitivity to reaction time, over-reduction of nitrite to ammonia, and variability in reproducibility limited its effectiveness. Additionally, side reactions and maintenance issues, including zinc oxidation and clogging, hinder its suitability for our continuous process.

Vanadium Chloride reduction method was finally chosen for its efficiency, rapid reaction time, and robustness under varying conditions. This method, combined with UV-VIS spectrophotometric analysis and MATLAB-based data processing, enabled real-time nitrate monitoring with over 93.05% accuracy. Key parameters such as residence time, flow rate, and heat transfer were optimised to enhance system performance. A reaction temperature of 85°C enabled complete reduction of vanadium species within 2 minutes, ensuring safe operation, consistent repeatability, and high precision. To address axial dispersion in flow-through systems, a novel sample-and-hold configuration was implemented, utilising seven parallel reactors with 17-second intervals to achieve

discrete temporal resolution and accurate measurement. The system achieved a high-frequency sampling rate of 210 samples per hour (105 samples per CDI cycle), allowing near real-time tracking of nitrate fluctuations during semi-batch CDI operation.

A Stella model was developed to simulate nitrate removal via CDI, providing high resolution insight into nitrate adsorption and desorption dynamics. The model predicted transient nitrate responses that did not far exceed the system's temporal resolution, which guided the implementation of a discrete sampling interval of 17 seconds. The integration of experimental validation with system simulation underscores the effectiveness of this combined approach in achieving accurate, real-time nitrate monitoring. The outcomes of this research contribute to the advancement of automated water quality analysis systems and offer a scalable, field-deployable solution for mitigating nitrate pollution in drinking water supplies.

Acknowledgements

I extend my sincere gratitude to my supervisor, Dr. Peter Kovalsky, for his invaluable guidance, support, and encouragement throughout this research. His expertise, insightful advice, and patience played a crucial role in the successful completion of my thesis.

I am grateful to the University of Waikato for providing dedicated staff who are committed to mentoring students in the master's Research Program.

A special thanks to Marko Aleksic for his assistance with the Sample Holder (3D design and Printing) and data analysis. I deeply appreciate the support of my colleagues and fellow researchers—Mathavan, Prashant, Enola, and David, whose contributions and camaraderie fostered a positive research environment. I extend my best wishes to all members of the Nitrate detection team for their future endeavours.

I am sincerely thankful to my family and friends for their unwavering support and understanding during this journey. I offer my heartfelt thanks to my father, Jose Pynadath, my mother, Jolly Jose, and my siblings, Dona Jose and Jolbin Jose, for their constant support, encouragement, and belief in me.

Thank you all for your invaluable contributions and encouragement.

Declaration of Authorship

I hereby affirm that I am the sole author of this thesis, and the research presented within is entirely my own work. This thesis does not include any material previously published or authored by another individual.

JOJO JOSE

05-06-2025

Table of Contents

List of Figures

List of Tables

1 INTRODUCTION

Nitrate (NO_3^-) is an abundant component of the nitrogen cycle and supports agricultural and ecological productivity. However, anthropogenic activities such as fertiliser overuse, industrial discharges, and urban wastewater have significantly elevated nitrate levels in water bodies, leading to environmental and health challenges (da Ascenção et al., 2024; Guimarães et al., 2014). One of the major ecological concerns is eutrophication, which results in harmful algal blooms and oxygen depletion in aquatic systems, affecting biodiversity and water quality (Richards et al., 2022). From a health standpoint, elevated nitrate levels in drinking water have been linked to methemoglobinemia in infants, a condition that impairs the blood's ability to carry oxygen, as well as to the formation of carcinogenic N-nitroso compounds within the human body, which are associated with an increased risk of cancer. Recent studies link nitrate exposure to increased risk of colorectal cancer. While the World Health Organisation (WHO) recommends a maximum of 10 mg/L nitrate-nitrogen, New Zealand's standard is 11.3 mg/L. However, current research suggests that these limits will not prevent long-term health risks for humans, particularly infants.(Richards et al., 2022)

As a result, nitrate levels in drinking water are regularly monitored using established laboratory methods. However, it is still difficult to perform real-time or online testing directly in the field. Developing such capabilities is important for improving and speeding up nitrate removal technologies.

1.1 Analytical Methods for Nitrate Detection and Characterisation

Traditional detection methods, including spectrophotometry and ion chromatography, offer accuracy but are limited by complexity, time, and reliance on hazardous reagents such as cadmium (Guimarães et al., 2014). Safer reductants, such as vanadium chloride and zinc, have emerged as effective alternatives (da Ascenção et al., 2024).

Innovative methods such as second-derivative UV spectroscopy and flow-injection analysis improve accuracy and enable real-time monitoring. Electrochemical sensors, employing electrodes like copper or silver, further enhance detection capability, especially in field applications (Azmi et al., 2017).These innovations facilitate rapid, environmentally sustainable, and dependable nitrate detection, contributing to effective water quality management and adherence to regulatory standards.

1.2 Nitrate Removal by Capacitive Deionisation

Capacitive deionisation (CDI) is a new and promising method for removing salts and nitrates from water. It operates by utilising materials such as activated carbon and graphite to store electrical charge. This technology has already been successfully implemented in areas like industrial laundry, cooling systems, and agriculture. Researchers are now working to enhance CDI's usefulness for providing clean drinking water, particularly in regions where access to safe water is limited(Porada et al., 2013). To support this, there is also a need for developing simple and accurate methods to measure nitrate removal in CDI systems, which will help confirm the efficiency of the technology.

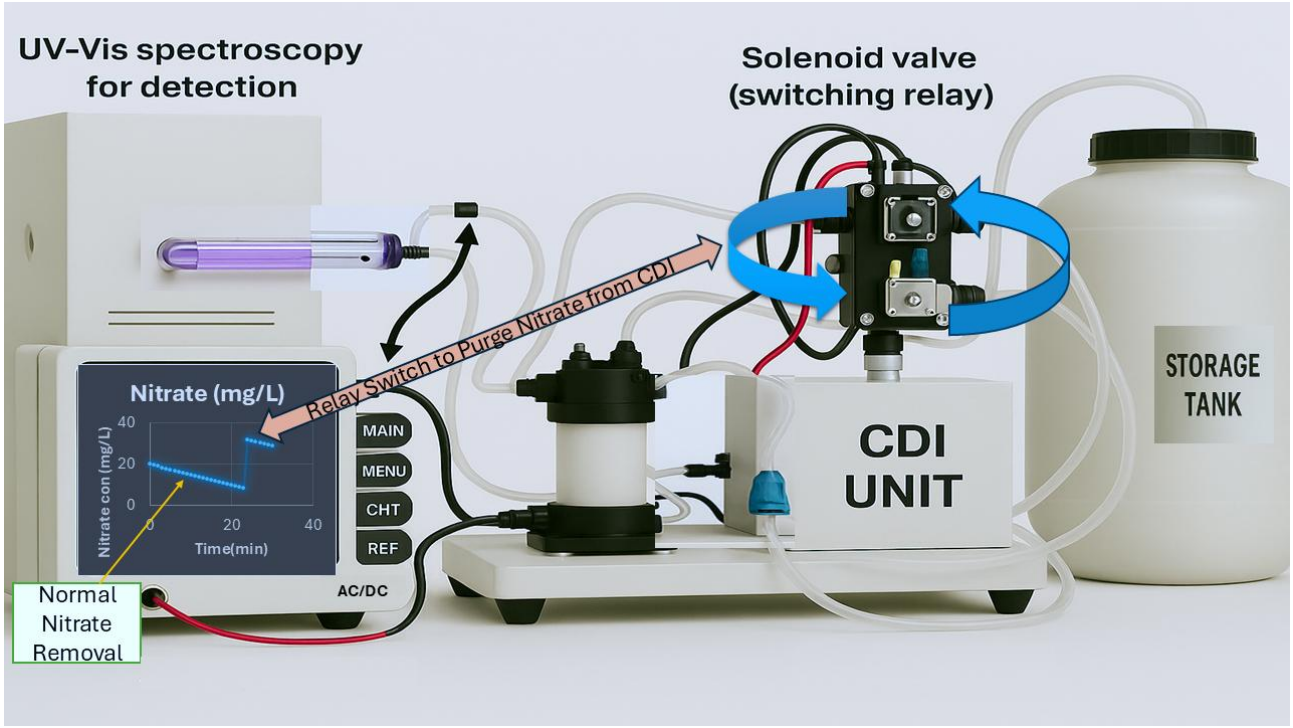

Figure 1 Conceptual drawing of an integrated online nitrate detection system using UV-Vis spectroscopy. Here a relay switches CDI operation between nitrate adsorption and nitrate desorption in a semi-batch CDI system. A device capable of displaying nitrate level on a screen in real-time clearly indicates the instantaneous increase in nitrate level and in response operate the relay based on actual nitrate levels as opposed to arbitrary valve timings..

To better illustrate the motivation and direction of this research, Figure 1 presents a conceptual drawing of the integrated online nitrate detection system developed in this study. The system combines UV-Vis spectroscopy for real-time nitrate concentration measurement with a solenoid-controlled switching relay to manage the adsorption and desorption cycles within the Capacitive Deionisation (CDI) unit. A storage tank supplies the nitrate-containing solution, which passes through

the CDI system where ions are removed. During the adsorption phase, nitrate levels decrease, and this trend is continuously monitored by the UV-Vis detector.

Whilst the nitrate measurement system developed in this thesis is a flow-cell spectrophotometer designed to sample continuously from the CDI nitrate removal system; complications related to the slow nature of spectrophotometric based nitrate measurement techniques focussed the project on a design that was semi-batch rather than continuous. For this purpose, we describe this technique as "sample-and-hold" as will be the focus in later chapters.

1.3 Scope and Objectives

This study focuses on developing a rapid, reliable, and cost-effective online nitrate detection system integrated with a CDI unit for point-of-use water treatment. The system is designed to support real-time monitoring and validate CDI performance using synthetic nitrate solutions and UV-Vis spectrophotometry. To overcome the limitations associated with the slow kinetics of nitrate reduction, a novel sample-and-hold mechanism is implemented, enabling high-resolution measurements. The overall design incorporates principles of chemical kinetics, flow regulation, and optical detection to optimise system performance.

The specific objectives of this study are as follows:

1. Investigate the chemical behaviour and limitations of the Palintest and zinc reduction methods for nitrate detection,
2. Design a sample-and-hold system optimised for online spectrophotometric nitrate detection using vanadium chloride (VCl_3),
3. Calibrate and validate the detection system using UV-Vis spectrophotometry against standard nitrate solutions,
4. Apply Levenspiel's tracer theory and conduct dye testing to evaluate flow dynamics, system accuracy, and real-time responsiveness,
5. Demonstrate high-sensitivity nitrate detection during CDI operation, capable of delivering results in under one minute.

2 LITERATURE REVIEW

2.1 Overview of Nitrate Contamination Sources

Nitrate contamination is a serious global problem affecting the environment and human health. It mainly comes from human activities, especially farming. The overuse of nitrogen-based fertilisers and the poor management of animal waste led to high nitrate levels in soil and water. These substances undergo a process called nitrification, where ammonium (NH_4^+) is converted to nitrite (NO_2^-) and then to nitrate (NO_3^-). Since nitrate is highly soluble, it easily leaches into groundwater and surface water through runoff from farms (Rogers et al., 2023; Singh et al., 2022).

Industrial activities, including fertiliser manufacturing, food processing, and improper disposal of nitrogenous waste, intensify nitrate pollution. Leachate from landfills and effluents from industries containing compounds such as ammonia and urea increased the nitrogen content in aquatic environments. In urban and peri-urban areas, leakage from septic tanks, sewer systems, and the absence of proper sanitation infrastructure contribute significantly to nitrate enrichment of groundwater (Serio et al., 2018; Shukla & Saxena, 2018). Additionally, atmospheric deposition of nitrogen oxides (NO_x and N_2O) from fossil fuel combustion also adds to the nitrate load via precipitation, impacting soil and surface water chemistry.

Another important factor is deforestation. Forests play a crucial role in the natural nitrogen cycle by serving as sinks that store nitrogen in biomass and soil. When forests are cleared for farming, construction, or logging, the nitrogen stored in trees and soil is released into the environment. The loss of vegetation also results in reduced nitrogen uptake, making it easier for nitrate to leach into water bodies. Therefore, deforestation disrupted the natural balance and contributed to increased levels of nitrate in surface and groundwater. (Shukla & Saxena, 2018).

In addition to human activities, there are also geogenic sources of nitrate. Natural deposits of nitrogen-containing minerals, such as nitre and nitratine, release nitrates into soil and groundwater through weathering processes. This form of contamination is particularly common in arid and semi-arid environments where such minerals are naturally present (Ayub et al., 2019). Lightning activity is another natural contributor, as it converts atmospheric nitrogen into nitrate and ammonia, which then deposit on land through precipitation. Figure 2 represents key aspects of the geologic nitrogen cycle that influence nitrate distribution (Shukla & Saxena, 2018). Environmental factors such as rainfall,

soil structure, and vegetation also influence the extent of nitrate transported through the landscape (Carroll et al., 2014).

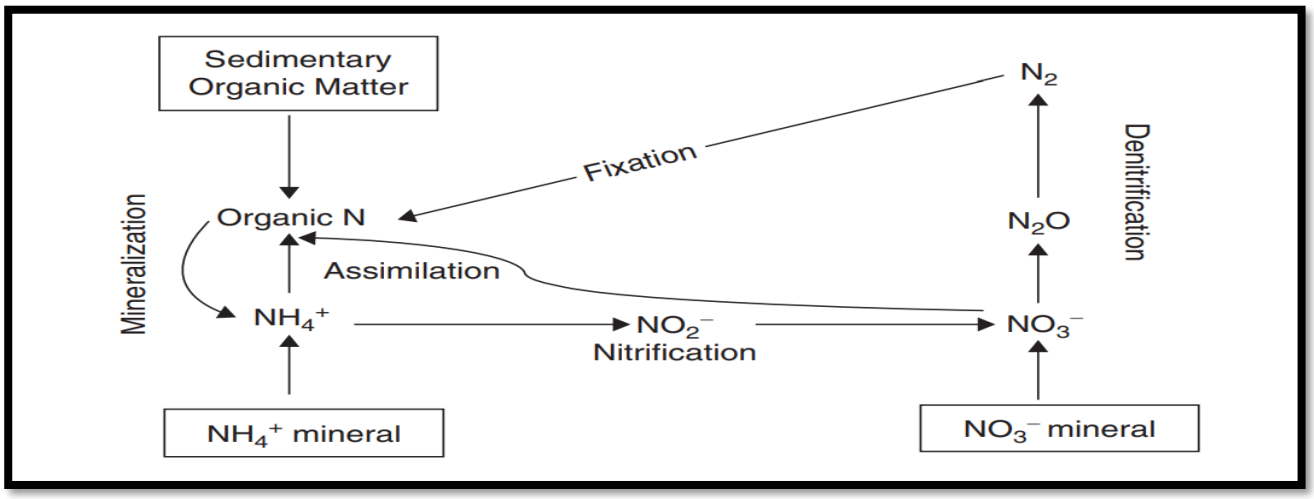

Figure 2 Simplified geologic nitrogen cycle showing key processes such as mineralisation, nitrification, assimilation, and denitrification (Shukla & Saxena, 2018).

In summary, nitrate pollution results from a combination of agricultural practices,, industrial activities, air pollution, and natural sources such as soil and rocks. While human activities are the primary contributors , natural processes also influence the amount of nitrate that enters water systems. Recognising both human-made and natural sources is essential for developing effective strategies to reduce pollution and ensure water remains safe and clean.

2.2 Health and Environmental Impacts of Nitrate

2.2.1 Health Impacts of Nitrate

Nitrate contamination in drinking water poses significant health risks, particularly to vulnerable populations such as infants and pregnant women. One of the most critical health effects is methemoglobinemia, or "blue baby syndrome," which occurs when ingested nitrate is converted into nitrite in the body. Nitrite reacts with haemoglobin in red blood cells to form methaemoglobin, an altered form that cannot transport oxygen effectively. As a result, oxygen delivery to tissues is impaired, leading to symptoms such as cyanosis, nausea, weakness, and elevated heart rate. In severe cases, methemoglobinemia can be fatal, especially in infants under six months who lack fully developed enzyme systems to reverse the oxidation process (Health, 2018). To reduce this risk, the

U.S. Environmental Protection Agency (EPA) has established a maximum contaminant level (MCL) of 10 mg/L nitrate-nitrogen in drinking water (Ward et al., 2005). Historical outbreaks in rural areas that relied on shallow wells near agricultural activity highlighted the need for such regulations, as these sources often contained both nitrate and bacterial contaminants.

Beyond acute effects, long-term nitrate exposure is increasingly linked to chronic diseases, particularly cancer. The main concern lies in the endogenous formation of *N-nitroso compounds*, potent carcinogens produced when nitrite reacts with dietary amines under acidic stomach conditions (Schullehner et al., 2018). Multiple epidemiological studies have reported associations between elevated nitrate levels in drinking water and increased risks of colorectal and gastric cancers. A Danish cohort study found that even nitrate levels above 2 mg/L nitrate-nitrogen were linked to a significant rise in colorectal cancer incidence (Grout et al., 2023). However, the evidence is nuanced. Factors such as *Helicobacter pylori* infection, high red meat consumption, and genetic predisposition may modulate individual risk, while antioxidants found in nitrate-rich vegetables may inhibit nitrosation reactions (Ward et al., 2018). Furthermore, prenatal exposure to nitrate is linked to adverse birth outcomes, including low birth weight, premature birth, and congenital abnormalities. Studies indicate that maternal nitrate exposure above 5 mg/L nitrate-nitrogen raises the risk of preterm birth by nearly 47% (Stayner et al., 2022). In animal models, nitrite-induced oxidative stress has also been linked to disrupted neurodevelopment, raising concerns about long-term child health(Temkin et al., 2019). The biochemical pathways through which nitrite interacts with oxygenated and deoxygenated haemoglobin, contributing to both toxicity and vasodilation, are illustrated in Figure 3 (Kim-Shapiro et al., 2005).

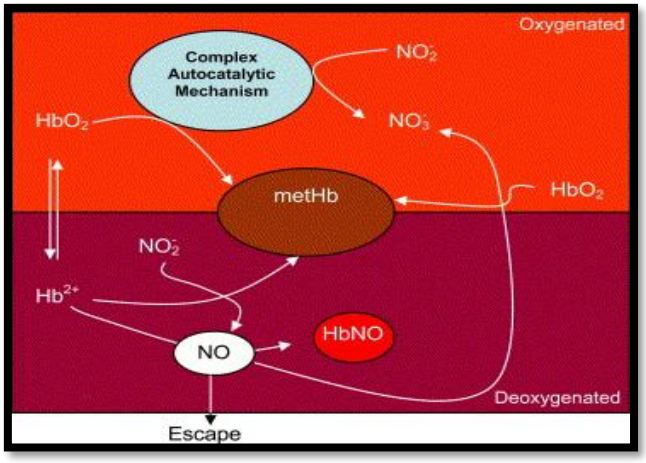

Figure 3 Schematic of the reactions between nitrite and haemoglobin in oxygenated and deoxygenated conditions.(Kim-Shapiro et al., 2005)

Nitrate exposure may also affect thyroid and cardiovascular health. Nitrate competes with iodine for uptake in the thyroid gland, potentially leading to hypothyroidism and goitre. This is particularly concerning for pregnant women and populations with iodine-deficient diets. Additionally, prolonged exposure to nitrate in drinking water may disrupt nitric oxide (NO) signalling in blood vessels, contributing to hypertension; however, further research is needed to confirm these effects (Ward et al., 2018). Interestingly, not all health impacts are negative; nitrate from vegetables may enhance cardiovascular function by serving as a precursor to NO, promoting vasodilation and reducing blood pressure. However, the balance between these potential benefits and documented risks remains complex. Understanding individual susceptibility and exposure patterns is essential for refining risk assessments and ensuring effective regulatory measures. As research continues to uncover both direct and indirect health effects of nitrate, integrating advanced water monitoring and treatment strategies will be critical to protecting public health in nitrate-affected areas regions.

2.2.2 Environmental Impacts of Nitrate

Nitrate pollution is a growing environmental issue that affects water quality, soil health, and atmospheric stability. It arises from the use of nitrogen-based fertilisers in agriculture, industrial discharges, and untreated sewage entering water bodies. These human activities increase nitrate concentrations in surface water and groundwater, leading to serious ecological and public health concerns. One of the most critical effects is eutrophication, a process where excess nutrients promote rapid algal growth in aquatic environments. This depletes oxygen levels in water, causing the death of aquatic organisms and reducing biodiversity (Prickett et al., 2024). In addition to water pollution, nitrate accumulation degrades soil fertility, disrupts microbial processes, and reduces agricultural productivity over time (McDowell et al., 2021). Nitrate also contributes to climate change by increasing the emission of nitrous oxide, a greenhouse gas with a significantly higher warming potential than carbon dioxide (Dench & Morgan, 2021).

Eutrophication is one of the most visible impacts of nitrate pollution, especially in lakes, rivers, and estuaries. Nutrient runoff from farms, urban areas, and residential properties enters nearby water bodies and triggers algal blooms. These blooms reduce sunlight penetration and, when they decay, microbial activity increases, consuming dissolved oxygen and creating hypoxic or anoxic conditions. This process harms fish, shellfish, and other aquatic organisms. Figure 4 illustrates how various sources such as agricultural runoff, septic systems, and urban discharge contribute to nutrient over-enrichment and eutrophication (Malone & Newton., 2020). Regions like the Gulf of Mexico and the

Baltic Sea have large "dead zones" where marine life cannot survive due to oxygen depletion caused by nitrate-driven eutrophication (Sebilo et al., 2013). Harmful algal blooms also release toxins that affect drinking water supplies and marine ecosystems, resulting in serious ecological and economic damage.

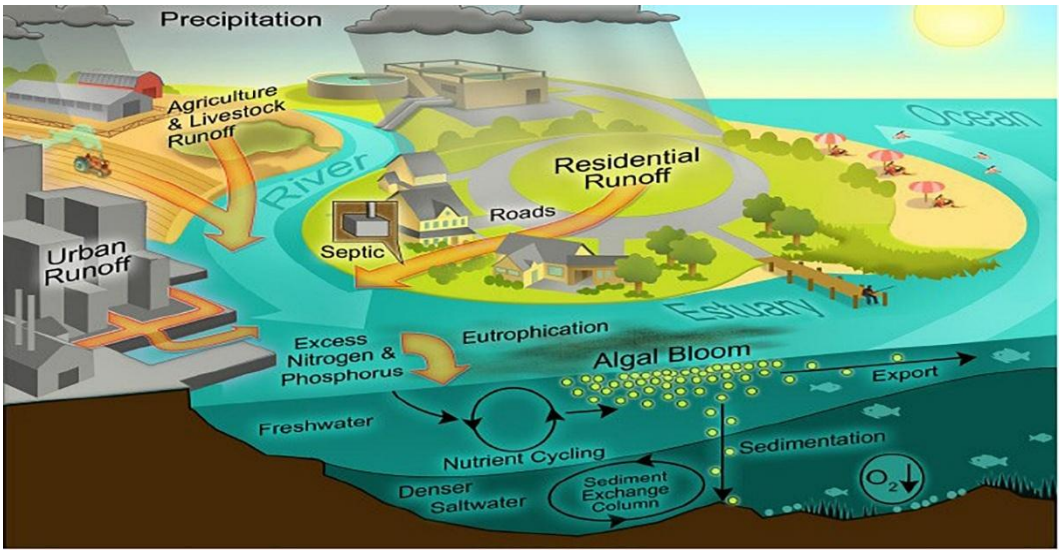

Figure 4 Nutrient Enrichment Pathways and Eutrophication Effects.(Malone & Newton., 2020)

Groundwater contamination is another significant problem linked to nitrate pollution, particularly in regions where agriculture is intensive. Nitrate is highly soluble and does not bind well to soil particles, allowing it to travel easily through the soil and enter groundwater. In the Indo-Gangetic Plain, for example, groundwater nitrate levels have reached values far above safe drinking water limits due to the overuse of fertilisers and poor wastewater management (Verma et al., 2023) . Figure 5 shows the nitrogen cycle and highlights the pathways through which nitrate enters groundwater, including leaching from fertilisers, animal waste, and failing septic systems. Once in groundwater, nitrate can persist for many years, affecting water quality and posing risks to humans and ecosystems. In addition, nitrate pollution alters soil chemistry, potentially releasing toxic heavy metals such as arsenic and uranium into the water (Bonotto et al., 2019). This creates a multi-layered contamination problem that is difficult to address with simple remediation.

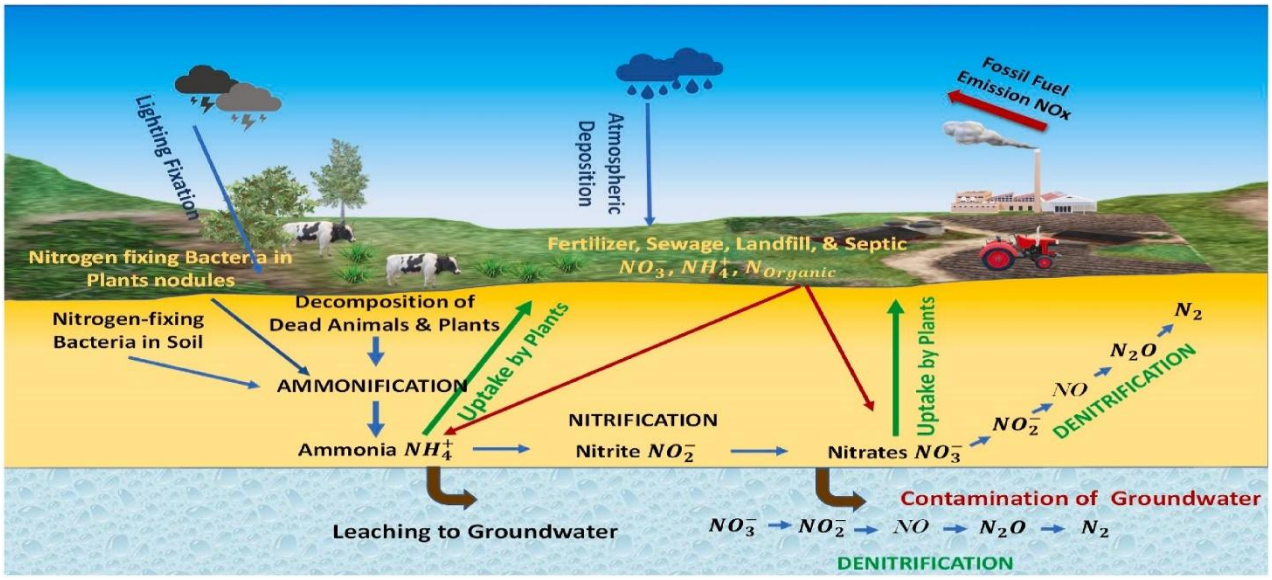

Figure 5 Nitrogen Cycle and Groundwater Contamination Pathways (Verma et al., 2023).

Nitrate pollution has a strong connection to climate change. During microbial denitrification, soil and groundwater microorganisms reduce nitrate to nitrogen gases, including nitrous oxide (N_2O), which is a highly potent greenhouse gas. Agricultural areas with significant nitrate leaching, such as the Indo-Gangetic Plain, are major sources of nitrous oxide emissions (Dench & Morgan, 2021). Figure 5 also shows how nitrate leaching and denitrification processes contribute to emissions of nitrogen-based greenhouse gases. climate change can intensify this issue by increasing temperatures, which accelerates microbial activity in soil and groundwater, thereby raising the rate at which soil and groundwater microbes transform nitrate into greenhouse gases. Additionally, changes in rainfall patterns and increased soil erosion due to climate change can further enhance nitrate mobility in the environment, creating a feedback loop where climate change and nitrate pollution exacerbate each other (Stuart et al., 2011).

Soil degradation caused by nitrate pollution results in reduced agricultural productivity and impacts food security. When excessive nitrate accumulates in the soil, it leads to acidification, which negatively affects soil microbes essential for nutrient cycling (Serio et al., 2018). This decreases the availability of nutrients like phosphorus and potassium and weakens root development in plants. Over time, nitrate leaching also removes important nutrients such as calcium and magnesium from the soil, diminishing its fertility (Rizeei et al., 2018). As a result, the declining soil fertility caused by nitrate leaching forces farmers to use more fertiliser to maintain yields, which raises costs and worsens pollution. Nitrate pollution also promotes the growth of invasive plant species, decreasing native biodiversity and disrupting natural ecosystems. (McDowell et al., 2021). To address these issues,

sustainable agricultural practices such as precision fertilisation, crop rotation, conservation tillage, and the use of buffer zones are essential. These methods can help restore soil health, reduce nitrate runoff, and protect water and air quality.

2.3 Historical Methods for Nitrate Detection

Historically, nitrate detection depended on colorimetric and chemical reduction methods. The Diphenylamine Spot Plate Test, one of the earliest qualitative techniques, offered an immediate visual indication of nitrate presence but was subjective and prone to interferences (Bedwell et al., 1995) . The Griess Assay, developed in 1879, was among the first quantitative methods, where nitrite (a reduced form of nitrate) reacted with sulfanilic acid and N-(1-naphthyl)-ethylenediamine dihydrochloride (NED) to form an azo dye detected at 540 nm (Wang et al., 2017). However, this method necessitated an extra nitrate-to-nitrite reduction step, complicating real-time monitoring.

The Cadmium Reduction Method, introduced in the mid-20th century, involved passing a sample through a cadmium column to reduce nitrate to nitrite, which was then detected through the Griess reaction (APHA 2000). Although highly sensitivity (0.01 mg/L NO_3^--N detection limit), concerns over cadmium toxicity prompted the development of alternative techniques. This method also faced challenges related to extended processing times, waste disposal issues, and reagent stability, which limited its applicability for real-time uses.

To improve efficiency, researchers developed early automated systems; however, these still required manual sample preparation and batch processing. These limitations prompted researchers to explore modern technologies that could enhance the speed, accuracy, and field applicability of nitrate detection methods.

2.4 Spectrophotometric Methods

Spectrophotometry, particularly UV-based techniques, became popular due to their simplicity and speed. The UV Absorption Method, first introduced in the 1960s, capitalised on nitrate's absorbance at 220 nm. However, dissolved organic matter (DOM) interferes at this wavelength, requiring a correction at 275 nm (Alahi & Mukhopadhyay, 2018). This method is fast, reagent-free, and ideal for field applications, but its accuracy declines in complex water matrices.

Second-Derivative UV Spectroscopy was introduced by researchers in the 1990s to address organic matter interference. By differentiating the spectral response, this method enhanced nitrate signal detection while reducing background noise (Holm et al., 1997). Despite these advancements, UV-based techniques still struggle with low detection limits in highly turbid samples.

Recent innovations in portable UV-based sensors have enhanced the feasibility of spectrophotometric methods for real-time applications. These include fibre-optic sensors and microfluidic platforms that combine UV detection with automated sample handling.

2.5 Chromatographic Methods

With the demand for high-precision nitrate analysis, Ion Chromatography (IC) and High-Performance Liquid Chromatography (HPLC) have emerged as leading laboratory techniques. IC, first introduced in the 1970s, separates nitrate ions via anion-exchange chromatography, followed by conductivity or UV detection. This method provides high specificity and sensitivity but requires costly instrumentation and skilled operators (Alahi & Mukhopadhyay, 2018).

HPLC, particularly with post-column photochemical reaction and chemiluminescence detection, improves sensitivity for food, water, and biological samples (Kodamatani et al., 2009). However, like IC, HPLC is not suitable for real-time or in-field applications due to extensive sample preparation and analysis time.

Efforts to integrate chromatographic techniques into real-time monitoring systems have led to advancements in automated sample injection, on-site preconcentration, and effective miniaturised chromatography systems. These innovations are advantageous for industrial and environmental monitoring, where high accuracy is essential.

2.6 Nitrate Detection using Zinc Reduction Method.

Nitrate concentration is commonly quantified using various analytical techniques, including spectrophotometry, chromatography, and electrochemical analysis. Researchers have developed these methods to ensure accurate and reliable quantification in both environmental and industrial applications. Among these, the zinc reduction method has gained significant attention as a cost-effective and environmentally friendly alternative to the widely used cadmium reduction technique, which is increasingly restricted due to cadmium's toxicity (Oladosu et al., 2017). This method

involves the chemical reduction of nitrate to nitrite using zinc powder in an acidic medium, followed by the quantification of nitrite through the Griess reaction, which produces a red azo dye measurable at wavelengths between 540 and 543 nm (Nelson et al., 1954). While the zinc reduction method offers lower toxicity and ease of use, its accuracy and efficiency rely on optimizing reaction conditions to ensure complete nitrate-to-nitrite conversion. This review explores the principles, optimisation strategies, analytical performance, and recent advancements in zinc-based nitrate detection, highlighting its potential as a reliable method for nitrate analysis.

2.6.1 Principle and Mechanism of Zinc Reduction for Nitrate Detection

The zinc reduction method relies on the chemical transformation of nitrate into nitrite under acidic conditions with the presence of zinc. The core reaction governing this process is shown in Equation (1):

$$NO_3^- + Zn(s) + 2H^+ \rightarrow NO_2^- + Zn^{2+} + H_2O \quad (1)$$

Following the reduction step, nitrite reacts with sulfanilamide and N-(1-Naphthyl)-ethylenediamine dihydrochloride (NED) in the Griess reaction. The initial step involves the formation of a diazonium salt, as shown in Equation (2) , followed by a coupling reaction that produces a red-coloured azo dye, as shown in Equation (3):

$$NO_2^- + C_6H_7SO_2NH_2 \rightarrow \text{Diazonium Salt} \quad (2)$$

$$\text{Diazonium Salt} + C_{12}H_{16}N_2 \rightarrow \text{Azo Dye (Red Color)} \quad (3)$$

This reaction results in a red-coloured azo dye, which is quantified using spectrophotometry. In comparison to the cadmium reduction method, zinc reduction is safer, more cost-effective, and eliminates hazardous cadmium waste. However, the efficiency of zinc reduction highly depends on reaction conditions such as pH, reaction time, and the presence of interfering ions. If the reduction is incomplete, nitrate concentrations may be underestimated, making optimization a crucial step in this methodology (Merino, 2009).

2.6.2 Optimisation and Analytical Performance of Zinc Reduction

2.6.2.1 Reaction Conditions and Buffer Systems

Reaction parameters such as pH, reaction time, zinc dosage, and buffer composition play a critical role in determining the efficiency of the zinc reduction method. Studies have established that the optimal pH range for zinc-mediated nitrate reduction is between 8.0 and 8.5. This pH range, maintained using ammonium chloride or borate buffers, ensures efficient nitrate-to-nitrite conversion. At higher pH levels, hydrogen gas evolution competes with the reduction process, lowering efficiency (Merino, 2009). The quantity of zinc used is another critical factor, with optimal dosages ranging from 50 to 100 mg per 5 mL sample. Insufficient zinc leads to incomplete reduction, while excessive zinc may cause side reactions, such as further reduction of nitrite to nitrogen gas, resulting in inaccurate measurements (J. Wu et al., 2016).The reaction time for complete reduction has been optimized to approximately 30 minutes. Longer reaction times may result in over-reduction, converting nitrite to ammonia, which affects measurement accuracy. (Jiwarungrueangkul et al., 2023). In seawater applications, the presence of chloride ions can interfere with zinc reduction, necessitating the use of borate buffers instead of ammonium buffers. These modifications enhance reaction stability and increase reproducibility in high-salinity environments (Oladosu et al., 2017).

2.6.2.2 Sensitivity and Detection Limits

The sensitivity of zinc reduction-based nitrate detection depends on reaction conditions, instrumentation, and sample matrix. The detection limit of the modified zinc reduction method is as low as 0.1 μM (1.4 μg-N/L) in seawater, making it suitable for monitoring marine and drinking water. (Jiwarungrueangkul et al., 2023). In food and wastewater samples, detection limits typically range from 3 to 5 mg/kg (Merino, 2009).

A major advancement in this method is the development of microplate spectrophotometry, which allows for high-throughput analysis with a detection limit of 0.5 μM and covers a linear range up to 100 μM (J. Wu et al., 2016). This adaptation reduces analysis time while enhancing precision. However, interference from organic matter, salinity, and reaction by-products can impact accuracy, necessitating modifications such as pre-treatment steps or alternative buffer systems to enhance method performance.

2.6.3 Comparison with Cadmium Reduction

The cadmium reduction method has long been regarded as the gold standard for nitrate detection, offering high accuracy. However, cadmium's toxicity and environmental risks have led to restrictions on its use. The chemical reaction governing cadmium-based nitrate reduction is presented in Equation (4):

$$NO_3^- + Cd + 2H^+ \rightarrow NO_2^- + Cd^{2+} + H_2O \quad (4)$$

While cadmium reduction yields faster results, it requires careful handling and proper waste disposal due to its toxicity. Unlike cadmium, zinc is safer to use, cheaper, and easier to apply in field testing. However, zinc reduction takes longer and is more affected by factors like salinity and organic matter, which can lower its efficiency (Nelson et al., 1954). Advances in buffer selection and reaction optimisation have improved the reliability of zinc reduction, making it a practical and environmentally friendly option for nitrate detection in various applications.

2.6.4 Recent Advances and Field Applications

2.6.4.1 Online and Automated Detection Methods

Automation has significantly enhanced the feasibility of zinc reduction for real-time monitoring. Sequential Injection Analysis (SIA) has been successfully integrated with zinc reduction, achieving a reduction efficiency of 94.7% while enabling continuous nitrate monitoring (Oladosu et al., 2017). This automated system minimises reagent consumption and reduces manual handling errors.

Another significant development is microplate spectrophotometry, which allows for the simultaneous analysis of multiple samples. This method can process 96-well plates in under 10 minutes, making it ideal for high-throughput environmental and water quality testing. (J. Wu et al., 2016).

2.7 Nitrate Detection Using Vanadium Chloride

Traditional methods for nitrate detection often involve toxic reagents like cadmium, prompting a shift towards safer alternatives such as vanadium chloride (VCl_3) reduction. This review explores various methodologies employing VCl_3 as a reductant for nitrate determination, evaluating their accuracy,

sensitivity, and applicability for online detection systems. The primary objective is to provide an overview of advancements in nitrate detection using VCl_3, including optimisation techniques, analytical methodologies, and potential real-time applications.

2.7.1 Nitrate Reduction by Vanadium Chloride

Vanadium (III) chloride (VCl_3) has been extensively studied as a reductant for nitrate determination. Unlike cadmium-based methods, VCl_3 provides a safer and effective means to convert nitrate NO_3^- to nitrite (NO_2^-), which is subsequently quantified using the Griess assay (Pai et al., 2021). The reduction reaction facilitated by VCl_3 is shown in Equation (5).

$$NO_3^- + 3V^{3+} + 3H^+ \rightarrow NO_2^- + 3V^{4+} + H_2O \quad (5)$$

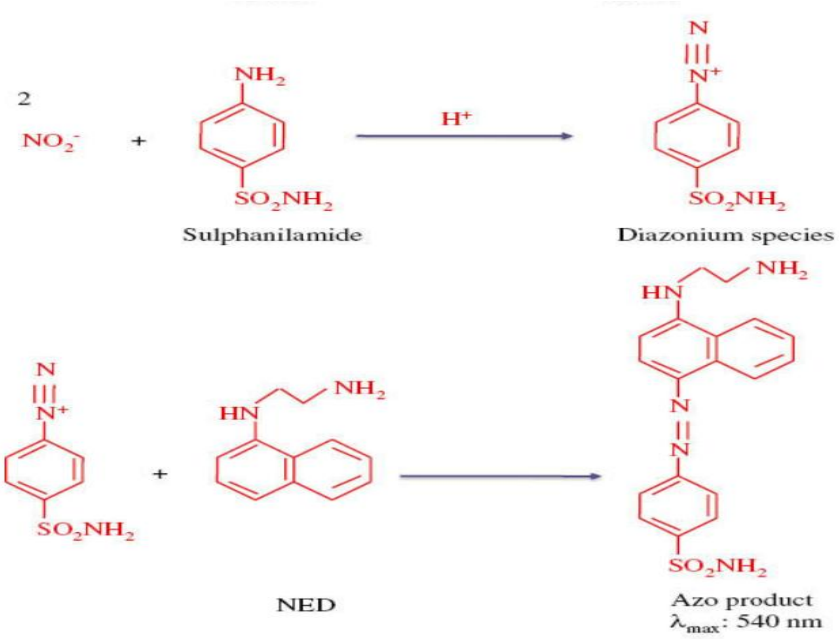

(6)

The reduction process involves the reaction of nitrate with VCl_3 under acidic conditions, yielding nitrite and ultimately forming a coloured azo dye when reacted with sulfanilamide and N-(1-naphthyl)-ethylenediamine dihydrochloride (NED), as illustrated in Equation (6) (Schnetger et al., 2014). The efficiency of this reduction depends on reaction parameters such as temperature, reagent concentration, and acidity. Recent research has demonstrated that optimising these parameters can significantly improve sensitivity and detection limits. Compared to cadmium reduction, the use of VCl_3 minimises toxic waste generation, making it an environmentally favourable alternative.

Furthermore, advancements in automated systems have facilitated the integration of VCl_3 reduction into real-time monitoring setups, allowing for continuous assessment of nitrate concentrations in various water bodies.

2.7.2 Analytical Techniques for Nitrate Detection using VCl_3

Several analytical techniques have been developed using VCl_3 reduction, including Spectrophotometry, flow injection analysis (FIA), and Chemiluminescence detection.

2.7.2.1 Spectrophotometric Methods

Spectrophotometry remains the most widely used technique for nitrate detection due to its simplicity and cost-effectiveness. The reaction product of the Griess assay exhibits maximum absorbance at 540–543 nm, facilitating straightforward quantification (Miranda et al., 2001). Studies have optimised parameters such as reagent concentration, temperature, and reaction time to enhance sensitivity, achieving detection limits as low as 0.2 μM (Pai et al., 2021)This method involves adding VCl3 to nitrate-containing samples, allowing the reaction to proceed under controlled conditions, and measuring the resultant absorbance. The accuracy of spectrophotometric methods depends on reagent stability, sample matrix composition, and potential interferences. Recent advancements have focused on developing portable spectrophotometric devices for in-field applications, improving the feasibility of real-time nitrate monitoring in environmental settings.

2.7.2.2 Flow Injection Analysis (FIA)

Flow Injection Analysis (FIA) is a widely used automated technique for nitrate detection. It offers rapid analysis, reduced reagent consumption, and high reproducibility. The FIA system operates by injecting a discrete sample into a continuous carrier stream, which transports the sample through a reaction zone before detection. In FIA systems utilising VCl_3 reduction, nitrate is first reduced to nitrite before undergoing spectrophotometric detection via the Griess reaction.

Recent advancements in FIA systems have focused on improving sensitivity and robustness. Lin (2022) developed a reverse flow injection method for nitrate determination in coastal waters, integrating a custom-made linear light path flow cell (Lin et al., 2022). This approach enhanced detection sensitivity by increasing the optical path length while minimising reagent consumption.

Additionally, sulfamic acid was introduced to eliminate interfering nitrite species, allowing for direct nitrate determination without complex corrections.

Another notable improvement in FIA-based nitrate detection is the use of syringe-pump-based environmental-water analysers, as demonstrated by (Fang et al., 2019). This method integrates an online filtration system for continuous nitrate monitoring in estuarine environments. By utilising an automated reagent mixing process, the system significantly minimises manual intervention while preserving analytical precision.

FIA systems also enable real-time nitrate monitoring, particularly in environmental studies where temporal variations in nitrate concentrations are critical. FIA's rapid response time and automation make it an ideal choice for high-throughput water quality assessment in field applications.

2.7.2.3 Chemiluminescence Detection

Chemiluminescence-based nitrate detection leverages the ability of VCl_3 to reduce nitrate to nitric oxide (NO), which is then quantified using NO-sensitive chemiluminescent detectors(Braman & Hendrix, 1989). This technique offers high sensitivity but requires specialised instrumentation, limiting its application for routine water quality monitoring. Chemiluminescence detection provides sub-nanomolar detection limits, making it suitable for highly sensitive environmental and biological studies. However, its reliance on expensive equipment and the need for controlled reaction conditions present challenges for widespread adoption.

2.7.3 Optimisation of Reaction Conditions

Key factors influencing the efficiency of VCl_3-based nitrate detection include reaction temperature, acidity, and reagent concentrations.

2.7.3.1 Temperature and Reaction Time

Reaction temperature significantly impacts the kinetics of nitrate reduction by VCl_3. Studies have shown that reaction rates increase with temperature due to enhanced molecular collisions and energy transfer. Higher temperatures (60–80°C) improve nitrate reduction kinetics, reducing analysis time and improving detection limits (Pai et al., 2021). However, excessive heating may lead to reagent degradation and potential side reactions, which can interfere with detection accuracy (Braman & Hendrix, 1989).

A study by Fang demonstrated that the reaction rate increases exponentially with temperature, with significant efficiency gains between 30°C and 90°C (Fang et al., 2018). However, excessively elevated temperatures caused bubble formation, which destabilised the analytical setup.

The temperature dependence of the reaction kinetics is mathematically expressed using the Arrhenius equation (Equation (7)).

$$k = Ae^{\frac{-E_a}{RT}} \tag{7}$$

where k is the reaction rate constant, A is the pre-exponential factor, E_a is the activation energy (J/mol), R is the universal gas constant (8.314 J/(mol.K)) and T is the temperature in Kelvin. This equation indicates that increasing temperature exponentially enhances reaction rates. However, practical considerations such as equipment limitations and reagent stability must be considered when determining optimal operating temperatures (Schnetger et al., 2014).

Additionally, reaction time influences the extent of nitrate reduction. Shorter reaction times may result in incomplete conversion of nitrate to nitrite, whereas excessively long reaction times may lead to side reactions that reduce method precision. Optimising reaction time is essential to ensure complete reduction while maintaining analytical efficiency (Pai et al., 2021).

2.7.3.2 Acidic Conditions

The pH of the reaction medium plays a critical role in the reduction process. Vanadium chloride functions effectively as a reducing agent under acidic conditions, typically within the pH range of 1 to 3. The presence of hydrogen ions is essential for electron transfer in the reduction reaction:

Studies have indicated that the optimal acidity for nitrate reduction is achieved using hydrochloric acid (HCl) or sulfuric acid (H_2SO_4) within the concentration range of 0.5–2.0 M (Schnetger et al., 2014). At higher acid concentrations, side reactions may occur, leading to inconsistencies in detection. Conversely, lower acid concentrations can slow down the reduction process, affecting the overall sensitivity of the method (Miranda et al., 2001) .

Maintaining the correct acidity is also crucial in preventing interference with subsequent colorimetric reactions such as the Griess assay. If the pH is too low, it can suppress the formation of the azo dye

required for spectrophotometric detection. Therefore, buffer systems or careful control of acid concentration are necessary for achieving accurate and reproducible results (Fang et al., 2021).

2.7.3.3 Reagent Concentration and Stability

The concentration of vanadium chloride is another critical factor in optimising nitrate detection. Higher concentrations of VCl_3 increase the nitrate reduction rate; however, excessive reagent concentrations can lead to reagent wastage and potential interference with detection methods. Studies suggest that an optimal concentration of VCl_3 ranges between 0.02 and 0.1 M to ensure efficient reduction while minimizing side reactions (Pai et al., 2021).

Furthermore, reagent stability is a concern in long-term monitoring applications. Vanadium chloride solutions can degrade over time, particularly under exposure to light and air, leading to reduced reactivity. To mitigate this issue, reagent solutions are often stored under controlled conditions, such as refrigeration at 4°C or in inert gas-sealed containers. Additionally, stabilizing agents may be added to extend reagent shelf life (Braman & Hendrix, 1989).

Another consideration is the stability of colorimetric reagents used in conjunction with VCl_3 reduction. Sulfanilamide and N-(1-naphthyl)-ethylenediamine dihydrochloride (NED) solutions are prone to oxidation, which can alter their reactivity and lead to errors in nitrate quantification. Ensuring the freshness of these reagents is critical for maintaining method reliability (Miranda et al., 2001).

2.7.3.4 Effect of Sample Matrix and Interfering Substances

The composition of the sample matrix can significantly affect the efficiency of nitrate reduction and detection. Environmental water samples, for instance, often contain dissolved organic matter, heavy metals, and other anions (e.g., Sulphate, phosphate) that can interfere with nitrate reduction. These interferences may lead to signal suppression or enhancement, impacting the accuracy of the results (Schnetger et al., 2014).

Pre-treatment methods such as filtration, dilution, or chemical masking agents are employed to address matrix effects. Filtration removes particulate matter that may interfere with flow injection analysis, while dilution reduces the impact of high ionic strength. Masking agents such as EDTA (ethylenediaminetetraacetic acid) are sometimes used to bind interfering metal ions, improving the selectivity of the detection method (Pai et al., 2021).

Additionally, the use of internal standards or calibration methods helps in correcting for matrix interferences. By analysing known concentrations of nitrate in a controlled matrix, adjustments can be made to account for potential deviations caused by sample composition (Fang et al., 2021).

2.7.3.5 Automation and Optimisation for Online Monitoring

With increasing demand for real-time water quality monitoring, the automation of nitrate detection systems has gained attention. Flow Injection Analysis (FIA) and Sequential Injection Analysis (SIA) have been optimised to integrate online monitoring capabilities. These automated systems offer continuous monitoring with minimal human intervention, reducing variability and improving response times (Miranda et al., 2001).

A key feature of automated systems is the integration of microfluidics, which allows precise control of reagent mixing, sample injection, and detection. Miniaturised optical detectors, such as LED-based spectrophotometers, have been incorporated into FIA setups to enhance sensitivity while reducing reagent consumption. By optimising reaction conditions in automated systems, the efficiency and reproducibility of nitrate detection can be significantly improved (Pai et al., 2021).

2.8 Electrochemical Methods

Electrochemical techniques have gained popularity for their potential in real-time and portable nitrate sensing. Among them, Nitrate Ion-Selective Electrodes (ISEs) were developed in the 1970s, providing rapid and portable detection by measuring the electrochemical potential difference across a nitrate-selective membrane (Bedwell et al., 1995) . Despite their convenience, ISEs suffer from low sensitivity and interference from chloride and bicarbonate ions.

Voltametric and Amperometry Methods represent significant advancements, utilising modified electrodes such as carbon nanotubes and nano-metal coatings to enhance nitrate detection. These methods offer high sensitivity, low detection limits, and real-time monitoring capabilities (Azmi et al., 2017). However, their widespread adoption is limited by electrode stability and maintenance challenges.

The recent development of nano-enabled electrochemical sensors has improved selectivity and robustness, making them ideal for continuous water quality monitoring. Furthermore, integration with

wireless data transmission enables remote, automated monitoring, making electrochemical methods increasingly suitable for smart water management systems.

2.9 Flow Injection Analysis (FIA) and Automated Detection

The development of Flow Injection Analysis (FIA) in the early 2000s represented a major advancement in automated and continuous nitrate monitoring. FIA systems continuously inject samples into a reagent stream, enabling rapid analysis with minimal reagent consumption. Coupled with spectrophotometry or electrochemical detection, FIA provides high-throughput, accurate, and real-time analysis (Alahi & Mukhopadhyay, 2018).

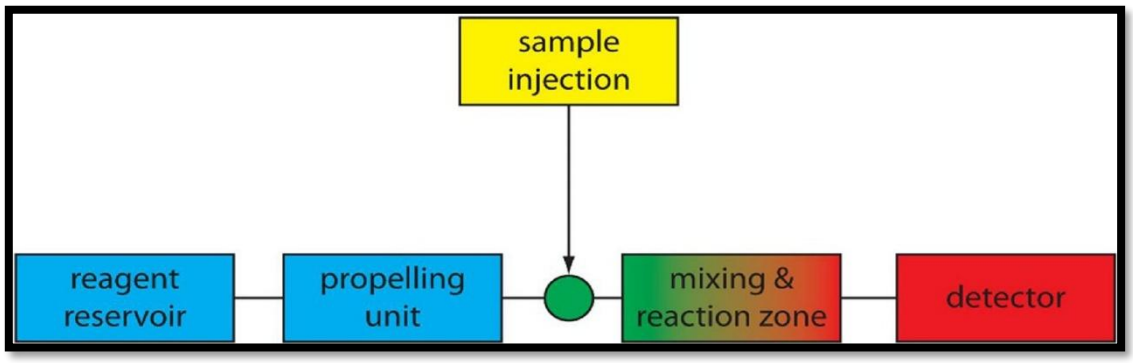

Figure 6 Schematic Representation of a Flow Injection Analysis (FIA) System for Nitrate Detection (LibreTexts, 2020)

Figure 6 illustrates the basic workflow of a Flow Injection Analysis (FIA) system, highlighting its key components and operational sequence. The system consists of a reagent reservoir, which stores the necessary chemical reagents for the reaction process. The propelling unit ensures a continuous and controlled flow of the reagent stream, into which the sample is injected at a designated sample injection point. This injected sample is then transported to the mixing and reaction zone, where it interacts with the reagents, leading to the desired chemical reaction. The resulting product is subsequently carried to the detector, which measures the reaction outcome, typically using spectrophotometry or electrochemical detection (Alahi & Mukhopadhyay, 2018). The streamlined design of FIA, as depicted Figure 6 enables rapid mixing, precise reagent usage, and efficient analysis, making it highly suitable for real-time nitrate monitoring. Furthermore, FIA automation minimizes human intervention, reduces sample handling errors, and enhances reproducibility in water quality assessments.

Recent advancements in FIA include Vanadium (VCl_3) reduction methods, which replace toxic cadmium while maintaining high sensitivity (Wang et al., 2017). These systems are increasingly integrated into online monitoring platforms, particularly for environmental water quality assessments. The development of lab-on-chip FIA systems allows for enhanced portability and miniaturisation, making FIA a promising solution for on-site and continuous water monitoring.

2.9.1 Optical and Chemiluminescent Sensors

Optical and chemiluminescence-based methods have significantly improved nitrate detection limits. Chemiluminescence sensors, which measure light emission when nitrate reacts with ozone, achieve nanomolar detection limits, making them ideal for trace analysis in marine and atmospheric studies (Wang et al., 2017).

Fluorescence-based sensors leverage fluorophores that change intensity upon nitrate binding, allowing real-time detection in drinking water and agricultural runoff (Sharma et al., 2021). However, these methods often require specialised instrumentation and are sensitive to background fluorescence interference. The emergence of smartphone-integrated optical sensors has improved accessibility, enabling point-of-use monitoring in decentralised water treatment systems (Fang et al., 2021).

2.10 Colorimetry vs. Spectrophotometry in Nitrate Detection

Colorimetry and spectrophotometry are two vital analytical techniques employed in chemical and environmental sciences for detecting and quantifying substances based on light absorption. These techniques play a crucial role in nitrate detection, especially in water quality monitoring and environmental assessments. Colorimetry is often favoured for its quick and cost-effective detection, while spectrophotometry offers greater accuracy and sensitivity.

2.10.1 Principles of Colorimetry

Colorimetry is a technique that measures the concentration of a substance based on colour intensity. It operates on Beer-Lambert's Law, which states that the absorbance of light is directly proportional to the concentration of the analyte and the path length of the sample (Miranda et al., 2001). A colorimeter directs light through a sample and measures how much of the light is absorbed or transmitted. The measurement is based on three primary colours (Red, Green, and Blue - RGB) within

the visible light spectrum (400-700 nm) (Singh et al., 2019). A comparison with standard solutions determines the analyte concentration.

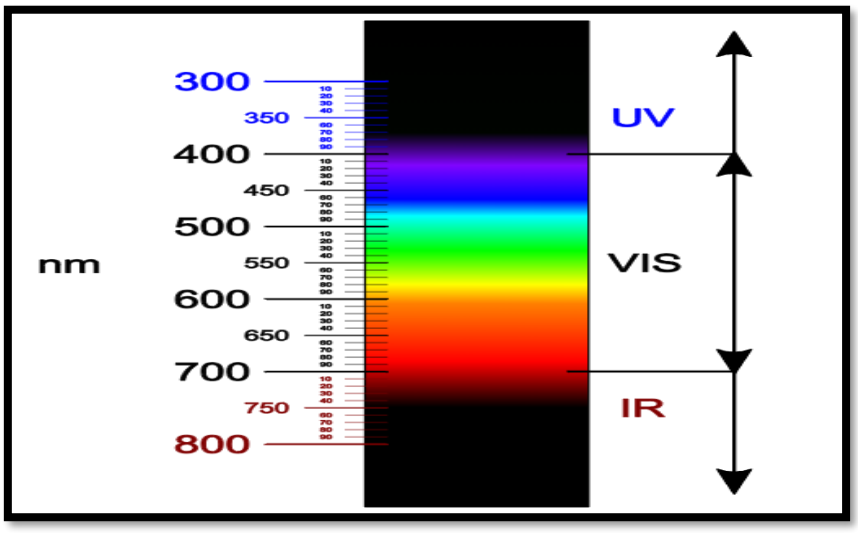

Figure 7 The electromagnetic spectrum showing UV, visible, and IR regions, highlighting the visible light range (400-700 nm) used in colorimetry (Jankovic, 2018)

A fundamental aspect of colorimetry is the visible light spectrum, which ranges from 400 to 700 nm, as illustrated in Figure 7 The ultraviolet (UV) region is below 400 nm, and the infrared (IR) region extends beyond 700 nm. The visible spectrum consists of different wavelengths corresponding to specific colours, where absorption of wavelengths results in the perception of different colours in solutions.

Colorimetry is widely used for detecting nitrates in water using the Griess reaction, where nitrate is reduced to nitrite and reacts with sulfanilamide and N-(1-naphthyl) ethylenediamine to form a pink-coloured azo dye, measurable at 540 nm (Tsikas, 2007). This method is favoured for its simplicity and cost-effectiveness (Cadeado et al., 2022), but it is limited to coloured substances and can suffer from interference from other coloured compounds (Kazemzadeh & Ensafi, 2001). Additionally, it has lower sensitivity compared to spectrophotometry.

2.10.2 Principles of Spectrophotometry

Spectrophotometry measures the intensity of light at specific wavelengths after it passes through a sample. It allows for high quantitative accuracy, enabling the detection of both colored and colourless compounds across a broad wavelength range (UV-visible-infrared, 200-2500 nm) (Yasir & Dadi,

2022). A spectrophotometer consists of a light source, a monochromator to select a specific wavelength, and a detector that measures the intensity of light after passing through the sample (Singh et al., 2019).

A typical spectrophotometer consists of five essential components, as shown in Figure 8 . The light source generates the initial beam, which is focused by a collimator lens to form a parallel beam. The monochromator (either a prism or grating) separates the light into its component wavelengths, and a wavelength selector (slit) ensures that only the chosen wavelength reaches the sample. The sample solution (in a cuvette) allows the selected wavelength to pass through, absorbing part of the light. A detector (photocell) then measures the intensity of the transmitted light after it has passed through the sample, while a digital display or meter shows the absorbance reading, which is used for quantitative analysis.

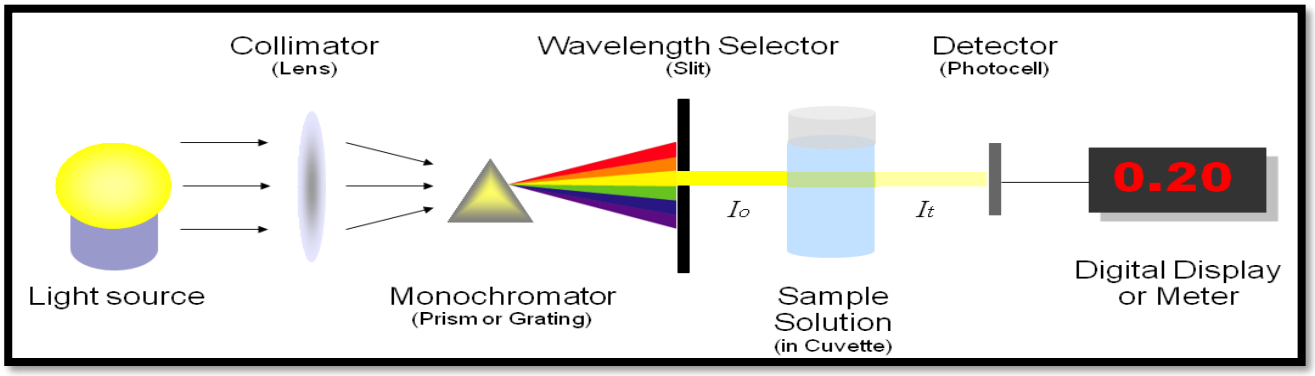

Figure 8 Schematic diagram of a spectrophotometer showing key components involved in light absorption measurement (Shim, 2020).

Spectrophotometry is more advanced than colorimetry because it allows precise measurement of absorbance at specific wavelengths, reducing interference and increasing accuracy (Norman & Stucki, 1981). It is extensively used in water quality analysis, biomedical research, and industrial applications, particularly for analysing nitrate levels in water and biological samples due to its high sensitivity and low detection limits. This method offers high accuracy and precision by measuring absorbance at specific wavelengths, making it applicable to both coloured and colourless substances while reducing interference from other chemicals(Yasir & Dadi, 2022) . However, spectrophotometry requires higher costs and trained personnel for calibration and operation.

2.10.3 Comparative Analysis of Colorimetry vs. Spectrophotometry

Colorimetry and spectrophotometry differ significantly in terms of wavelength range, measurement principle, accuracy, applications, and cost. Colorimetry operates within the visible light range (400–700 nm), which restricts its application compared to spectrophotometry, which covers ultraviolet (UV), visible, and infrared wavelengths (200–2500 nm). Colorimetry measures RGB colour intensity, while spectrophotometry measures absorbance at specific wavelengths, allowing for higher precision. A colorimeter is commonly employed for basic analyses such as water testing and food analysis, whereas a spectrophotometer is employed in advanced research, clinical diagnostics, and industrial applications. In terms of cost and complexity, colorimetry is affordable and easy to use, while spectrophotometry is more expensive and requires skilled personnel (Norman & Stucki, 1981; Singh et al., 2019).

2.11 Nitrate Removal Using Capacitive Deionisation (CDI)

CDI has emerged as a promising electrochemical technology for removing nitrates and other ionic contaminants from water sources. CDI utilises a low-voltage electrical field to attract and remove charged ions, such as nitrates, from water by adsorption onto high-surface-area porous carbon electrodes. This process is advantageous over conventional methods due to its low energy consumption, high water recovery, and ease of regeneration (Porada et al., 2013). Several enhancements, such as membrane capacitive deionisation (MCDI), flow-electrode CDI (FCDI), and ion-selective CDI, have improved ion selectivity and removal efficiency. In addition to nitrate removal, detecting nitrate contamination rapidly and in real time is crucial for water quality monitoring and environmental management. Recent advancements in electrochemical and capacitive sensing technologies have enabled online monitoring of nitrate concentrations with high sensitivity and precision.

This literature review of CDI technology for nitrate removal, exploring recent advancements in electrode materials, process optimisation, and nitrate detection methods. It also explores the integration of CDI with real-time nitrate sensing technologies as a potential solution for continuous water treatment and monitoring.

2.11.1 Conventional Methods for Nitrate Removal and their Limitations

Traditional methods for nitrate removal from water include biological denitrification, ion exchange, reverse osmosis (RO), and electrodialysis (ED). Biological denitrification utilises bacteria to reduce nitrates into nitrogen gas, but it requires strict environmental controls and a consistent carbon source, making it unsuitable for rapid and large-scale applications (Lacasa et al., 2011). Ion exchange is widely used due to its high selectivity for nitrates, but the process generates brine waste, which requires additional disposal treatment (Kim & Choi, 2012). Reverse osmosis (RO) is another highly effective method for nitrate separation, but it suffers from high energy consumption, membrane fouling, and frequent maintenance requirements (Epsztein et al., 2015).

Electrodialysis (ED) is a process that employs ion-exchange membranes to remove nitrates selectively, but operational challenges such as scaling, membrane degradation, and high capital costs limit its widespread adoption (Ortiz et al., 2008).Given these limitations, researchers have explored alternative, energy-efficient technologies such as capacitive deionisation (CDI) as a more sustainable solution for removing nitrate from drinking water and wastewater.

2.11.2 Capacitive Deionisation (CDI) for Nitrate Removal

2.11.2.1 Working Principle of CDI

Capacitive deionisation (CDI) is an emerging electrochemical water purification technology that removes ionic contaminants by applying a low voltage across high-surface-area porous carbon electrodes. CDI operates through electrostatic adsorption, wherein anions and cations migrate toward oppositely charged electrodes, effectively deionising the feed water (Anderson et al., 2010). Unlike conventional ion exchange or reverse osmosis systems, CDI is energy-efficient and produces minimal secondary waste, making it a promising technology for water desalination and nitrate removal (Porada et al., 2013). The efficiency of CDI largely depends on the electrode material, its ability to selectively attract ions, and operational settings such as voltage and water flow rate.

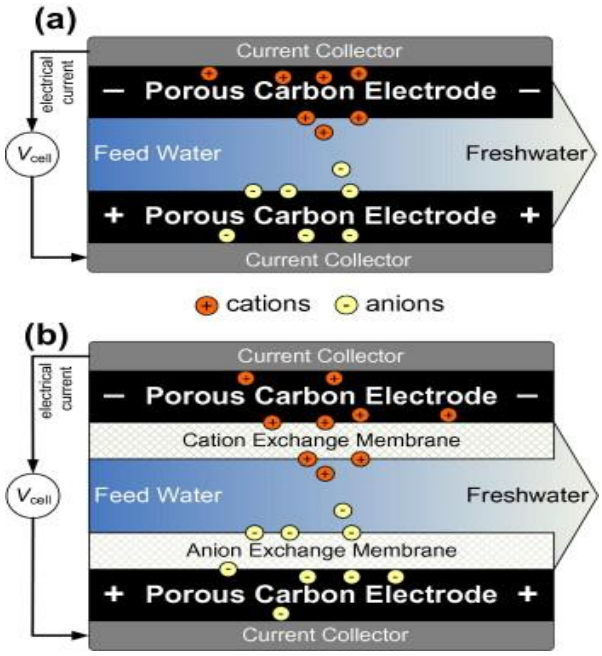

Figure 9 Schematic of (a) Conventional CDI, where ions accumulate on oppositely charged porous carbon electrodes, and (b) MCDI, which uses ion-exchange membranes for selective ion transport, improving efficiency and desalination performance (Porada et al., 2013).

Figure 9 illustrates the working principles of two different CDI configurations: (a) conventional CDI and (b) membrane capacitive deionisation (MCDI). In the conventional CDI system, charged ions in the feed water migrate toward oppositely charged porous carbon electrodes, forming an electrical double layer that stores these ions until the electrodes are regenerated (Porada et al., 2013). In contrast, MCDI enhances ion selectivity and charge efficiency by incorporating ion-exchange membranes. These membranes allow selective transport of specific ions, thereby reducing co-ion repulsion and improving desalination efficiency (Tang et al., 2015).Due to its improved charge efficiency, MCDI has been shown to achieve higher salt removal capacities and lower energy consumption than conventional CDI.

2.11.2.2 Recent Advancements in CDI for Nitrate Removal

Significant advancements in CDI technology have focused on improving nitrate selectivity, energy efficiency, and scalability. Membrane capacitive deionisation (MCDI), as mentioned earlier, utilises ion-exchange membranes to increase nitrate removal efficiency and prevent co-ion expulsion (Porada et al., 2013). Flow-electrode capacitive deionisation (FCDI) further improves ion removal rates by incorporating suspended carbon particles as electrodes, enabling continuous ion adsorption and desorption, which enhances nitrate recovery (Fang et al., 2018).

Researchers have developed innovative electrode materials to improve nitrate adsorption. Nitrogen-doped carbon electrodes have demonstrated outstanding performance, with adsorption capacities reaching 149.35 mg/g, significantly surpassing traditional carbon-based electrodes (Li et al., 2023). Additionally, asymmetric CDI electrodes, where one electrode is modified with SiO_2 and Al_2O_3, have been introduced to enhance nitrate selectivity (Lado et al., 2017).

A study by Tang (2015) investigated the simultaneous removal of fluoride and nitrate from brackish groundwater using CDI (Tang et al., 2015). Their research developed a one-dimensional transport model to describe the competitive adsorption behaviour between nitrate and chloride, which plays a crucial role in optimising CDI efficiency for real-world applications.

2.12 Summary

This chapter reviews the main causes of nitrate contamination, its harmful effects, and the different methods used for detecting and removing nitrate from water. Most nitrate pollution comes from human activities like using too much fertiliser, poor wastewater handling, and industrial waste. Natural sources, such as certain minerals and rainwater containing nitrogen compounds, also contribute. Because nitrate dissolves easily in water, it can quickly spread through soil and into rivers or underground water. This creates serious health risks, especially for babies and pregnant women, including a condition called "blue baby syndrome" and increased chances of cancer. In the environment, high nitrate levels can cause algal blooms, reduce oxygen in water, damage soil quality, and release greenhouse gases that worsen climate change.

The chapter also examines methods for detecting nitrate in water. Older methods, like the zinc reduction technique, are simple and low-cost but can be unreliable and hard to use for continuous testing. A better method is using vanadium chloride, which reacts faster and works well with UV-Vis spectrophotometry for real-time measurement. In addition to detection methods, the chapter introduces Capacitive Deionisation (CDI) as a modern approach for nitrate removal, which operates by applying an electrical charge to selectively remove ions from water. The insights gained from this literature review provide a foundation for the design and testing of the integrated nitrate detection and CDI system described in the following chapter.

3 REQUIREMENTS FOR A NITRATE DETECTION SYSTEM FOR CAPACITIVE DEIONISATION (CDI)

Conventional nitrate removal techniques, such as ion exchange, reverse osmosis, and biological denitrification, often involve prohibitive costs, energy-intensive processes, and complex operations. The literature consistently highlights these limitations, particularly the high energy demands, and operational burdens associated with reverse osmosis and electrodialysis systems (Epsztein et al., 2015). Capacitive deionisation (CDI) is an emerging, energy-efficient, and sustainable alternative for nitrate removal, utilising electrically charged porous electrodes to adsorb ions from water selectively. This chapter focuses on modelling nitrate adsorption and desorption in a membrane capacitive deionisation (mCDI) system using a dynamic modelling software called Stella. The platform facilitates the visualisation of how water and nitrate concentrations move through the CDI system by tracking material flow and ensuring conservation of mass. It provides a clear picture of how concentrations change over time, making it easier to understand the system's behaviour during adsorption and desorption cycles Using graphical elements such as stocks, flows, and converters, the model simulates adsorption-desorption cycles and predicts system response under semi-batch conditions. The primary focus is on simulating sodium chloride behaviour to validate the model structure, followed by the introduction of nitrate as a secondary species. This approach enables the estimation of nitrate removal rates and supports the design of accurate sampling mechanisms. The experimental data used to calibrate the model serves as a key link between theoretical development and practical implementation, forming the basis for the automated nitrate detection system described in the subsequent sections.

3.1 Stella Software

Stella is a generic dynamic modelling tool developed by ISEE Systems, designed to simulate the behaviour of systems over time through an intuitive, graphical environment. Stella provides a flexible modelling framework that we use as a platform to construct and simulate material balance models for the quantities of interest such as water and participating salt species.

Stella simplifies model development by providing an intuitive interface that uses graphical elements. These elements include stocks, which represent the accumulation of a substance (for example, nitrate concentration); flows, which indicate the rate of movement into or out of the stocks; converters, which are used to define mathematical relationships or constants; and connectors, which link elements and

define logical or mathematical dependencies. Users construct models by dragging and connecting these elements, making the software accessible to users with limited programming experience.

To simulate system behaviour over time, Stella relies on numerical integration techniques. The software offers two primary methods: Euler's method, a straightforward first-order approach, and the Runge-Kutta 4th order method (RK4), which is more accurate and stable for a wider range of systems.
Stella Blocks

In Stella, models are built using a set of core elements called blocks, which are used to visually represent material accumulation and flow.

3.1.1 Stocks

Stocks represent the quantity of a material in the context of the models presented in this study. They can represent quantities such as mass of water, chloride, or nitrate. Stocks integrate incoming and outgoing flows over time, enabling the simulation of dynamic changes in the respective quantities in the context they represent.

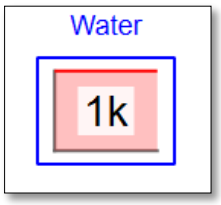

Figure 10 Stock block showing water accumulation of 1k units in a Stella model.

Figure 10 illustrates a stock block labelled *Water*, showing a stored value of 1kg.The numerical value inside the stock indicates the current quantity stored at a point in time, and the block's boundary helps identify it as a core element in Stella modelling used for tracking accumulation.

3.1.2 Flows

Flows are the pathways through which material enters or leaves a stock. They represent dynamic rates such as flow rate of materials in and out of stocks. Flows are typically connected to stocks and are calculated based on equations or input data defined by converters.

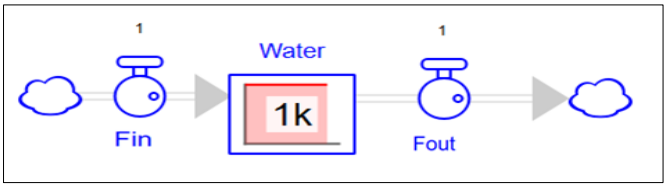

Figure 11 Fin and Fout connected to a stock holding 1k units of stored water.

Figure 11 shows a Stella model with a stock labelled *Water*, currently holding 1kg of stored water. The stock connects to two flow elements, *Fin* and *Fout*, that represent the dynamic flow of water into and out of the stock. This structure simulates how water accumulates over time, enabling the simulation of the stock quantity over the duration of the simulation.

3.1.3 Converters

Converters are used to define variables, constants, or algebraic expressions in the system. They often hold process parameters such as reaction coefficients, pump settings, or conductivity sensor calibration factors. Converters support modularity and flexibility, making the model easy to tune or expand.

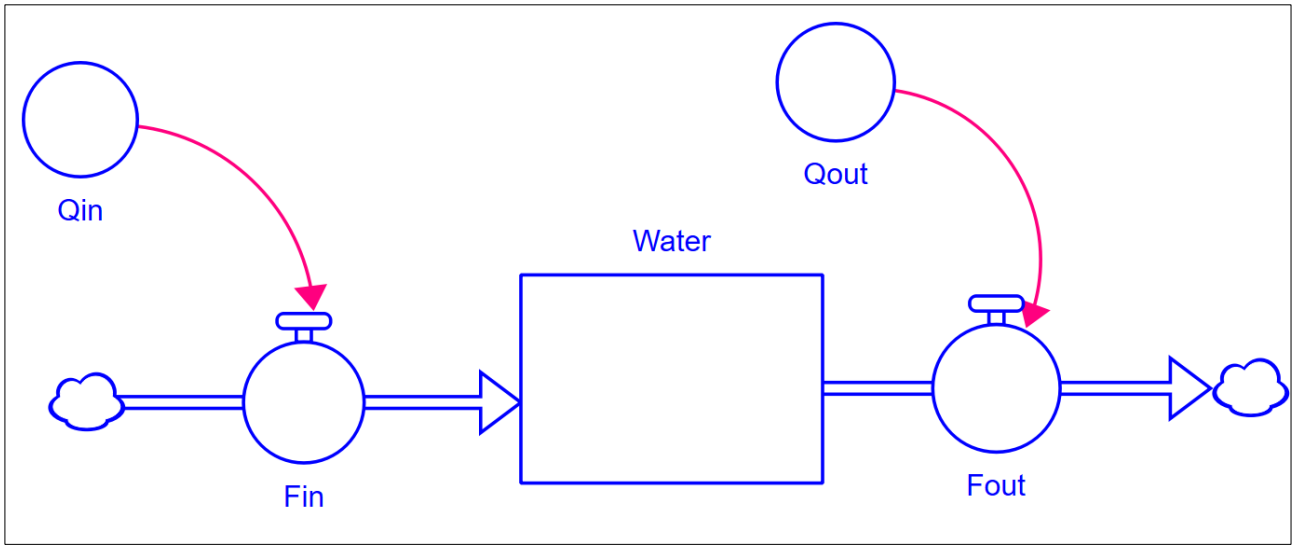

Figure 12 Converters Qin and Qout provide values for Fin and Fout connected to the Water stock thus controlling the rate of material in and out.

Figure 12 illustrates the role of converters in a Stella model. Two converters, labelled *Qin* and *Qout*, are connected to the *Fin* and *Fout* elements, respectively. These converters provide values or equations that determine the flow rates entering and exiting the stock labelled *Water*. By adjusting

the converters, users can easily modify system behaviour without altering the overall structure of the model, making the simulation more dynamic and adaptable.

3.1.4 Use of Stella Blocks to Facilitate Material Balance Calculations

With an understanding of Stella's fundamental building blocks, we can now explore how these blocks are applied to simulate unit operations and components in a system designed for nitrate detection and removal using CDI.

The general form of a material balance involves a conserved quantity. This quantity is contained within a discrete process and is expressed mathematically by the material balance equation shown in the equation (8):

$$Accumulation = Input - Output + Generation - Consumption. \quad (8)$$

In this work, none of the modelled quantities are generated or consumed, simplifying calculations.

3.1.4.1 Implementing a Tank in Stella

Th simplest form of a discrete process in this work can be considered a tank, or a simple geometrical structure containing the solvent (*M water*). In Stella, a tank is implemented using a Stock block that accounts for the quantity of water by storing the amount of fluid at any given time during the simulation. At the same time, a unique dynamic variable is created in the simulation called *M Water*.

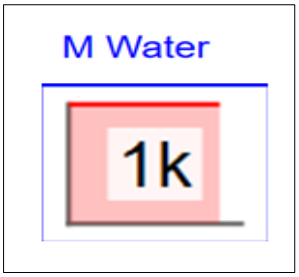

Figure 13 Stock block representing a tank with 1k units of water in a Stella model.

Figure 13 shows a stock block labelled *MWater,* representing a tank containing 1k units of stored water in a Stella model that is not changing with time. This block simulates the accumulation of fluid

volume over time and serves as the core element for modelling tank behaviour or any material quantity we wish to track in the calculation.

3.1.4.2 Implementing a Pump in Stella

A pump is modelled as a flow block whose rate is controlled by a converter. The flow rate can be constant or dynamically adjusted using feedback from sensors or controllers. This is important when simulating pulsed flow, batch operation, or pressure-driven delivery in CDI systems.

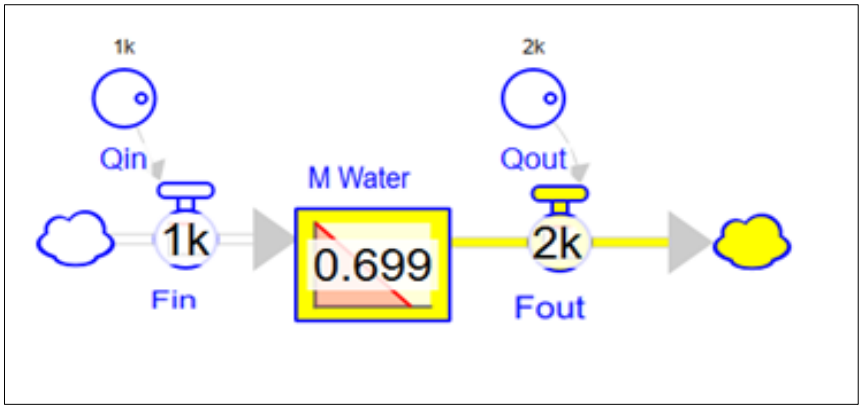

Figure 14 Pump-controlled flow system with converters Qin and Qout regulating inflow and outflow around a water stock. The imbalance between flow in and out results in a reduction in the quantity of material.

Figure 14 This shows a Stella model where a pump is implemented using a flow block, with the flow rate controlled by converters labelled Qin and Qout. At the end of the simulation, the stock quantity has reduced from a starting quantity of 1kg to 0.699g, while Fin and Fout are influenced by converter values set to 1k per unit time and 2k per unit time, respectively. This simulates a tank where more liquid is being pumped out than being pumped in.

3.1.4.3 Implementing a Chemical Species in Stella as a CSTR

The dynamic behaviour of dissolved chemical species such as nitrate can be effectively modelled in Stella using separate stock blocks for each species. These stocks represent the species' mass within a particular tank or system unit. To simulate the realistic transient behaviour of chemical species passing through system components, each component is modelled using the continuous stirred-tank reactor (CSTR) assumption. This assumes that the contents of each “tank” are perfectly and continuously mixed, where a tank is any discrete component in the system with a known finite

volume. Under this condition, the outlet concentration is equal to the internal concentration of the tank, as expressed in mathematical Equation (9):

$$C_{out} = C \tag{9}$$

The dynamic behaviour of the species within the reactor is described using a mass balance expression based on the accumulation principle. The general form of the equation is provided in Equation (10):

$$\frac{dC}{dt} = \frac{Q}{V}(C_{in} - C) \tag{10}$$

In this equation, *C* is the concentration of the chemical species inside the tank (*mg/L*), C_{in} is the inlet concentration (*mg/L*), *Q* is the volumetric flow rate (*L/s*), and *V* is the tank's volume (*L*). This equation captures the rate of change in concentration as a function of flow rate and the difference between inlet and internal concentrations.

Assuming an initial concentration of zero inside the tank, i.e., *C(0) =0*, and a constant inlet concentration C_{in} , solving this first-order differential equation yields the expression shown in Equation (11):

$$C(t) = C_{in}(1 - e^{-kt}) \tag{11}$$

This result indicates that the internal concentration increases over time, following an exponential rise. As time progresses ($t \rightarrow \infty$), the exponential term $e^{-kt} \rightarrow 0$, and the concentration inside the reactor asymptotically approaches the inlet concentration C_{in} . This behaviour reflects the typical response of a CSTR to a step change in inlet concentration and is characteristic of well-mixed systems.

Within Stella, the chemical mass is tracked using a stock block, while the water volume is modelled using a separate stock. The concentration inside the tank is then calculated as the ratio of these two stocks. The formal definition of this concentration is provided in the Equation (12):

$$C = \frac{M_{Chem}}{V_{water}} \tag{12}$$

Where M_{chem} is the chemical species mass (mg) and V_{water} is the water volume (L). This real-time computation ensures that all downstream flows accurately reflect the chemical conditions within the tank.

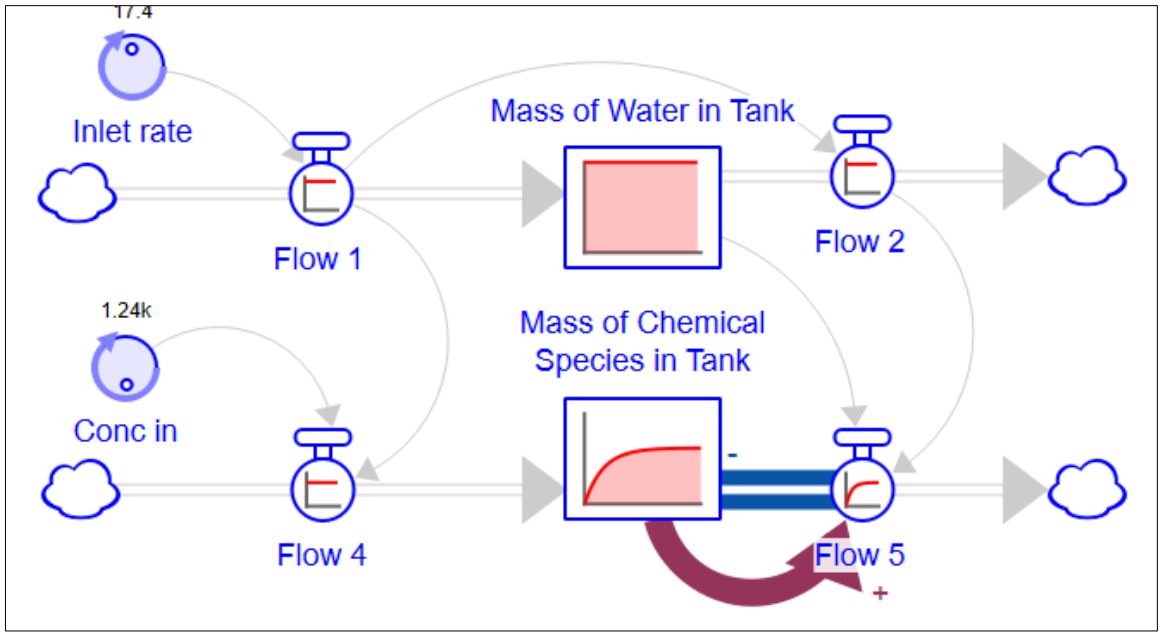

Figure 15 Model showing separate stocks for water and chemical species with flows based on inlet rate and concentration.

Figure 15 shows a Stella model with two separate stock blocks representing the mass of water and the mass of a chemical species in a tank. *Flow 1* and *Flow 2* manage the water movement, with the inlet rate defined by a converter labelled Inlet rate. *Flow 4* and *Flow 5* handle the transport of the chemical species, where the concentration input is controlled by the converter labelled *Conc in*.

The rate at which the chemical leaves the tank (denoted as *Flow 5* in the Stella model) is dependent on the internal concentration and the water outflow rate (*Flow 2*). This relationship is mathematically expressed in Equation (13):

$$\text{Flow 5} = \text{C} \times \text{Q}_{\text{out}} \tag{13}$$

Where:

C is the concentration of the species in the tank (*mg/L*),

Q_{out} is the volumetric flow rate of water leaving the system (*Flow 2*).

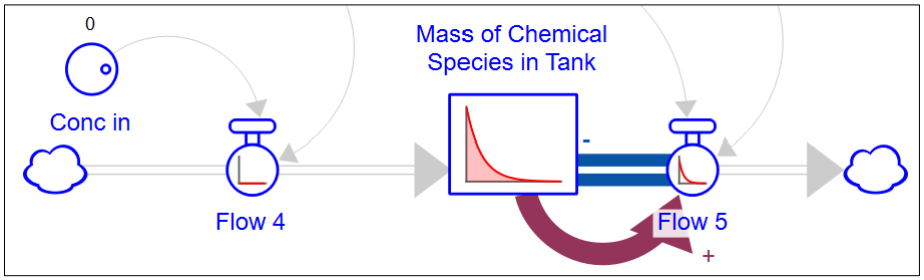

Figure 16 Stella model of a CSTR showing exponential decay of chemical species with zero inlet concentration.

Figure 16 illustrates an alternate scenario in which the tank initially contains a known quantity of a chemical species and is flushed with clean water (i.e., inlet concentration is zero). In such a case, the internal concentration decreases over time following exponential decay behaviour, characteristic of first-order systems. This behaviour is mathematically represented by Equation (14).

$$C(t) = C_0 . e^{-kt} \tag{14}$$

where C_0 is the initial concentration (mg/L), $k = \frac{Q}{V}$ is the system's dilution or washout rate constant (s^{-1}), and t is the time (s).

3.1.4.4 Implementing Recycle in Stella

A recycle loop is modelled by connecting a process's outflow back to its input, often through an intermediate converter or stock to account for delay, mixing, or secondary treatment. This approach is essential in modelling semi-batch and batch processes with continuous feedback.

3.1.4.5 Implementing a CDI Cell

The implementation of a Capacitive Deionisation (CDI) cell within the Stella modelling environment was achieved by constructing two flow blocks *NaClincell* and *NaCl adsorbdesorb*. The *NaClincell* block represents the mass of salt (NaCl) dissolved in the water phase inside the CDI module. This encompasses the dynamic fluctuations in salt concentration during operation. The *NaCl adsorbdesorb* block captures the mass of salt electrostatically adsorbed onto or desorbed from the electrode surfaces during each operational cycle. It is also associated with the quantity called the salt adsorption rate (SAR) and nitrate adsorption rate (NAR). Determination of this parameter is the focus of the experimental section of this chapter.

These two stocks are interconnected through flow pathways that model ion migration, driven by external factors such as applied voltage, electrode saturation, and desorption cycles, as illustrated in Figure 17.

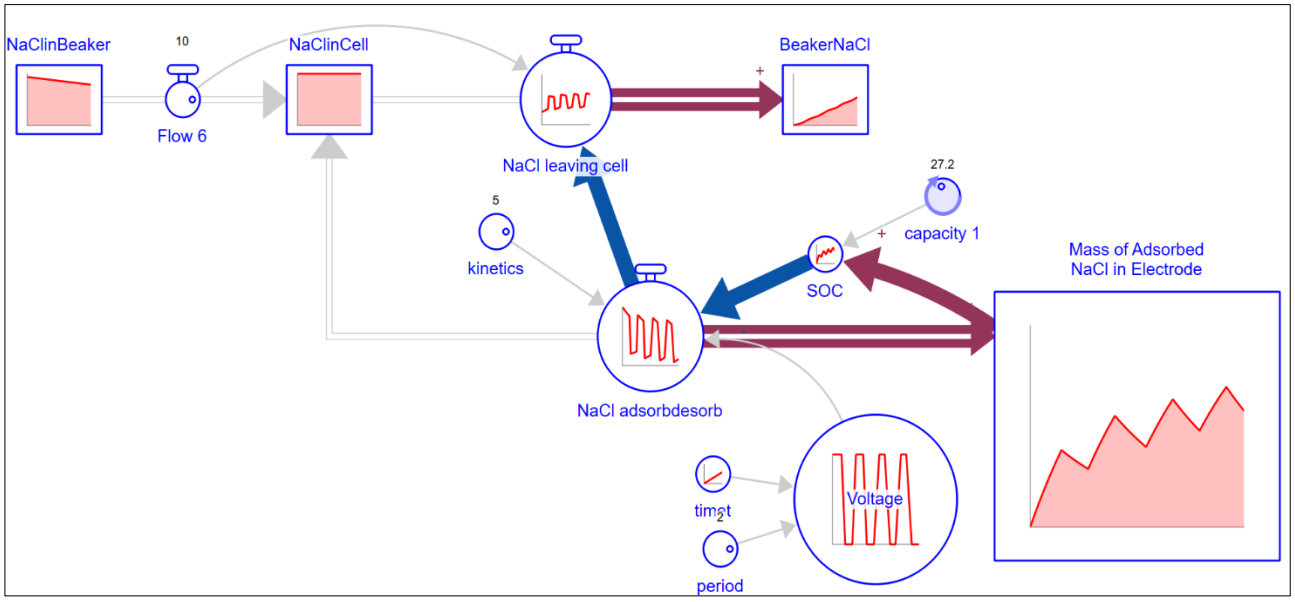

Figure 17 Stella model representation of NaCl transport and adsorption within the CDI system. It simulates the movement of dissolved salt and its periodic adsorption-desorption behaviour on the electrode surfaces

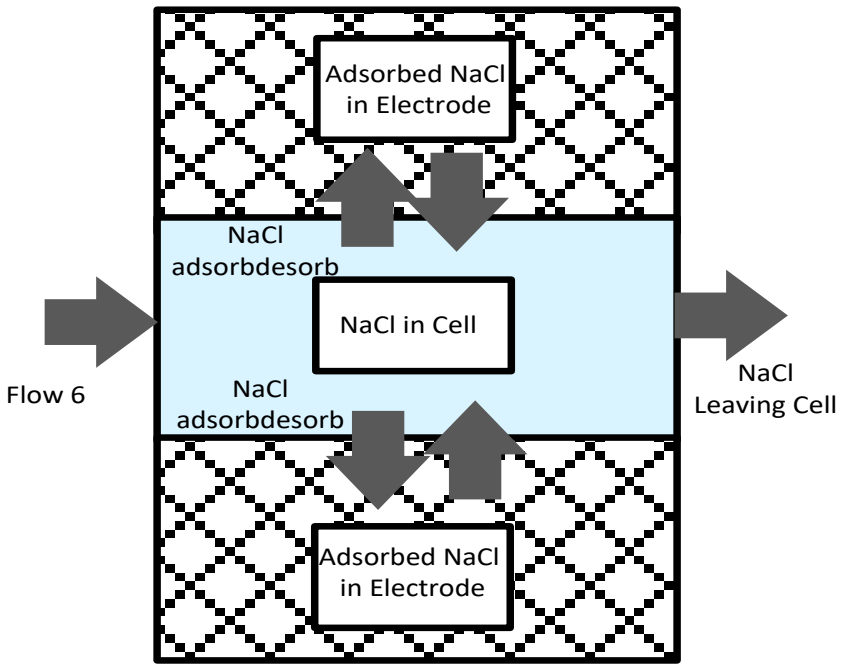

Figure 18 Equivalent representation of Stella model of CDI cell illustrating the identity of stocks and flows

Figure 18 illustrates the Stella model framework developed to simulate the CDI cell's ion transport and adsorption dynamics. During the adsorption phase, as voltage is applied, ions (Na^+ and Cl^-) are removed from the solution and adsorbed on the electrode surfaces, resulting in a reduction of *NaClincell* and a corresponding increase in *NaCl adsorbdesorb*. Conversely, during the desorption phase, when the applied voltage is reversed or removed, the adsorbed ions are released back into the water phase, causing an increase in *NaClincell* and a simultaneous decrease in *NaCl adsorbdesorb*. This cyclic exchange between the two stocks accurately captures the operational dynamics of CDI technology, including adsorption efficiency and regeneration behaviour. By tracking the free and adsorbed ions separately, the Stella simulation allows a more precise depiction of mass balance, ion storage capacity, and system performance over multiple cycles. This framework provides a robust foundation for extending the model towards more complex systems involving nitrate removal and multi-species ion competition.

3.2 Stella Model for Semi-Batch Capacitive Deionisation (CDI) NaCl Removal

In batch mode operation, a fixed volume of water is treated multiple times by continuously recirculating it through the CDI cell. This system functions as a single-pass configuration that separates the output into two streams: purified water and salt-rich water. The purified water is then returned to the feed tank for reuse. Semi-batch operation is a variation of this approach, where fresh water is periodically added to the feed tank. This ensures that the treatment process continues smoothly and prevents the feed tank from running empty.

In this section, NaCl removal is examined to represent the background salinity associated with all groundwater containing nitrates. By first understanding the behaviour of NaCl during semi-batch operation, subsequent modifications can be made to the model to introduce nitrate as a secondary anionic species. This can be achieved by incorporating specific nitrate adsorption kinetics, electrode modifications, and selectivity factors.

3.2.1 Model Setup for Semi-Batch CDI

The water loop models the flow of NaCl-laden water through the CDI stack, ensuring continuous circulation and treatment. The salt loop represents the transport of Na^+ and Cl^- ions from the solution into the charged electrodes. During the adsorption phase, an external voltage is applied, causing the positively charged Na^+ ions to migrate toward the negatively charged electrode and the negatively

charged Cl^- ions to move toward the positively charged electrode. These ions are held within the micropores of the electrode, effectively lowering the salt concentration in the treated water.

Once the voltage is reversed or removed, desorption occurs , releasing the ions back into the solution and regenerating the system for further ion removal. Figure 19 illustrates how the water loop and salt loop work together during the adsorption and desorption phases in the CDI system.

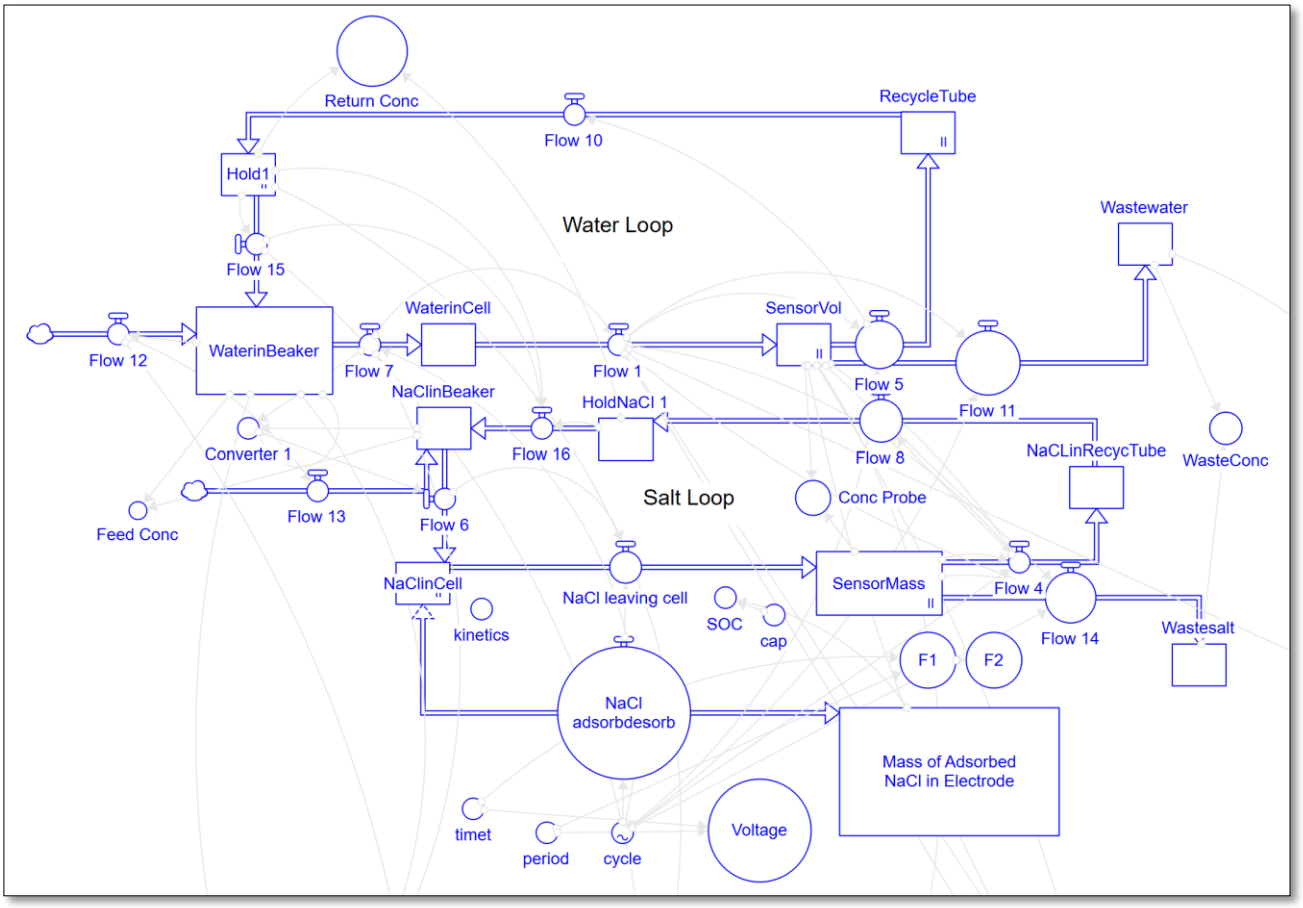

Figure 19 Stella Model Representation of Capacitive Deionisation (CDI) for NaCl Removal, Showcasing Water Loop, Salt Loop, and Adsorption-Desorption Dynamics

3.2.2 Simulation of Semi-Batch CDI for NaCl Removal

The simulation of semi-batch operation in a capacitive deionisation system offers a detailed representation of how sodium chloride is removed from water through controlled adsorption and desorption cycles. In this configuration, a fixed volume of saline water is circulated through the system, enabling repeated contact with the electrodes for ion removal without continuous feed replenishment. The Stella model developed for this simulation integrates water flow, ion transport,

and sensor monitoring into a cohesive framework that reflects the dynamic performance of a laboratory-scale CDI system. The layout and functionality of this simulation are illustrated in Figure 20.

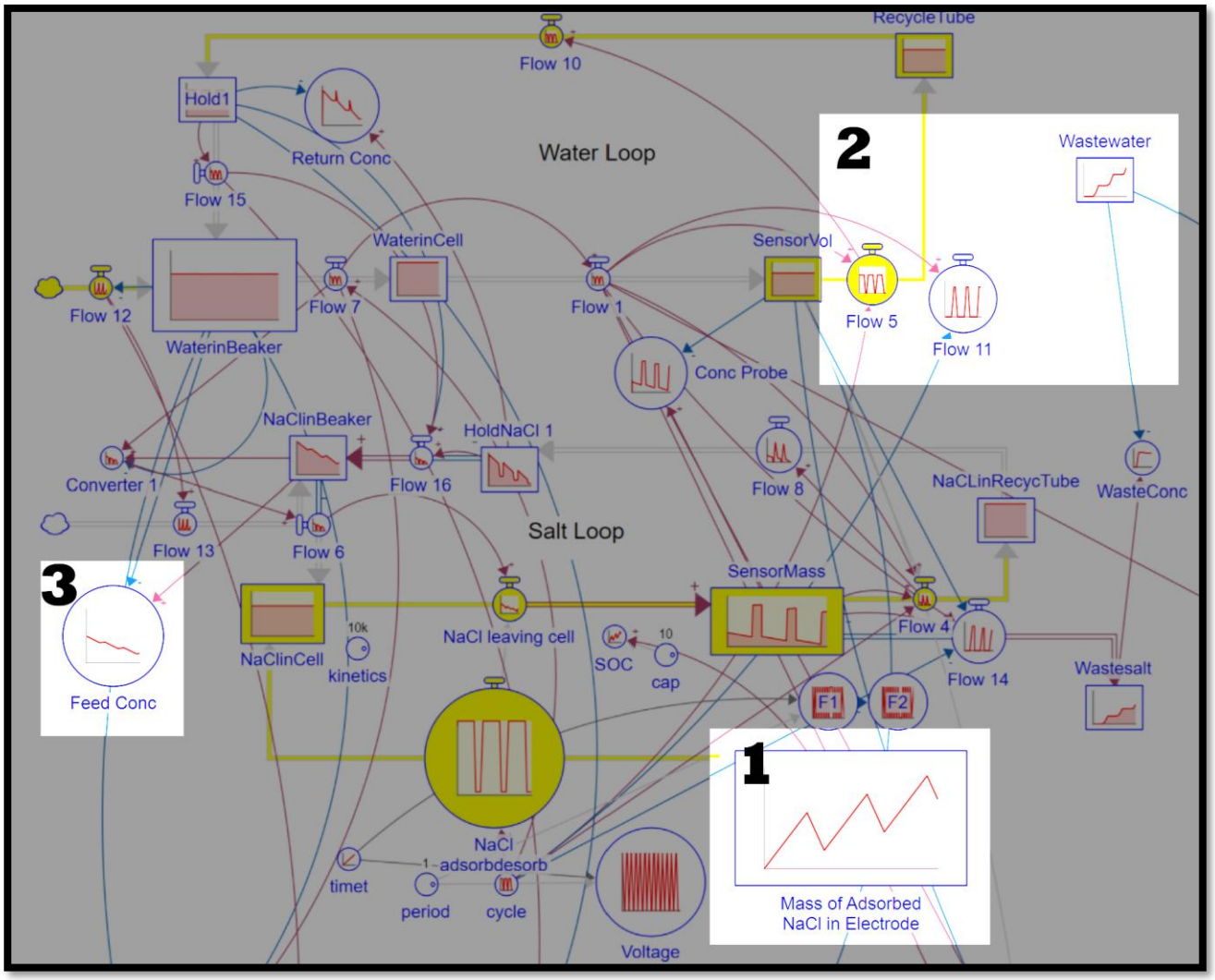

Figure 20 Stella simulation model of the capacitive deionisation (CDI) system illustrating water and salt flow loops, with key indicators for adsorbed NaCl mass (1), phase-shifted recycle and waste flow dynamics (2), and declining feed concentration (3) under cyclic adsorption-desorption operation

During the adsorption phase, sodium and chloride ions are drawn from the bulk solution and held on the surfaces of the activated carbon electrodes. This process leads to a gradual decrease in the salt concentration within the circulating water. The simulation tracks this behaviour by calculating the rate at which ions are removed and storing the total mass of salt adsorbed on the electrodes. Once the electrodes approach saturation, the system enters the desorption phase. At this point, the applied electrical potential is reversed, causing the release of stored ions into a separate waste stream. The

simulation reflects this reversal by showing a rapid increase in salt concentration in the waste flow, confirming the successful regeneration of the electrodes.

Here we note the following:

1) As the voltage alternates between positive and negative, salt is adsorbed and desorbed as indicated by increasing mass with time and decreasing mass, respectively. Note that the adsorb and desorb times are not equal as per the real operation of CDI,

2) The recycle flow (*Flow 5*) and waste flow (*Flow 11*) are in opposite phases and correspond to when desalted water is being recycled back to the batch tank and when waste desorb water is being purged. Note that the collection wastewater tank is accumulating in steps at approximately 15 min intervals as per the real operation of a semi-batch process,

3) Subsequently, as salt is adsorbed and purged to the wastewater tank from the loop, the batch is gradually lowered in salt concentration.

3.3 Stella Model for Nitrate Removal by CDI

The nitrate loop was adapted from the NaCl loop, applying similar ion transport principles to nitrate removal described in the previous section. Here we detail the model adaptation and test the model by way of a simple simulation of nitrate removal.

3.3.1 Model Setup for Simulated Nitrate Removal

The Stella Model Representation of (Figure 21) illustrates the addition of the Nitrate Loop to the baseline model already containing the Water Loop and the Salt Loop. The Nitrate Loop is identical to the Salt Loop except for the following modifications.

- The value for the nitrate removal rate (NRR) is entered in the block called *Nitrate adsorbdesorb 1,*
- The initial quantity of nitrate is entered into the stock *NitrateinBeaker1* as a starting boundary condition,
- *Flow 18* indicates the quantity of nitrate added as a top up to maintain a constant quantity of working solution in the batch.

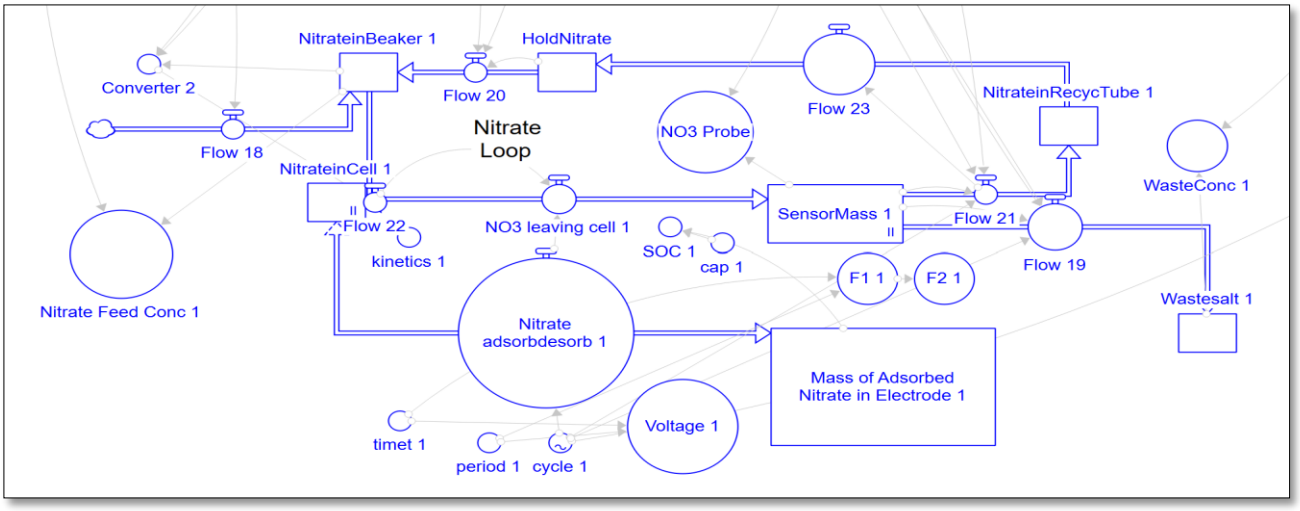

Figure 21 Stella model representation of the nitrate loop describing the mechanism by which nitrate removal occurs in a semi-batch system.

3.3.2 Results of Simulated Nitrate Removal

The Nitrate Feed Concentration Graph Figure 22-(a) illustrates the CDI system's efficiency in reducing nitrate levels over time, where the initial feed concentration of 20 mg/L steadily declines to approximately 2 mg/L at 69 minutes, demonstrating a 90% reduction. This confirms that the simulation of the Nitrate Loop effectively removes nitrate ions from the working batch solution and transfers them to the waste stream.

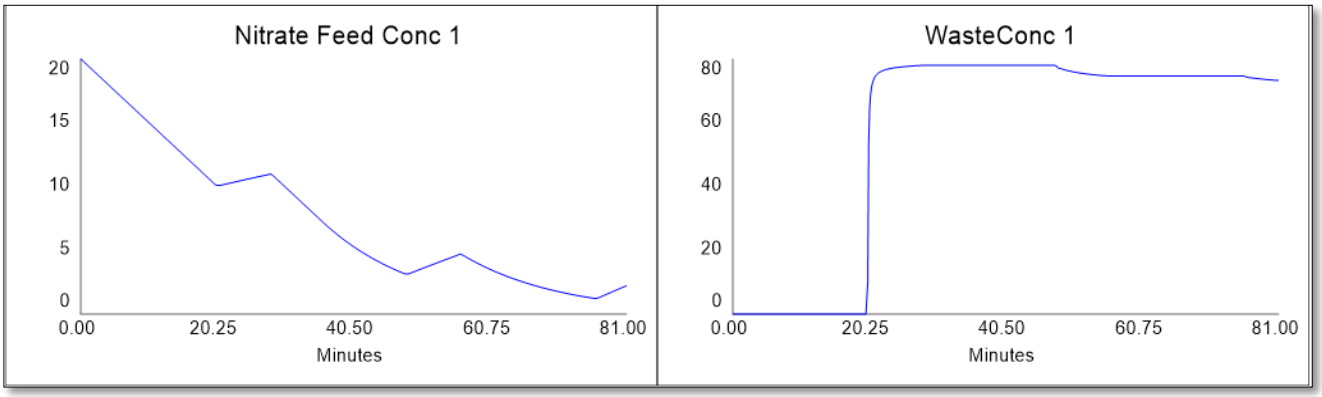

Figure 22 (a) Nitrate concentration in the feed decreases over time, indicating effective removal of nitrate by the CDI system. (b) Waste concentration shows a rapid increase followed by stabilisation, reflecting the desorption phase during CDI operation.

Correspondingly, Figure 22-(b) shows a rapid increase in waste nitrate concentration during the desorption phase, followed by stabilisation. This indicates successful nitrate transfer from the feed to

the waste stream during each cycle of CDI operation, reinforcing the system's ability to compartmentalise nitrate removal and disposal within defined temporal phases.

Figure 23-(a) represents the rate of nitrate adsorption and desorption over time, measured in milligrams per minute. The CDI system exhibits cyclic behaviour, where a nitrate removal rate (NRR) of 10 mg/min was arbitrarily used for the adsorption phase. During desorption, nitrate release is time-compensated at -17 mg/min according to the 5:3 ratio as previously discussed. The sudden negative spikes at 20, 48, and 76 minutes indicate rapid desorption, suggesting that nitrate ions are being expelled when the voltage is reversed. The gradual decline in the adsorption rate in the later cycles (from the 40-minute mark onwards) can be observed and noted.

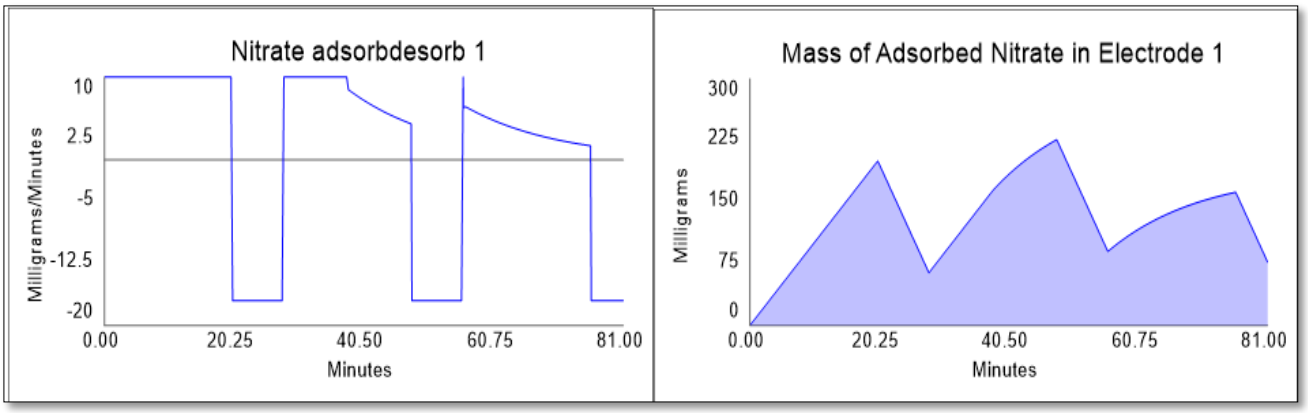

Figure 23-a Nitrate adsorption-desorption rate over time, showing cyclic behaviour with adsorption peaking at 10 mg/min and rapid desorption reaching -17 mg/min. Figure 23 -b Mass of adsorbed nitrate in CDI electrode, displaying periodic adsorption peaks up to 225 mg, with declining peaks suggesting partial electrode saturation.

Figure 23-(b) presents the mass of adsorbed nitrate in the CDI electrodes over 81-minutes. The adsorption mass follows a cyclic pattern, increasing steadily to 200 mg at 20 minutes, dropping slightly, then peaking at 225 mg at 47 minutes. The fluctuations indicate periodic adsorption-desorption cycles, confirming the cyclic nature of CDI operation.

The declining peaks after 40 minutes indicate that the electrode cannot be supplied with nitrate by the feed solution at the requested rate of 10 mg/min. This coincides with the nitrate concentration in the tank approaching low levels, approximately 5mg/L in this case. Thus, the cell is starved of nitrate, resulting in nitrate-free effluent, leaving the cell at 0mg/L concentration. This situation is also true of real operation, as documented by Lee and Choi, who achieved outlet conductivity as low as 0.11 µS/cm during membrane capacitive deionisation (MCDI) of a dilute NaCl solution, effectively

demonstrating an ion-starved effluent under low feed concentrations.(Lee & Choi, 2012) It is this starvation effect that accounts for the gradual decline in the adsorption rate noted earlier.

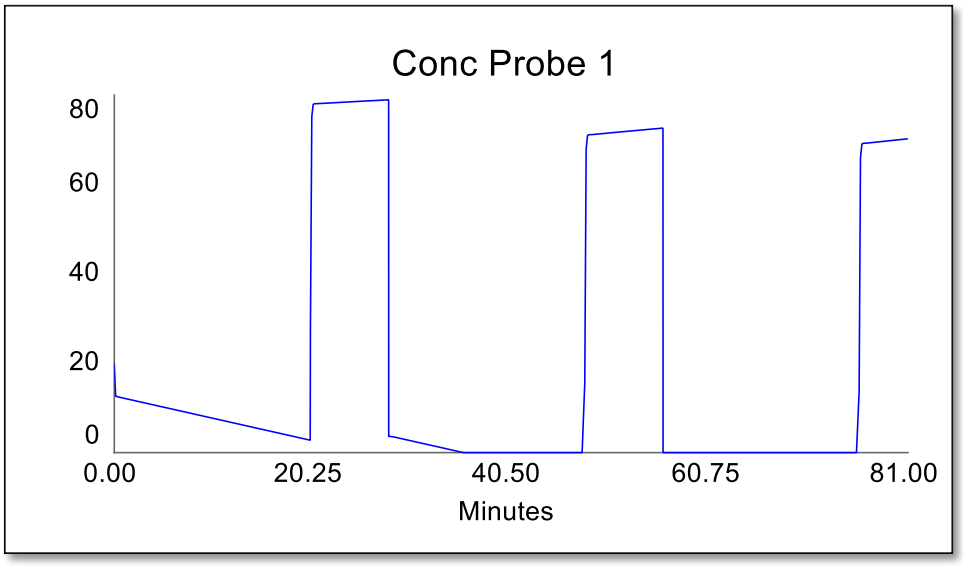

Figure 24 Periodic adsorption-desorption cycles of nitrate in the CDI system, showing effective removal and abrupt desorption spikes.

Figure 24 illustrates the periodic nitrate adsorption-desorption cycles observed in the CDI system. Effective nitrate removal is indicated by a gradual decline in concentration , while the sharp desorption spikes show efficient regeneration. This cyclic pattern is characteristic of batch-mode CDI performance and reinforces the simulation trends.

3.4 Experimental Study for Parameter Fitting Stella Model of Semi-Batch CDI Process

For the Stella model, a simplification was made for how salt removal is implemented quantitatively. Rather than using a salt removal model where the salt removal rate is a function of the state of charge (SOC) as described by other workers (Porada 2013), a fixed value model has been developed for Stella and comprises one value for adsorption and one value for desorption(Porada et al., 2013). This model can be applied individually to any species undergoing adsorption/desorption, provided there are no significant selectivity effects . This is expected to be the case with just chloride and nitrate present, as these anions have similar molecular weights and diffusion coefficients.

3.4.1 Methodology for Fitting Parameters to Stella Model

In these experiments, different methods were used to estimate how quickly salt was removed during CDI operation. For the background salt (NaCl), the removal rate was calculated by measuring how quickly the water's conductivity decreased over time, as recorded by the outlet sensor AT1. This slope was then compared to the values generated by the "Conc Probe" component in the Stella model, which simulates how the salt concentration is expected to change during the process.

Three different tank volumes (10 L, 15 L, and 20 L) were tested to ensure consistency and evaluate system performance under varying conditions. The main objective of selecting these batch sizes was to determine whether the salt removal rates remained consistent across different operating volumes. These specific volumes were chosen because they represent typical capacities in household nitrate treatment systems and small-scale portable water purification units. This approach ensures that the findings apply to real-world domestic and field-based nitrate removal scenarios.

3.4.2 Experimental Setup

3.4.2.1 Semi-Batch VS3 Process Configuration

The experimental setup, illustrated in Figure 25, consisted of a storage tank containing 10L, 15L, and 20L solutions of NaCl and nitrate. A micro diaphragm pump was measured to operate at a flow rate of 1.36 LPM to circulate the solution through the VS3 CDI module (26.6 cm × 22.5 cm × 8 cm (*LxWxH*); approximately 5 kg). The VS3 module was selected for the experiment as it was equipped with activated carbon electrodes and anion and cation exchange membranes to improve nitrate removal. A solenoid valve was incorporated into the system to control the flow direction for adsorption and desorption cycles. This switch directed the treated solution either back to the storage tank during adsorption or to waste during desorption. Supply of DC voltage to the CDI VS3 was provided by a programmable switching mode power supply (Powertech MP3094, 0–15 VDC, 0–40 A), which was integrated with an H-Bridge circuit to enable digital switching between the adsorption and desorption phases.

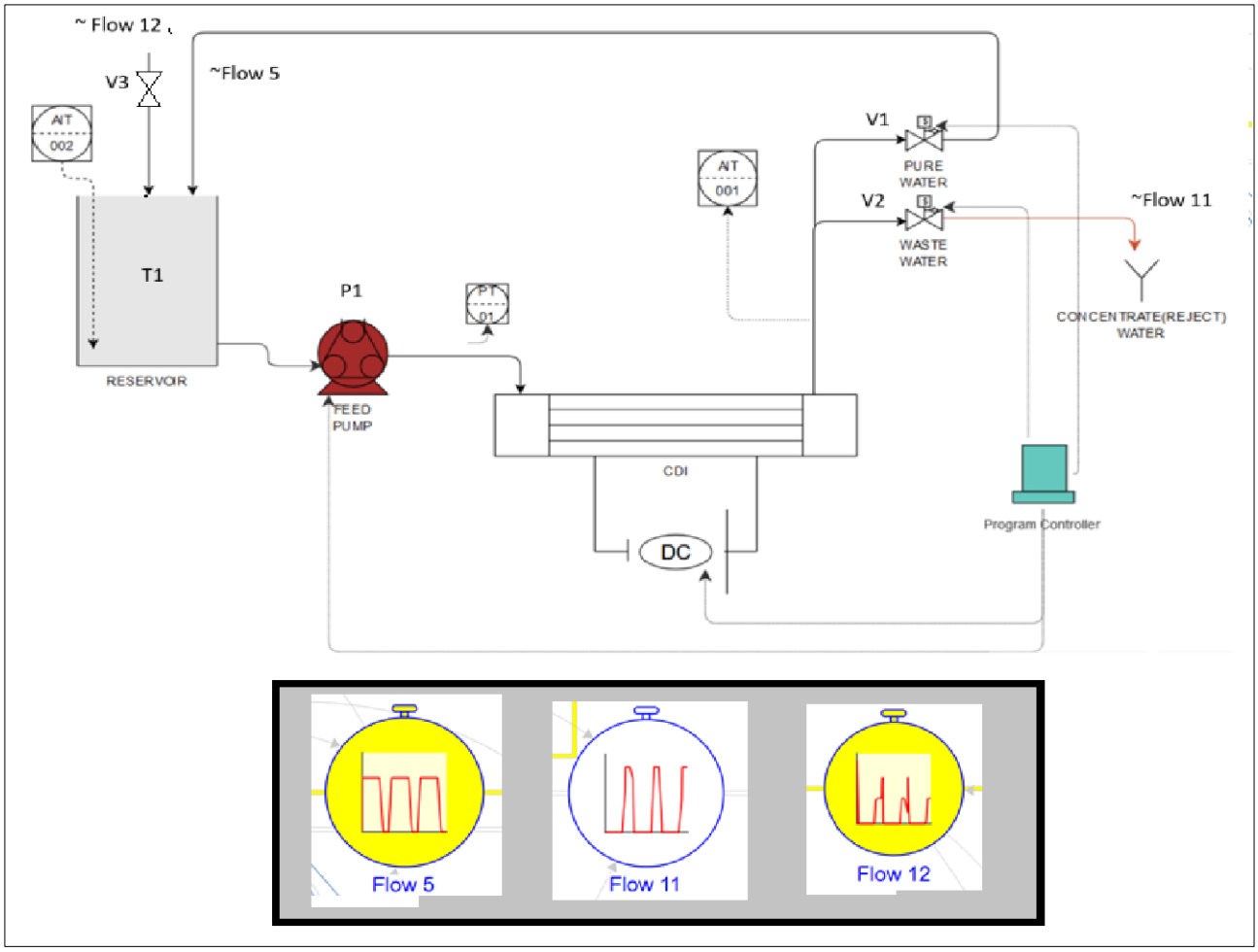

Figure 25 shows the experimental setup for the semi-batch CDI system using the VS3 module with activated carbon electrodes and ion-exchange membranes. Flow 5 represents treated water, Flow 11 is the waste stream during desorption, and Flow 12 is the nitrate feed from the storage tank

Flow 12 represents the incoming nitrate feed from the storage tank to the CDI unit. During adsorption, *Flow 5* returns the treated water back to the storage tank, indicating successful ion removal. In contrast, during desorption, *Flow 11* is activated to discard the concentrated waste stream, ensuring regeneration of the electrodes. These flow directions were managed in coordination with the valve and control circuitry to ensure accurate cycle transitions.

The system also included a control panel connected to the switch, ensuring the adsorption and desorption cycles were regulated correctly. A Go Direct Platinum-Cell Conductivity Probe was installed at the CDI module outlet to continuously monitor the treated solution's conductivity. The nitrate stock solution was prepared with an initial concentration of 20 mg/L, while the NaCl solution was adjusted to a conductivity of 2000 µS/cm to simulate real wastewater conditions. Conductivity

readings were used to evaluate the efficiency of ion removal by monitoring changes in salt concentration over time.

3.4.2.2 Methodology

During the experiment, the prepared solution was pumped from the storage tank into the VS3 CDI module. In the adsorption mode, a voltage was applied across the electrodes, allowing ions to be attracted and stored in the micropores of the activated carbon electrodes. As a result, the conductivity of the solution gradually decreased, indicating ion removal. The treated clean water was then recirculated back to the storage tank, allowing continuous monitoring of its conductivity to assess the efficiency of the adsorption process. A stepwise outline of this procedure is provided in Table 1

Table 1 Stepwise Experimental Procedure for Ion Adsorption and Desorption in the VS3 Capacitive Deionisation (CDI) System

Step	Name	Function	Action
1	Initiate Software and Sensor Logging	Begin data logging for conductivity and voltage	Launch Vernier Go Direct® software and begin live recording from the platinum-cell conductivity probe (AT001) and voltage meter for real-time monitoring and post-analysis.
2	Fill Tank	Fill the storage tank with prepared nitrate and NaCl solution	Open V3 and charge tank (T1) until level is at 20L marker (as marked on side of tank).
3	Mixing and Homogenisation	Ensure homogeneous mixing of the prepared nitrate and NaCl solution to replicate synthetic feed conditions	Mix manually using a stirrer. Conductivity was checked periodically (AT2) until 2000 µS/cm was reached
4	Priming and System Start	Circulate DI water and stabilise flow by	Switched on the pump (P1) and allowed fluid circulation (F5) through the tubing. The system was made air bubble-free

		eliminating bubbles and airlocks	before the experiment. The suction and discharge tubing were set up with clearly visible tubing. The pump operating voltage varied to eliminate air bubbles from the suction discharge lines and CDI stacks. The conductivity sensor tubing was also observed to ensure a continuous, bubble-free flow before proceeding. The conductivity probe was confirmed to be calibrated.
5	Electrode Shunt Conditioning	Ensure electrodes start with zero charge before adsorption	Place the CDI stack in zero-voltage discharge (ZVD) or "shunt" condition. This ensured the electrodes were fully discharged, preventing pre-adsorption and allowing accurate material balance.
6	Start Adsorption Cycle	Remove nitrate and NaCl ions via electrostatic adsorption	Activate the manual toggle switch to initiate the adsorption phase. The product solenoid valve (V1) was kept open, recirculating treated water back to the tank (T1). Conductivity (AT001) was monitored continuously.
7	Conductivity Monitoring	Track removal efficiency during the adsorption phase	Measured conductivity at the CDI outlet using AT001, while tank conductivity was monitored using AT002. Both sensors recorded values every second to track removal efficiency.
8	Start Desorption Cycle	Regenerate electrodes by reversing the voltage, releasing stored ions from the electrode to the waste	The programmed controller toggled the CDI polarity. Valve V2 was opened to release concentrate through Flow 11 to

			waste. Conductivity rise confirmed ion release.
9	Cycle Completion	End of adsorption-desorption sequence	Marked the cycle complete when conductivity at AT001 dropped below 700 µS/cm. At this point, pump P1 was stopped, or Flow 12 was redirected back to T1 for recirculation.

When the electrodes reached saturation, the system was switched to desorption mode. In this phase, the stored ions were released by reversing the voltage polarity. The desorbed ions were expelled from the CDI module and directed to waste through the solenoid switch valve. The desorption process ensured the electrodes were regenerated and ready for the next adsorption cycle. Conductivity measurements were taken at various time intervals to track ion removal rates and system performance.

3.4.3 Results and Discussion

3.4.3.1 NaCl Removal Performance

The effect of batch volume on salt removal performance was examined using 10L, 15L, and 20L solutions of NaCl and nitrate, each with a total initial conductivity of 2000 µS/cm. Conductivity measurements were collected using the Vernier Go Direct® graphical sensor during the semi-batch CDI operation. The results are presented in Figure 26, which plots the time taken for each solution to reach a target conductivity of 700 µS/cm.

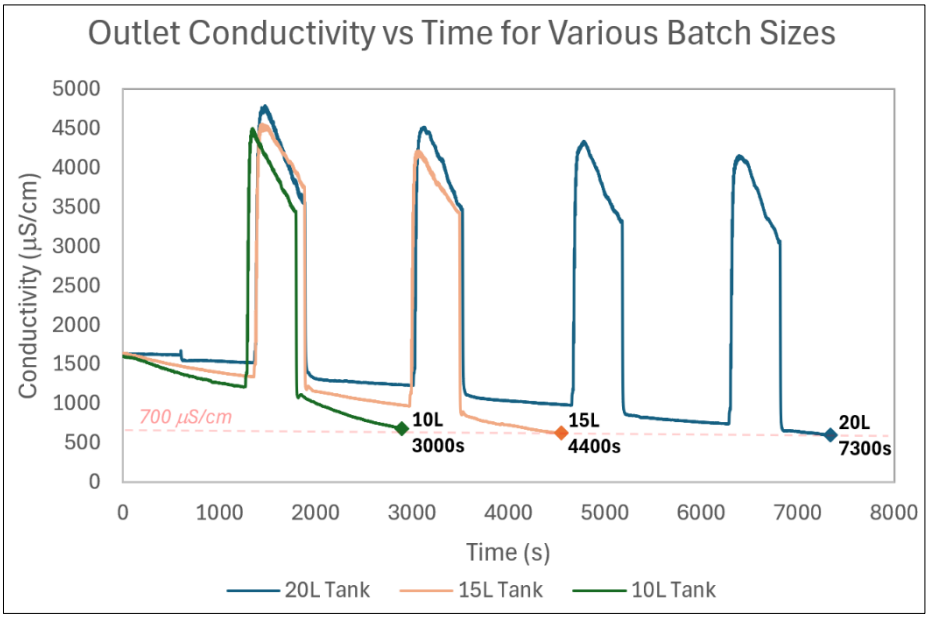

Figure 26 Outlet conductivity vs. time for various batch volumes (10L, 15L, and 20L) during semi-batch CDI operation, showing adsorption until the 700 µS/cm threshold and subsequent desorption behaviour.

The results demonstrate a clear volume-dependent trend in conductivity reduction. The 10-litre batch reached the conductivity threshold of 700 µS/cm in the shortest time, followed by the 15-litre and then the 20-litre batches. This sequence does not indicate that the CDI system operated more efficiently in smaller volumes; instead, it illustrates the governing influence of mass balance. Since the ion removal rate of the CDI unit remained approximately constant across all tests, batches with lower total ionic content naturally achieved the desired conductivity faster.

The 20-litre batch required more time due to its larger volume and correspondingly higher total ion load. In essence, a fixed removal capacity distributed over a greater quantity of ions translates into a longer treatment duration. This confirms that system performance should be evaluated not only on rate curves but also in terms of the absolute ion load to be treated.

In the desorption phase, all three volumes exhibited a pronounced increase in conductivity, signifying successful ion release from the electrodes. However, the rate of conductivity recovery varied with volume. The 10-litre solution demonstrated the fastest return to peak conductivity, consistent with its lower ion mass. Conversely, the 20-litre solution experienced a slower recovery due to the extended time required to re-equilibrate its higher ion content. This behaviour underscores the importance of considering both adsorption and desorption dynamics when scaling CDI operations.

Overall, the findings reinforce that while the removal mechanism remains unchanged, batch volume strongly influences the apparent kinetics and dynamic conductivity profile of semi-batch CDI cycles.

3.4.3.2 Determination of Salt Removal Rate (SRR)

Analysis of the data presented in Figure 26 was performed to calculate the slope of the lower portion of the outlet conductivity (AT1) curve. AT1 was chosen over the tank conductivity sensor AT2 due to limitations in the accuracy of this sensor, due to inadequate mixing during operation. By comparing the slope of the curve produced by the Stella simulation and the actual slope based on experimental data, the offset error between the two can be used to measure the accuracy of the salt adsorption parameter (SRR). Thus, the best SRR that fits the experimental data can be found by minimising the offset error.

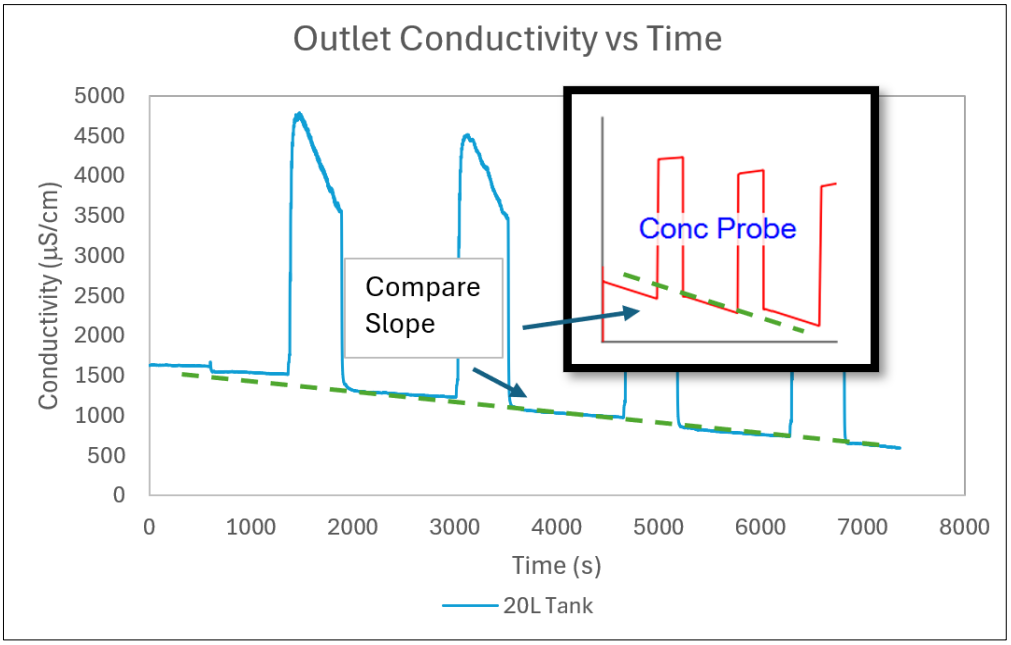

Figure 27 Comparison of outlet conductivity decay slopes during CDI cycles with theoretical concentration probe response.

Figure 27 illustrates the conductivity decay at the outlet of the CDI system during the adsorption phase, with a superimposed theoretical response profile used to validate the accuracy of the sample-and-hold system. The slope of the conductivity curve is calculated by selecting two linear points during the adsorption period, typically from the onset of conductivity decline to the point where it approaches a steady minimum. The slope is determined using the equation $Slope = \frac{\Delta y}{\Delta x}$, where Δy

represents the change in conductivity in microsiemens per centimetre and Δx the time interval in seconds.

With the slope S obtained by simple rise over run, the offset error is defined by Equation (15) as:

$$\mathrm{abs}(S_{\mathrm{model,V}} - S_{\mathrm{actual,V}}) \tag{15}$$

where S_{model} is the slope from Stella, and S_{actual} is from the analysis of experimental data. The subscript V denotes the volume of the tank. If the correct SAR is programmed into the Stella model, the offset error will be zero for all three tank volumes calculated independently. To obtain an offset error that encompasses all three tank simulations, the Sum of Error is defined as a cumulative measure of the deviation between simulated and actual slopes. This is expressed in the Equation (16) as:

$$\text{Sum of Error} = \sum_{V=1}^{3} \mathrm{abs}(S_{\mathrm{model,V}} - S_{\mathrm{actual,V}}) \tag{16}$$

where index values V or 1, 2 and 3 refer to values for 10L, 15L and 20L, respectively.

The Stella model was simulated for salt adsorption rates between 125 and 145 mg/min. These values were chosen as a range known to contain the best solution from trial and error. The values for these are presented in Table 2

Table 2 Conductivity decay slopes from Stella simulations and experiments for 10L, 15L, and 20L batches during CDI adsorption

	10L Batch	**15L Batch**	**20L Batch**
	Slope mS/cm per second	Slope mS/cm per second	Slope mS/cm per second
Stella 125 mg/min	-0.1336	-0.0952	-0.0741
Stella 135 mg/min	-0.1447	-0.1044	-0.0814
Stella 140 mg/min	-0.1507	-0.1090	-0.0851
Stella 145 mg/min	-0.1568	-0.1136	-0.0888
From Experiment	-0.1559	-0.1075	-0.0695

For the slope values presented, the Sum of Errors was calculated, and these values are presented in Table 3. Here we can see that the lowest value of the Sum of Error is for an SAR of 140 mg/min is a value of 0.0223.

Table 3 Offset errors between experimental and Stella-simulated conductivity slopes for 10L, 15L, and 20L batches, identifying 140 mg/min as the best-fit nitrate removal rate with the lowest cumulative error.

	10L Batch	**15L Batch**	**20L Batch**	
	Offset Errors	Offset Errors	Offset Errors	Sum of Error
Stella 125 mg/min	0.0223	0.0122	0.00462	0.0392
Stella 135 mg/min	0.0111	0.00307	0.0118	0.0261
Stella 140 mg/min	**0.00527**	**0.00153**	**0.0155**	**0.0223**
Stella 145 mg/min	0.000866	0.00614	0.0193	0.0263

Using the optimum calculated SAR of 140 mg/min, the Stella simulated concentration profile is compared with the actual in Figure 28. Here we can see close correspondence between the two figures with near identical slopes in the lower section of the curve. This indicates that the SAR value used in the simulation results in an overall reduction of NaCl in the system matching what was observed experimentally.

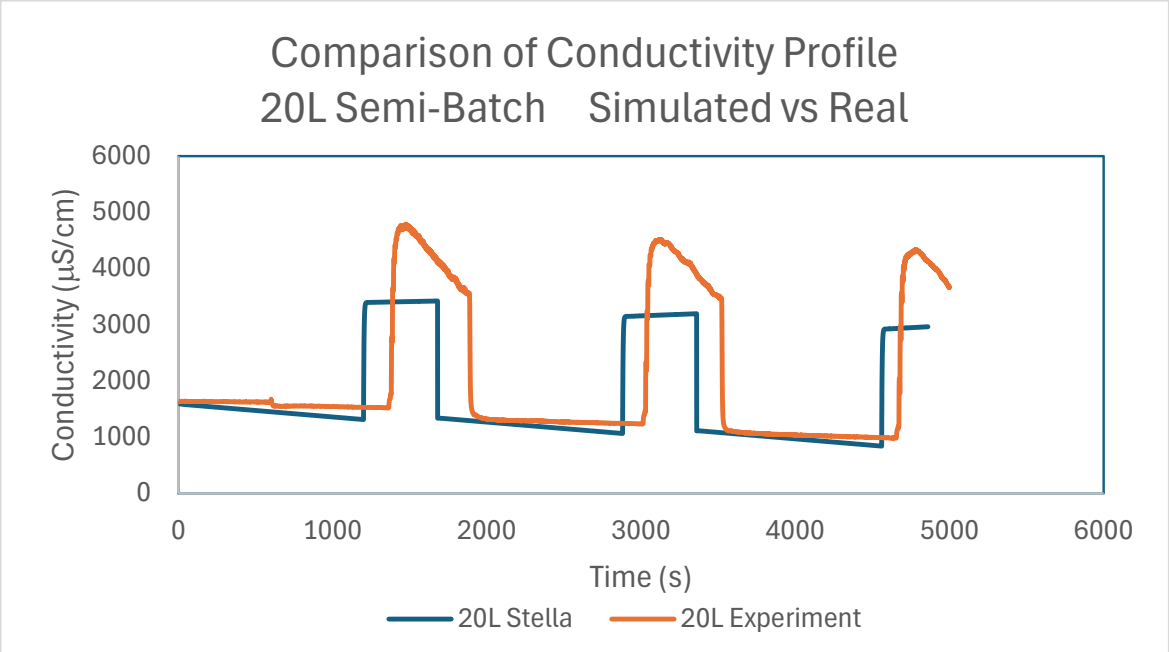

Figure 28 Comparison of simulated and experimental conductivity profiles for the 20L semi-batch CDI system, highlighting differences in peak height and adsorption dynamics between the Stella model and real experimental data

The technique used to calculate SAR is based on determining the slope of conductivity versus time within the linear portion of the adsorption curve. This is the period where conductivity decreases consistently due to ion removal and where the electrode surfaces are not yet saturated. The accuracy of this technique relies on several assumptions: uniform mixing in the tank, stable operating

conditions, and high-resolution conductivity data. In practice, when experimental conditions are well controlled, the SAR calculation yields consistent and reproducible results that closely align with modelled values, especially when using standardised volumes and flow rates.

However, a clear discrepancy was observed between the Stella model predictions and the experimental data. While Stella produced smooth, idealised curves with predictable cyclic behaviour, the real system exhibited more variable conductivity profiles. Notably, desorption phases exhibited sharper changes, and adsorption phases occasionally slowed unexpectedly. These differences are largely attributed to real-world factors such as ion transport limitations, electrode saturation dynamics, incomplete regeneration, and the presence of non-ideal flow conditions. Stella, although effective in capturing the general trends, simplifies or omits such physical and operational complexities.

An important limitation of the SAR approach is that it only applies to the linear portion of the conductivity curve. Over longer operational periods, the system tends toward a pseudo-steady state, where the conductivity does not fall to zero but instead stabilises due to the balance between incoming salt through top-ups and salt removal via CDI. This behaviour means that SAR cannot be extrapolated across the entire cycle. A similar limitation applies to nitrate removal: the nitrate removal rate (NRR) can only be accurately determined from the initial slope of nitrate concentration over time, often based on the first two measured values. This ensures that the calculation reflects the true removal rate prior to the onset of saturation or equilibrium.

Several sources of error can influence the SAR calculation. Experimental errors include fluctuations in flow rate due to pump variability, sensor drift or noise in the conductivity probe, and temperature fluctuations that affect conductivity measurements. Additionally, any inconsistency in the mixing of the solution in the batch tank or incomplete electrode regeneration during desorption can introduce error into the calculated SAR. In the Stella model, simplifications such as fixed kinetics and the exclusion of dispersion effects can also contribute to minor inaccuracies when compared to real system performance.

From a material balance perspective, the Stella model ensures that the amount of salt removed from the water phase matches the amount adsorbed on the electrodes, thereby satisfying mass conservation. In experimental systems, mass balance was generally observed when cycles were tightly controlled, and electrode saturation was avoided. However, minor imbalances were occasionally noted, especially over long-term operation. These could result from irreversible ion trapping within the

electrode matrix or the presence of additional ionic species not accounted for in the simplified model. Nonetheless, these discrepancies were small and did not undermine the overall validity of the approach.

In conclusion, the SAR technique, when properly applied within its limits, offers a reliable and accurate means of quantifying ion removal performance in CDI systems. Although it does not capture the full complexity of long-term operation, it is fit for purpose in assessing short-cycle performance, comparing operational conditions, and supporting Stella-based modelling. The strong correlation between initial model predictions and experimental results affirms the utility of this approach in both laboratory evaluation and design development of scalable nitrate and salt removal systems.

3.4.3.3 Determination of Nitrate Removal Rate (NRR)

The nitrate removal rate (NRR) was determined using a trial-and-error approach based on Stella simulations at different batch volumes. The model was simulated for a range of removal rates between 5 and 20 milligrams per minute. For each candidate rate, Stella was used to generate slope predictions of conductivity decline during the adsorption phase. These predictions were then compared against experimental results from three separate experiments conducted at batch volumes of 10 litres, 15 litres, and 20 litres. The objective was to identify the NRR that consistently matched observed system behaviour across all volumes.

The slope of conductivity decline, expressed in microsiemens per centimetre per second, was calculated from the early linear portion of the adsorption curve in both simulation and experiment. This linear region was selected because it reflects the period of most predictable ion removal, prior to the influence of saturation or equilibrium effects. The modelled and experimental slopes are presented in Table 4.

Table 4 Slope of conductivity decline for different nitrate removal rates from Stella simulations and experimental data across 10 L, 15 L, and 20 L batch volumes.

	10L Batch	**15L Batch**	**20L Batch**
	Slope mS/cm per second	Slope mS/cm per second	Slope mS/cm per second
Stella 5 mg/min	-0.4929	-0.332	-0.25
Stella 8 mg/min	-0.782	-0.526	-0.396
Stella 10 mg/min	-0.961	-0.656	-0.494
Stella 12 mg/min	-1.052	-0.784	-0.59133
Stella 14 mg/min	-1.097	-0.872	-0.688
Stella 16 mg/min	-1.1224	-0.9205	-0.756
Stella 18 mg/min	-1.138	-0.95	-0.7966
Stella 20 mg/min	-1.1467	-0.967	-0.8213
From Experiment	-1.1486	-0.7633	-0.7366

To quantify the accuracy of each simulated removal rate, the absolute offset between the experimental and simulated slopes was calculated for each volume using Equation ((15). The total deviation across the three volumes was then summed using Equation ((16). The resulting offset errors for each rate are provided in Table 5.

Table 5 Offset errors between experimental and Stella-simulated conductivity slopes for 10 L, 15 L, and 20 L batch volumes, identifying 16 mg/min as the nitrate removal rate with the lowest cumulative error

	10L Batch	**15L Batch**	**20L Batch**	
	Offset Errors	Offset Errors	Offset Errors	Sum of Error
Stella 5 mg/min	0.655	0.431	0.486	1.572
Stella 8 mg/min	0.366	0.237	0.34	0.943
Stella 10 mg/min	0.187	0.107	0.242	0.536
Stella 12 mg/min	0.0966	0.021	0.145	0.2626
Stella 14 mg/min	0.0516	0.108	0.0486	0.2082
Stella 16 mg/min	**0.0262**	**0.157**	**0.01933**	**0.20253**
Stella 18 mg/min	0.0106	0.186	0.06	0.2566
Stella 20 mg/min	0.0019	0.204	0.08466	0.29056

From these values, it was observed that a removal rate of 16 milligrams per minute yielded the lowest total offset across the three volumes. While other rates demonstrated strong alignment for individual volumes, only 16 mg/min consistently produced minimal error across all cases. This indicates that it is the most robust and volume-independent estimate for the nitrate removal rate in the system.

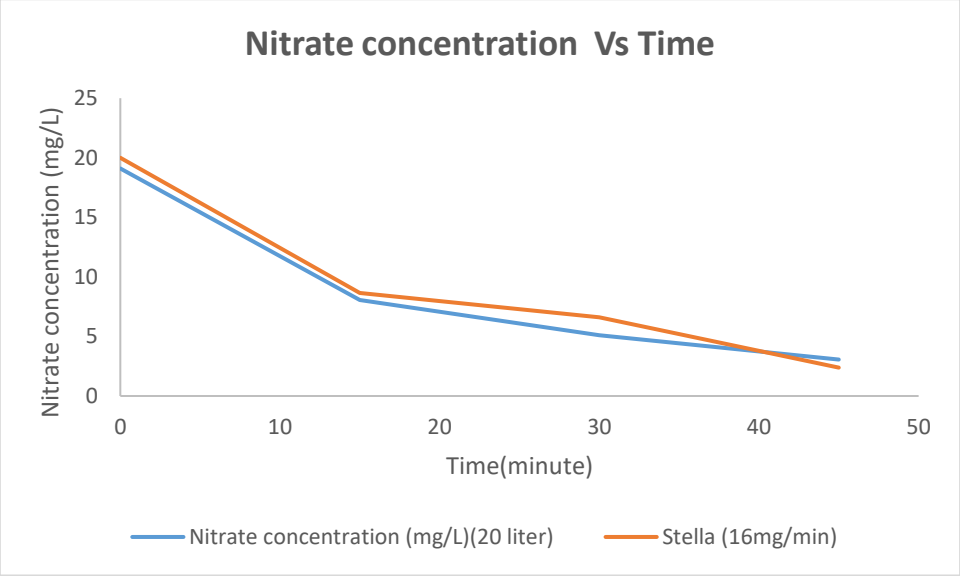

Figure 29 Comparison of experimental and Stella simulated nitrate concentration profiles for a 20 L batch, showing close agreement at a nitrate removal rate of 16 milligrams per minute during the adsorption phase.

This selection is further supported by the comparison presented in Figure 29, which shows the nitrate concentration profiles from both simulation and experiment. The Stella curve at 16 mg/min closely tracks the experimental data in the early adsorption phase, particularly in terms of slope. This confirms that the removal rate selected through simulation aligns well with the system's physical response.

Although the selection method is effective, it has certain limitations. The assumption of constant removal rate throughout the simulation does not capture the gradual decline in performance that may occur as electrodes become saturated. Additionally, the slope-based comparison is limited to the linear portion of the process and does not reflect behaviour near equilibrium. Experimental uncertainties, such as minor fluctuations in flow rate, probe sensitivity, or mixing, may also introduce minor errors in slope measurement.

Despite these limitations, the nitrate removal rate of 16 milligrams per minute is considered accurate and fit for modelling purposes. The value was identified through a structured simulation process using Stella and validated against experimental results collected from three independent batch volumes. Its consistent performance across multiple conditions supports its use in subsequent model-based analyses and system optimisation studies.

3.4.3.4 Nitrate Reduction in Different Volumes

The reduction of nitrate concentration (mg/L) over time in a capacitive deionisation (CDI) system reflects the interplay between the system's fixed ion removal rate and the total mass of ions present in different batch volumes. While initial experiments with 10 L, 15 L, and 20 L solutions showed varied times to reach near-zero nitrate concentrations, this variation is not due to differences in removal efficiency or kinetics between volumes. Rather, it arises from a straightforward mass balance consideration.

In each case, the nitrate removal rate (NRR) remains effectively constant, governed by the CDI unit's fixed operational parameters such as voltage, flow rate, and adsorption capacity. For example, if the CDI system removes nitrate at a rate of 10 mg/min, this removal rate is applied uniformly regardless of whether the system is treating 10 L or 20 L. However, a 20 L batch inherently contains twice the mass of nitrate as a 10 L batch at the same initial concentration. Consequently, achieving the same final concentration will require approximately double the time, assuming consistent removal conditions.

This observation mirrors findings in NaCl removal studies, where the salt removal rate (SRR) remains constant across varying batch volumes, with the time to reach target conductivity levels extending proportionally with volume. In the case of nitrate, the same principle holds. As illustrated in Figure 30, although the 10 L solution reaches near-zero concentration within approximately 30 minutes, this is not due to accelerated removal. It simply reflects that the total mass of nitrate present was smaller, enabling the fixed removal rate to reduce concentration more quickly.

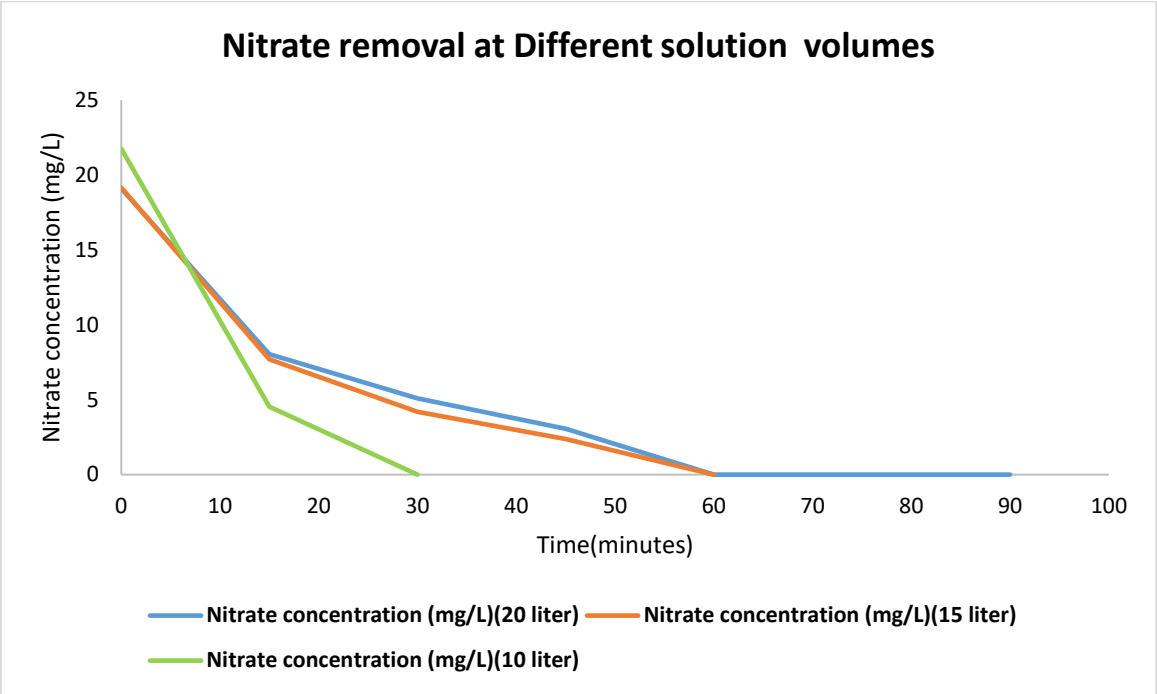

Figure 30 Nitrate concentration over time for 10 L, 15 L, and 20 L batches, measured from the storage tank and analysed in the lab.

Importantly, this reinforces that the CDI unit's performance metrics, including NRR, are independent of batch size. The apparent steep initial decline in nitrate concentration observed across all volumes during the first 10–20 minutes can be attributed to the high concentration gradient between the solution and the adsorbing electrode surfaces, which promotes rapid ion transport during the early stages of the process. As equilibrium is approached, the rate naturally declines due to reduced driving force, not due to limitations imposed by solution volume.

3.5 Implications for Continuous Sampling System Design

The Stella simulations provided essential quantitative insights necessary for designing a continuous sampling system capable of accurately monitoring nitrate concentrations during capacitive deionisation (CDI) operation. The expected adsorption-desorption cycle time was determined to be approximately 30 minutes per complete cycle, consisting of roughly 20 minutes of nitrate adsorption followed by 10 minutes of desorption. During the adsorption phase, the nitrate concentration at the CDI outlet was predicted to decrease to between 8 and 10 mg/L, while during the desorption phase, peaks of 30 to 35 mg/L were observed. Experimentally validated outlet flow rates stabilised at approximately 0.8 mL/min throughout both phases.

To achieve reliable real-time monitoring, the sampling system must respond to rapid concentration changes with a time resolution of better than 2 minutes. This equates to collecting a new sample approximately every 120 seconds. Given the system's diluted flow rate of approximately 0.8 mL/min, the total sample volume produced over a typical 30-minute cycle can be estimated using Equation (17) :

$$\text{Total sample volume per cycle} = 0.8\ \text{mL/min} \times 30\ \text{min} = 24\ \text{mL} \quad (17)$$

This relatively small waste volume can be easily managed using standard laboratory practices, but it must still be included in the planning for reagent preparation and waste disposal to ensure system sustainability over extended monitoring periods.

Due to the possibility of peak nitrate concentrations reaching up to 20 mg/L during desorption, inline dilution is critical to maintain compatibility with the vanadium chloride-based UV-Vis detection system, which is optimised for a range of 0–5 mg/L. A dilution ratio of approximately 1:4 was achieved by mixing roughly 0.2 mL/min of the CDI outlet stream with 0.6 mL/min of Milli-Q water, resulting in a diluted flow of approximately 0.8 mL/min. Following dilution, the maximum nitrate concentration entering the detector was approximately 5 mg/L, comfortably within the calibrated detection window (Equation (18)).

$$\text{Diluted nitrate concentration} = \left(20\frac{\text{mg}}{\text{L}} \times 0.2\frac{\text{mL}}{\text{min}}\right) \div 0.8\frac{\text{mL}}{\text{min}} = 5\ \text{mg/L} \quad (18)$$

Ensuring minimal dispersion within the tubing and connection lines was also identified as a critical design factor. Analysis of the residence time distribution (RTD) showed that the system's dispersion number (D/UL) must be maintained below 0.05 to detect changes in nitrate concentration during adsorption and desorption. This ensures that the concentration readings reflect the actual changes occurring in the CDI unit without being distorted or delayed by mixing effects in the tubing. To achieve this, narrow tubing (internal diameter less than 2 mm) and a consistent flow rate of about 0.8 mL/min were used. These parameters promote uniform flow behaviour that closely approximates ideal plug flow conditions, thereby minimising mixing and enhancing both the accuracy and temporal resolution of nitrate detection.

Overall, the results from the Stella simulations provide a quantitative framework to guide the engineering of a continuous sampling system capable of real-time, high-precision monitoring. The system must sample at two minutes or faster intervals, manage approximately 24 mL of waste per cycle, dilute the outlet stream to fit within a 0–5 mg/L nitrate detection range, and minimise dispersion to preserve measurement fidelity. These design parameters form the operational foundation for the subsequent development of the vanadium chloride-based flow cell system, enabling the rapid and reliable nitrate detection strategies discussed in the following chapters.

3.6 Summary of Key Learnings and Relevance to Vanadium Chloride Flow Cell Development

This chapter systematically develops the foundational requirements for a nitrate detection system tailored for CDI processes. Using Stella software as a dynamic modelling platform, we established material balance models that predicted nitrate's cyclic adsorption and desorption behaviour in CDI systems. The simulation results provided quantitative insights into expected nitrate concentration profiles, flow rates, and the dynamic variations that a real sampling system would encounter during CDI operation. Critical parameters such as adsorption-desorption cycle times, nitrate concentration ranges, and conductivity fluctuations were identified, providing benchmarks for the design and calibration of an online detection system.

The flow characterisation studies, particularly the residence time distribution (RTD) and dispersion analyses, further revealed that non-idealities such as axial dispersion would influence sample delivery to the detection unit. Understanding the dispersion number (D/UL) and normalised variance (σ^2/τ^2) allowed us to set thresholds for acceptable system performance, ensuring that detection responses would faithfully represent real-time changes at the outlet of the CDI unit. These findings directly informed the design specifications for the Vanadium Chloride flow cell system, guiding decisions on tubing dimensions, sample residence times, flow rates, and detection frequency. Moreover, estimates of waste generation and required sampling resolution were obtained, allowing efficient system integration without excessive reagent or sample wastage. Altogether, the insights derived from the Stella modelling, tracer analysis, and experimental validation form the theoretical and practical foundation necessary for the successful development of a continuous vanadium chloride-based nitrate detection system suitable for integration with capacitive deionisation technology.

3.7 Conclusion

This chapter details developing and applying a dynamic simulation model using Stella software to characterise nitrate removal behaviour in a semi-batch capacitive deionisation (CDI) system. Beginning with fundamental representations of flow, accumulation, and reaction within a process framework, Stella enabled accurate visualisation of water and ion dynamics using core modelling blocks such as stocks, flows, and converters. The semi-batch CDI process was simulated with sodium chloride to establish baseline adsorption-desorption performance, followed by integrating a nitrate-specific removal loop. Experimental data from lab-scale CDI trials were used to fit parameters, particularly the nitrate removal rate, and validate the model's predictive accuracy under various batch volumes. Results confirmed that Stella could simulate transient and cyclic ion behaviour, offering key insights into CDI performance and enabling system configuration optimisation.

Beyond simulation, the findings from this chapter have direct implications for real-time nitrate monitoring. The validated Stella model provides a foundation for designing and implementing a responsive detection system capable of capturing the dynamic nature of CDI operations. Specifically, understanding system kinetics and flow interactions supports developing a Vanadium Chloride-based flow cell system for continuous nitrate detection. The next chapter builds upon these findings by focusing on the experimental validation of the vanadium chloride method and the construction of a flow cell detection platform. This transition marks a critical step in moving from simulated to physical systems, ensuring that theoretical understanding is effectively translated into a reliable, real-world solution.

4 DEVELOPMENT AND VALIDATION OF VANADIUM CHLORIDE-BASED FLOW CELL SYSTEM FOR RAPID NITRATE DETECTION

4.1 Introduction

Following the simulation and modelling framework established in the previous chapter, this chapter transitions from theoretical design to experimental validation of a chemical detection method tailored for real-time nitrate monitoring. While the Stella-based semi-batch CDI model provided insights into dynamic nitrate removal behaviour, its practical utility depends on a rapid, accurate, and robust detection system capable of capturing transient concentration changes. To meet this need, the present chapter introduces a vanadium(III) chloride-based method for nitrate reduction, enabling subsequent spectrophotometric quantification through the Griess reaction. This method reduces nitrate to nitrite, which then forms a pink-coloured azo dye whose absorbance is measured at 540 nm. The resulting approach offers high reduction efficiency and analytical stability, providing a critical foundation for integrating chemical detection with capacitive deionisation (CDI) processes.

The method presented here, based on nitrate reduction via a vanadium reducing agent, has relatively fast reaction kinetics compared to commercially available alternatives such as Palintest. This observation aligns with previous reports indicating that vanadium-based reduction can achieve rapid and consistent colour development, with superior stability and safety when compared to cadmium-based kits. (Pai et al., 2021). The chapter outlines reagent preparation, sample-reagent ratio optimisation, and the construction of calibration curves under varying thermal conditions to support online detection. Furthermore, the Arrhenius equation is applied to assess activation energy, justifying the shift to higher operational temperatures for accelerated reaction rates. These findings collectively form the experimental basis for the flow cell design explored in the subsequent chapter, where continuous nitrate detection is implemented and validated.

4.2 Principles of Vanadium Chloride Reduction

The Vanadium Chloride (VCl_3) Reduction Method is an effective and safer technique for detecting nitrate in water samples. In this method, vanadium in the +3-oxidation state serves as a strong reducing agent. When introduced into an acidic environment, it reacts with nitrate ions (NO_3^-) and reduces them to nitrite ions (NO_2^-) (Equation (5)). This step is essential because the resulting nitrite

can be accurately measured using the Griess reaction, which forms a pink-coloured compound known as an azo dye.

The formation of this coloured dye involves two stages. First, nitrite reacts with sulfanilamide to form a diazonium salt. Then, this salt reacts with N-(1-naphthyl) ethylenediamine (NED) to produce the pink azo dye (Equation (6)). The intensity of this colour is directly related to the nitrite concentration, which reflects the original nitrate level in the sample. This is quantified by measuring the absorbance at a wavelength of 540 nanometres using a spectrophotometer (Schnetger et al., 2014).

Compared to traditional cadmium and zinc reduction methods, vanadium chloride offers several advantages. Cadmium is toxic and poses environmental hazards, while zinc is prone to inconsistent reactions due to interference from sample matrices and slower kinetics. In contrast, the vanadium chloride method is more reliable, faster, and better suited for automation and continuous monitoring systems.

For optimal results, the reaction requires careful control of conditions such as temperature, acidity, and reagent concentration. Typical operating temperatures range from 50 to 90 degrees Celsius, ensuring rapid and complete nitrate reduction. This method is particularly suitable for both laboratory analysis and field-based water quality monitoring.

The principles of vanadium chloride reduction lay a strong foundation for accurate and rapid spectrophotometric nitrate detection. In this study, these principles were applied to develop a reliable lab-scale method and to design a continuous flow system for online monitoring. A custom 3D-printed flow cell was engineered to integrate with a UV-Vis spectrophotometer, allowing the nitrate-reduced solution to pass vertically from top to bottom, ensuring steady absorbance measurements at 540 nm. This configuration supports real-time analysis by maintaining a consistent optical path length and minimising bubble interference. Most importantly, this setup was specifically designed to detect nitrate concentrations from the outlet stream of a CDI unit. Integrating the vanadium chloride method with flow cell technology enables the system to handle continuous samples from the CDI during its adsorption and desorption cycles. This is critical because the CDI process alters nitrate concentrations dynamically, requiring a detection method that is both responsive and stable under flow conditions. By bridging chemical reduction kinetics with real-time flow-based detection, this section forms the conceptual and practical basis for the later experimental validation of nitrate quantification from CDI systems.

4.3 Methodology

This section outlines the experimental procedure developed for the spectrophotometric detection of nitrate using vanadium chloride, with particular emphasis on reagent preparation, calibration standard development, and the optimised protocol for batch measurements. The approach was designed to support both laboratory-scale experimentation and online detection within a capacitive deionisation (CDI) system.

4.3.1 Reagent Preparation

The reagents used in this procedure included vanadium (III) chloride (VCl_3), sulfanilamide, and N-(1-naphthyl) ethylenediamine dihydrochloride (NEDD), which together formed the Griess reagent essential for nitrate quantification. The vanadium (III) chloride solution was prepared by dissolving 0.8 g of VCl_3 in approximately 20 mL of Milli-Q water, followed by the slow addition of 8.4 mL of concentrated hydrochloric acid (18 M HCl) under continuous stirring. The solution was then made up to a final volume of 100 mL using Milli-Q water. The resulting particle-free, deep blue solution was designated as Stock Solution A. A 2% (w/v) sulfanilamide solution (Stock Solution B) was prepared by dissolving 2.0 g of sulfanilamide in 100 mL of 10% (v/v) hydrochloric acid. Stock Solution C was prepared by dissolving 0.1 g of NEDD in 100 mL of Milli-Q water, yielding a 0.2% (w/v) solution (Schnetger et al., 2014).

The working Griess reagent was freshly prepared before each analysis by mixing five parts of the VCl_3 solution, one part of the sulfanilamide solution, and one part of the NEDD solution in a 5:1:1 volumetric ratio (Schnetger et al., 2014). This combined reagent formed an azo dye and served as both the reducing agent and the colorimetric detection medium for nitrate.

For the preparation of standard nitrate solutions compatible with the capacitive deionisation (CDI) system, a 20 mg/L nitrate stock solution was first prepared. This was achieved by accurately weighing 54.84 mg of sodium nitrate ($NaNO_3$), calculated based on its molar mass (85 g/mol), to yield a solution containing 62 mg/L of NO_3^-. The $NaNO_3$ was dissolved with 2.0 g of sodium chloride (NaCl) in approximately 1.5 litres of Milli-Q water in a clean 2 L volumetric flask. After complete dissolution, the solution was made up to the 2 L mark and thoroughly mixed. From this stock, standard solutions with nitrate concentrations of 5.0 mg/L, 3.5 mg/L, 1.6 mg/L, 1.0 mg/L, and 0.5 mg/L, corresponding to approximately 10 to 100 µM were prepared by serial dilution with Milli-Q water.

All solutions were clearly labelled with concentration and preparation date, and stored in clean, capped containers. To maintain analytical accuracy, solutions were freshly prepared or kept in a cool, dark environment, and all glassware used was cleaned and rinsed thoroughly with Milli-Q water.

4.3.1.1 Equipment Required.

- **UV-Vis Spectrophotometer**: Capable of measurements at 540 nm for absorbance analysis,
- **Water Bath**: Provided precise temperature control within the range of 45°C to 90°C (± 0.5°C) to ensure consistent reaction conditions,
- **Borosilicate Glass Test Tubes** (10 mL) used as reaction vessels for mixing and incubating samples,
- **Adjustable Micropipettes** (10–1000 µL) Equipped with low-retention tips to ensure accurate and precise liquid handling,
- **Quartz Cuvettes**: With a 1 cm path length, used to obtain reliable spectrophotometric measurements.

4.3.2 Optimisation and Sample-Reagent Ratio Selection

The method was optimised based on published experimental results to determine the ideal sample-to-reagent volume ratio for accurate detection. According to Schnetger (2014), various combinations of sample (S) and reagent (C) volumes were tested under standardised reaction conditions (45°C, 60 minutes). As shown in the Figure 31, the combination of 0.18 mL *S* and 0.15 mL *C* exhibited the best linear correlation between absorbance and nitrate concentration (R^2 = 0.99961) (Schnetger et al., 2014). This balance of high sensitivity and linearity made it the preferred option.

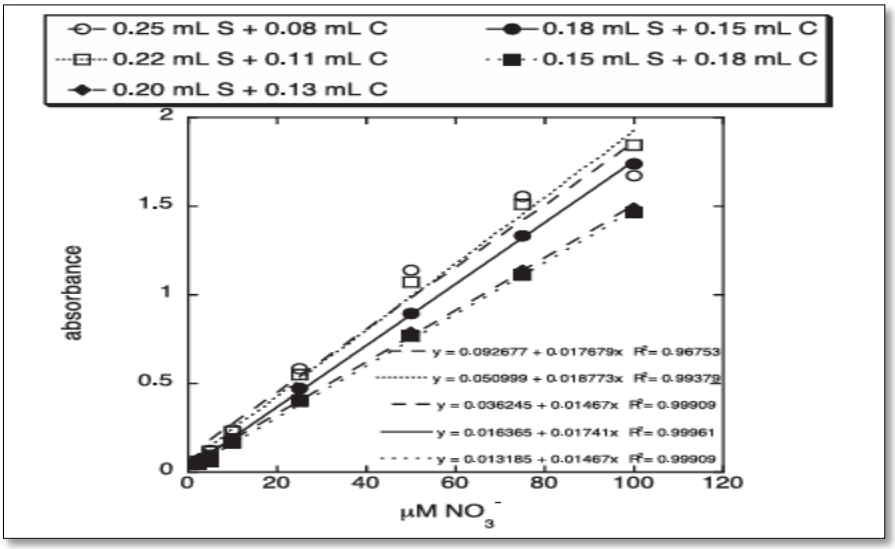

Figure 31 Absorbance vs Nitrate concentrations for various sample-to-reagent ratios with a given incubation temperature (45°C) and reaction period (60min). The optimal balance of linearity and sensitivity is attained with a 0.18mL sample (S) and 0.15mL reagent solution (C).(Schnetger et al., 2014)

To meet the 1 mL volume requirement of the spectrophotometric cuvette, the original ratio was proportionally scaled. Accordingly, 0.54 mL of nitrate sample was mixed with 0.45 mL of freshly prepared NOx reagent (a combination of Griess reagent and reduction reagent).

4.3.3 Procedure

This study aimed to identify the most efficient reaction conditions for rapid nitrate detection using the vanadium chloride method. Each experiment used a total volume of 0.99 mL, combining 0.54 mL of nitrate-containing sample with 0.45 mL of freshly prepared NOx reagent. This ratio was selected to ensure high analytical sensitivity while meeting the minimum volume requirements for UV-Vis spectrophotometric analysis. The reagent and sample were thoroughly mixed and transferred into a clean borosilicate test tube for controlled thermal treatment.

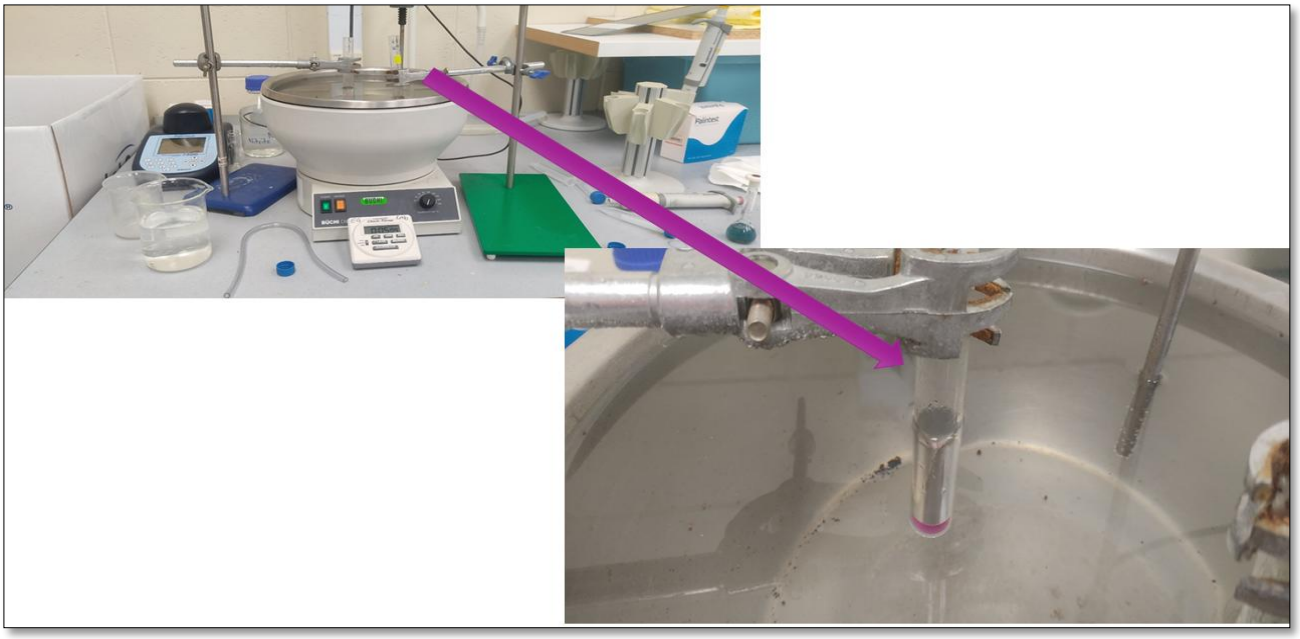

Figure 32 The primary stage of nitrate detection using vanadium chloride via a test tube-based laboratory method. The setup includes a heated water bath for reaction temperature control and a test tube containing the reagent and sample mixture for colorimetric analysis.

The test tube was vertically clamped in a temperature-regulated water bath (Figure 32) to maintain uniform heat distribution. Reaction conditions were systematically varied, with temperatures ranging from 45°C to 90°C and incubation times between 1 and 60 minutes, depending on the experimental objective. During this step, nitrate was reduced to nitrite, followed by the formation of a colored azo complex through the Griess reaction. After incubation, the test tube was removed and cooled to room temperature to stabilise the colour before analysis.

The final solution was pipetted into a 1 cm quartz cuvette for absorbance analysis at 540 nm using a calibrated UV-Vis spectrophotometer. Although the initial calibration curve (Figure 31) was performed at 45°C, the corresponding slow reaction kinetics and extended response time rendered this curve unsuitable for rapid online detection. Therefore, new calibration curves were developed at higher temperatures where the reaction kinetics are significantly accelerated to support faster detection and real-time monitoring applications.

4.4 Experiment Design

This methodology was developed to enhance the speed and reliability of nitrate detection using vanadium (III) chloride in a laboratory setting. The approach involved manual mixing of the sample

and reagent solutions in precise volumes to simulate real-time detection conditions. A fixed ratio of 0.54 mL of nitrate sample to 0.45 mL of freshly prepared NOx reagent was used to ensure reproducibility across different concentrations.

After mixing, the reaction mixture was subjected to thermal processing in a controlled water bath. Two temperature regimes were investigated to optimise the reaction kinetics and colour development. For detection at 65°C, a heating duration of 5 minutes followed by 5 minutes of ambient cooling was established as optimal. This allowed sufficient time for the reduction of nitrate to nitrite and subsequent formation of the coloured azo dye. At an elevated temperature of 85°C, the reaction proceeded more rapidly, allowing for a reduced heating duration of 1 minute, followed by 1 minute of cooling. These conditions were selected based on repeatability and stability of absorbance readings at 540 nm. The chosen protocols were designed to stabilise colour intensity before spectrophotometric analysis, supporting accurate quantification of nitrate concentrations under varied thermal conditions.

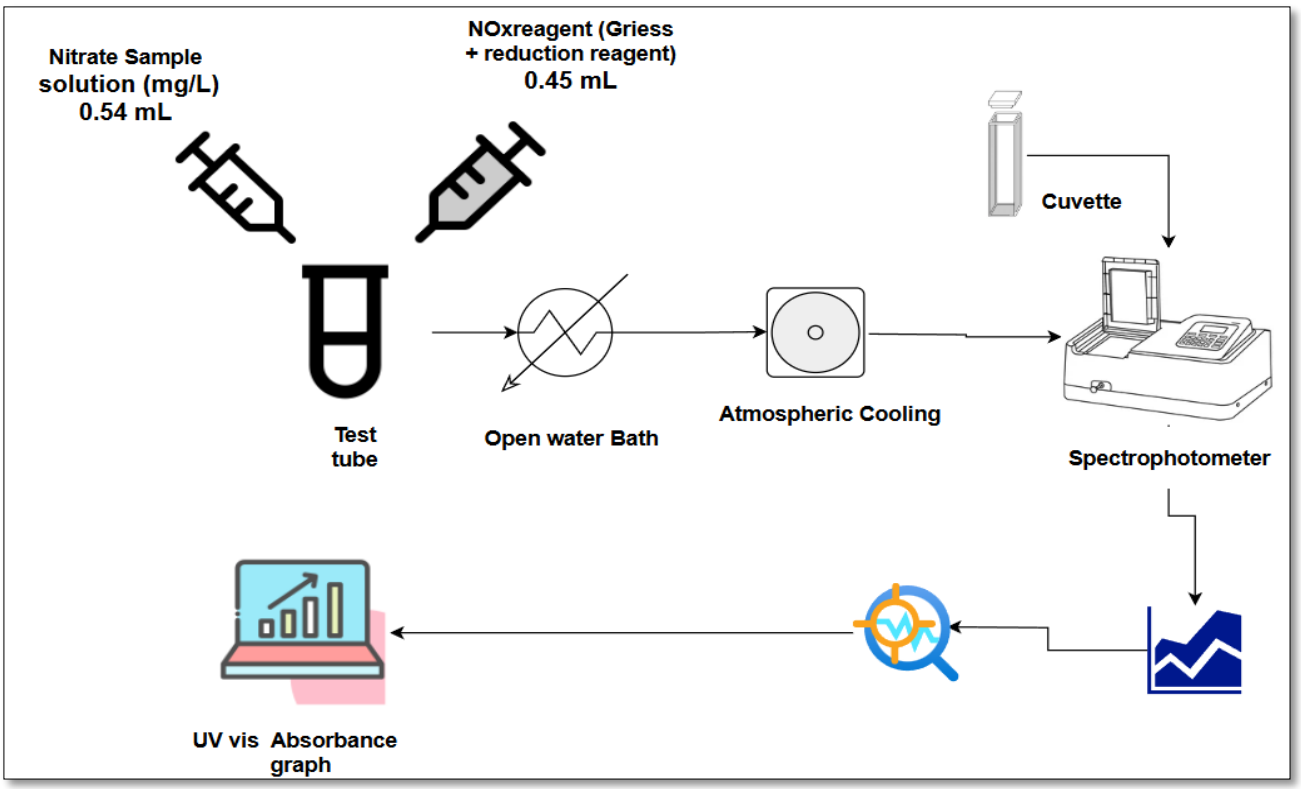

Figure 33 Workflow Diagram for the Analytical Procedure of Nitrate Detection Using UV-Vis Spectrophotometry

The absorbance of the pink azo dye produced during the Griess reaction was measured using a UV-Vis spectrophotometer at 540 nm. Figure 33 illustrates the workflow for the analytical procedure, from reagent mixing to data acquisition, highlighting the sample-to-reagent volume proportions and

data visualisation process. The spectrophotometer was calibrated using standard nitrate solutions ranging from 0.5 to 5 mg/L to ensure accuracy. All solutions were prepared from a 20 mg/L sodium nitrate stock and serially diluted with ultrapure water. Data was captured electronically and processed using compatible software to streamline analysis.

This methodology was designed with future automation in mind and serves as a protocol for integration into an online detection system.

4.5 Batch Calibration and Beer-Lambert Analysis

Beer-Lambert's Law was fundamental in interpreting the calibration data obtained during this study. This law, expressed in Equation (19),

$$A = \varepsilon \cdot l \cdot C \tag{19}$$

Where:

A is the absorbance,

ε is the molar absorptivity coefficient ($L \cdot mol^{-1} \cdot cm^{-1}$),

l is the optical path length (cm),

C is the concentration of the absorbing species ($mol \cdot L^{-1}$).

This relationship underpins spectrophotometric techniques by allowing concentration measurements to be derived from absorbance values, assuming constant path length and a uniform absorbing species.

To establish a strong analytical foundation for online nitrate detection, calibration curves were constructed at two operational temperatures: 65°C and 85°C. The aim was to assess whether the elevated temperature protocol could maintain or improve upon the linearity and sensitivity established under the slower, conventional method. In each trial, a fixed volume of nitrate solution was reacted with the vanadium chloride-based Griess reagent and incubated under controlled temperature conditions. Absorbance readings were recorded at 540 nm after sufficient reaction and cooling periods.

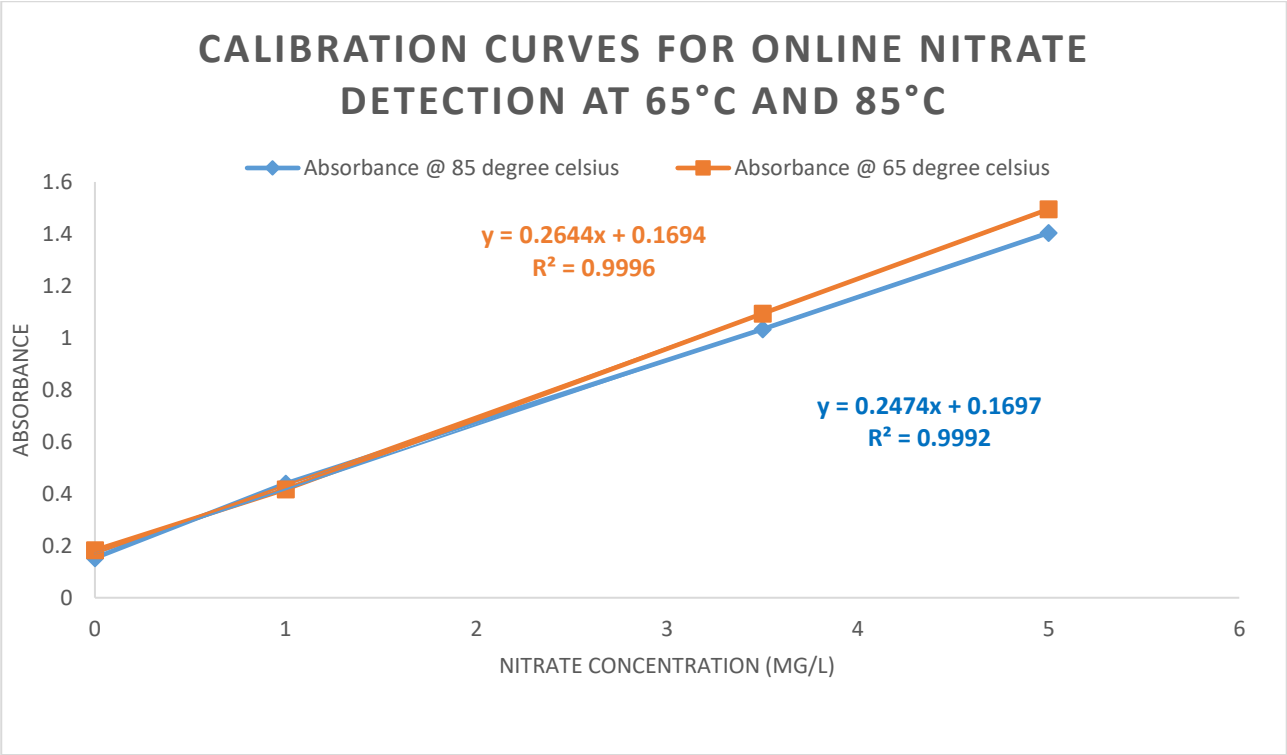

Figure 34 Comparison of calibration curves for nitrate detection at 65°C and 85°C, showing excellent linearity and suitability of the 85°C method for rapid online analysis.

Figure 34 shows the calibration results. The 65°C curve yielded the equation Y=0.2644X+0.1694, with an exceptional coefficient of determination R^2=0.9996. This slope reflects high molar absorptivity, confirming the strong colour development and reliable signal output across the 0–5 mg/L nitrate range. Comparatively, the 85°C calibration exhibited the equation Y=0.2474X+0.1697, with R^2=0.9992. Though the slope is slightly lower, the minimal intercept deviation and strong R^2 value indicate that the 85°C method preserves analytical robustness.

The slightly reduced slope at 85°C may be attributed to marginally faster reaction kinetics leading to a reduced window for complete chromophore development. However, the system's precision remained unaffected. This validation supports the transition to 85°C for online detection due to its balance of speed and analytical integrity. Hence, this section provides crucial justification for temperature selection in high-frequency nitrate monitoring systems.

4.6 Temperature Optimisation and Activation Energy Determination

To facilitate the transition from laboratory-based calibration to real-time detection, the nitrate reduction reaction was optimised for speed without compromising accuracy. A comparative study

was performed between two reaction conditions: 10 minutes at 65°C and 2 minutes at 85°C. The goal was to shorten reaction time while maintaining sensitivity, linearity, and colour stability. To quantitatively understand this enhancement, the Arrhenius equation was applied to calculate the activation energy (*Ea)* of the vanadium chloride reduction reaction. Using Equation (20) :

$$\ln \frac{t1}{t2} = \frac{E_a}{R}\left(\frac{1}{T_1} - \frac{1}{T_2}\right) \tag{20}$$

where:

t_1 and t_2 are the reaction times (in seconds) at two different absolute temperatures,

T_1 and T_2 are the corresponding temperatures in Kelvin,

Ea is the activation energy in joules per mole (J/mol), and

R is the universal gas constant, 8.314 J/mol.K.

Using the experimental conditions $t_1 = 600\ s$, $t_2 = 120$ s, $T_1 = 338\ K\ (65^oC)$, and $T_2 = 358\ K\ (85^oC)$, the calculated activation energy was approximately 80,957 J/mol or 81 kJ/mol. This high value confirmed the temperature-sensitive nature of the reaction, thus validating the strategic increase in temperature. Despite the increased rate, calibration curves at 85°C retained excellent linearity (R^2 = 0.9992). This indicated that accelerated detection was not only possible but preferable in continuous online monitoring systems. Additionally, the short reaction time reduced thermal stress on the system, minimised reagent degradation, and allowed rapid data acquisition, essential for dynamic environments such as CDI. By understanding the kinetics of the VCl_3 reaction, this section provided a scientifically grounded rationale for shifting from slow batch methods to fast, inline nitrate detection, supporting the broader goals of system integration and automation.

4.7 Evaluation of tube materials for effective heat transfer in Nitrate detection

In the process of online nitrate detection, selecting an appropriate tube material for heating the NOx reagent and nitrate sample mixture is crucial for ensuring efficient heat transfer and maintaining structural integrity at elevated temperatures. Various materials were tested in a water bath at 85°C to determine their ability to heat the liquid efficiently while retaining stability. This analysis was prompted by an observation that plastic (PVC) used in the round-bottom flask for the water bath

turned white at 85°C, indicating potential thermal degradation. To identify the most suitable material, different tube types, including glass, plastic, steel, Teflon, and LLDPE (Linear low-density polyethylene) were evaluated based on their internal temperature after heating and cooling.

Table 6 Evaluation of Tube Materials for Efficient Heat Transfer in Nitrate Detection at 85°C.

Material	Water bath Temperature (°C)	Time for heating and cooling	Temperature of reagent mixture (°C) (reagents before cooling)	Temperature of Mixture (°C) (reagents after cooling)
Glass tube	65	5 minutes	37.3	19.1
Glass tube	85	1 minute	52.8	26.3
Plastic tube	85	1 minute	33.3	23.5
Steel tube	85	1 minute	29.1	21.8
Teflon tube	85	1 minute	38.6	23.9
LLDPE tube	85	1 minute	40	25.9

Table 6 presents the results of the heating trials. Among all materials tested, glass tubes showed the highest internal liquid temperature (52.8°C after 1 minute in the 85°C water bath) and maintained a relatively higher temperature even after cooling for 1 minute (26.3°C). This suggests that glass has superior heat transfer properties, making it the most effective material for rapid and uniform heating of the reagent mixture. Teflon and LLDPE tubes demonstrated moderate performance, reaching 38.6°C and 40°C, respectively, but LLDPE softens at 80–90°C, making it unsuitable for continuous operation at 85°C. Plastic and steel tubes performed poorly, with internal liquid temperatures of 33.3°C and 29.1°C, respectively, indicating significant heat loss.

Operating above 85°C presents additional challenges due to material limitations and system stability. Many polymer-based tubes, including LLDPE and PVC, begin to soften or degrade near 90°C, risking leakage or rupture. Furthermore, maintaining precise thermal control becomes increasingly difficult as evaporation and steam formation accelerate beyond 85°C, especially in open or semi-open systems. Nevertheless, theoretical heating at higher temperatures could offer faster reaction kinetics. Based on a simple linear approximation from observed data, a reaction mixture that reaches 52.8°C after one minute at 85°C might reach approximately 56.4°C at 90°C and 60.1°C at 95°C, assuming similar heat transfer efficiencies. However, practical limitations such as equipment durability, increased vapour

pressure, and reagent stability constrain the operational temperature to 85°C for safe and reproducible nitrate detection.

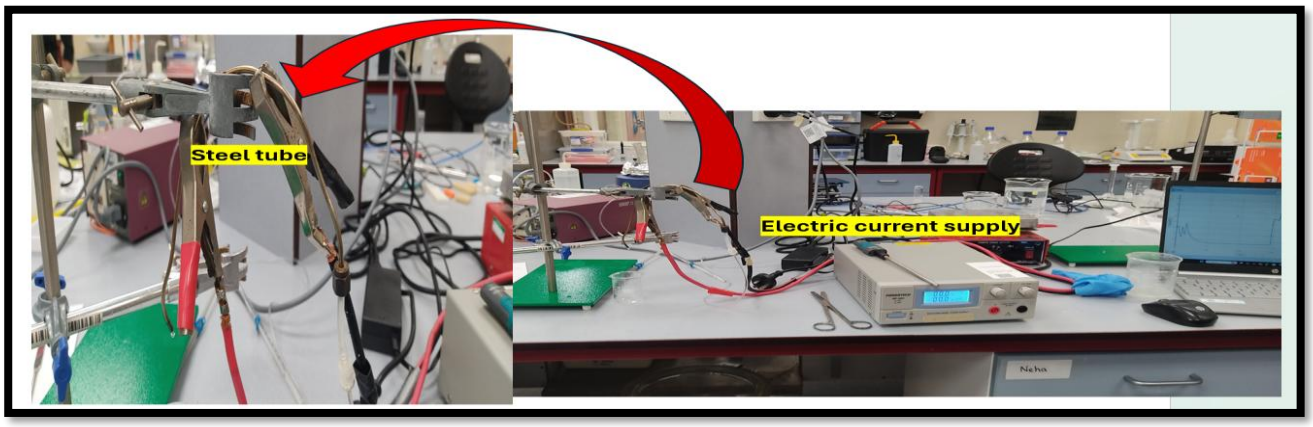

Figure 35 Experimental Setup for Testing Heat Transfer Using Electric Current in a Steel Tube for Nitrate Detection

To explore alternative heating methods, experiments were conducted where the mixture was passed through a steel tube while applying different voltages (as shown in Figure 35). Additionally, both copper and stainless-steel tubes were tested under various voltages (0V-2V) to determine whether direct electrical heating could provide efficient thermal control. However, this method proved ineffective in achieving stable and uniform heating. Instead, the applied potential (and currents approaching 30A) generated steam inside the tubing, leading to uncontrollable temperature variations that affected the reaction process. The inability to regulate temperature effectively resulted in inconsistent heating of the nitrate mixture, making this approach unsuitable for precise temperature control in the nitrate detection process.

Based on these findings, glass tubes remain the preferred choice due to their high thermal conductivity, stability at elevated temperatures, and effective heat retention. Teflon could be considered as an alternative if a non-glass material is required, but it is slightly less effective in heat transfer. LLDPE and PVC should be avoided due to their risk of deformation and degradation at high temperatures, which could compromise experimental accuracy and equipment longevity.

4.8 Summary

This chapter established the development and validation of a rapid nitrate detection system using the vanadium chloride reduction method. Careful optimisation of experimental parameters, including reaction temperature, sample-to-reagent ratio, and tubing material, resulted in significant

improvements in reaction speed, sensitivity, and reproducibility. It was confirmed that operating the system at an elevated temperature of 85°C enabled near-complete nitrate reduction within two minutes, making the method highly suitable for real-time detection. In addition, investigations into heat transfer efficiency and batch calibration analyses reinforced the robustness of the optimised detection protocol. Altogether, these findings created a strong experimental foundation for moving beyond batch experiments towards continuous monitoring applications.

The following chapter builds directly upon these results by implementing the optimised vanadium chloride detection method within a continuous flow-cell system. Chapter 5 will explore how fluid dynamic principles, including residence time distribution analysis and dispersion modelling, are incorporated to ensure stable and accurate real-time nitrate detection. The insights gained in this chapter, therefore, provide the necessary basis for developing an online nitrate detection platform suitable for integration with capacitive deionisation systems.

5 FLOW CELL IMPLEMENTATION OF VANADIUM CHLORIDE METHOD FOR CONTINUOUS MONITORING

Following the optimisation of the vanadium chloride-based nitrate detection method, the next stage involves implementing a continuous flow cell system for real-time monitoring. This chapter aims to examine the characteristics and limits of a flow cell system based on the reduction kinetics in the previous chapter. Ultimately, the target is to achieve a reactor design with a residence time of under two minutes while maintaining an adequate level of resolution in the measurement. An examination of the feasibility of a single tube plug flow reactor will be performed as a precursor to the final chapter, which presents a design that addresses the limitations of the continuous configuration.

A flow cell enables the controlled passage of liquid samples through a confined channel, facilitating rapid mixing, efficient heat transfer, and immediate spectrophotometric analysis. This transition bridges the gap between batch-mode experiments and continuous online monitoring, a necessary step for real-time nitrate detection in water treatment systems.

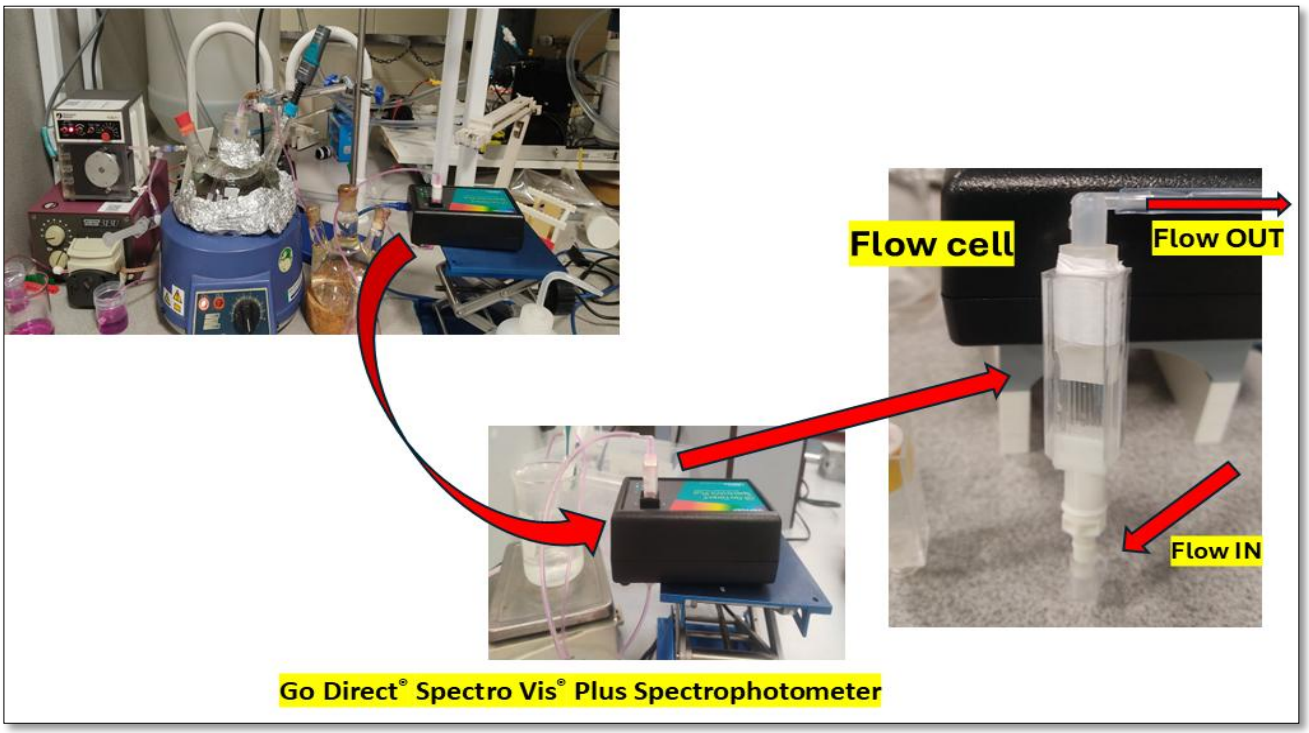

Figure 36 Flow cell used for continuous nitrate detection, shown integrated with the Go Direct® Spectro Vis® Plus spectrophotometer.

The flow cell used in this study was produced through 3D printing, based on modifications to a standard cuvette. A precision hole was drilled at the bottom of the cuvette, and customised flow connectors were printed to allow the smooth inflow and outflow of the sample, as illustrated in Figure 36. The flowing liquid within the cuvette is continuously monitored using the Go Direct® Spectro Vis® Plus Spectrophotometer, which enables absorbance measurements at the required wavelength for nitrate detection. The internal configuration of the spectrophotometer is based on a diffraction grating system coupled with a linear CCD array detector, enabling precise absorbance readings across multiple wavelengths, as shown schematically in Figure 37.

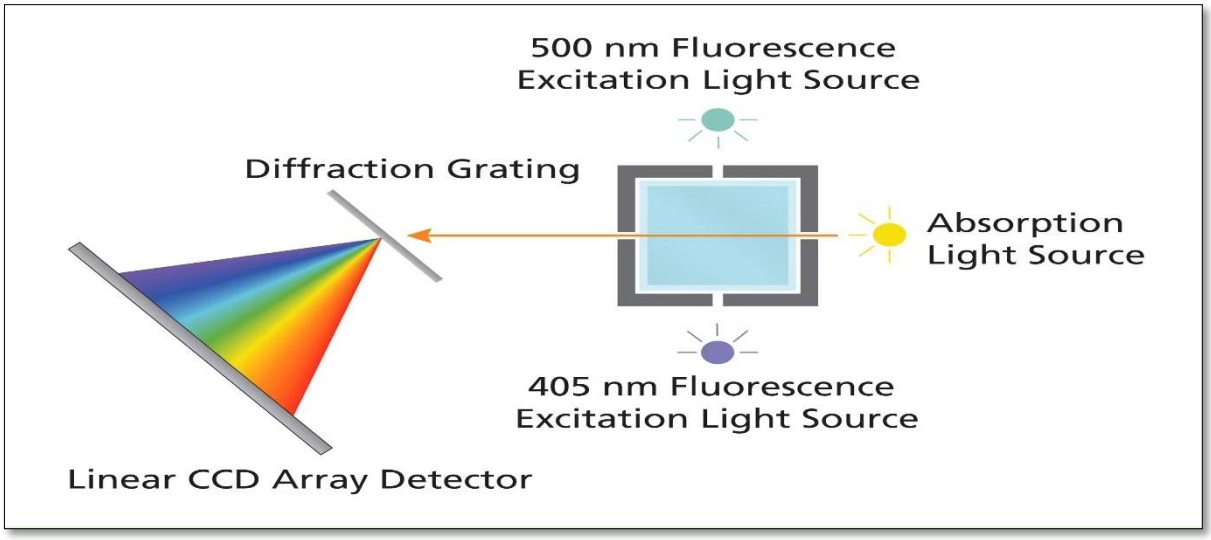

Figure 37 Schematic representation of the Go Direct® Spectro Vis® Plus Spectrophotometer showing diffraction grating and CCD array-based absorbance detection system (Vernier, 2021).

This chapter describes the design, methodology, and performance evaluation of the flow cell-based nitrate detection system, setting the stage for continuous, automated monitoring compatible with capacitive deionisation processes.

5.1 Theory of Flow Cell Design for Nitrate Measurement at 85°C

The design of a flow cell system for nitrate detection using vanadium chloride is based on the principles of chemical kinetics and fluid transport. At an elevated temperature of 85°C, the reduction of nitrate (NO_3^-) to nitrite (NO_2^-) becomes significantly faster, enabling rapid colorimetric detection using the Griess-based method. The purpose of the system is to ensure that the reaction proceeds to completion within the time that the solution flows through the heated zone. Therefore, residence time,

defined as the duration the fluid remains within the heated reactor, becomes the critical design parameter.

To achieve accurate and reliable nitrate measurements, the system was constructed with the aim of providing a residence time of approximately two minutes. The fluid path includes a one-metre-long tube that passes through a round-bottom flask maintained at 85°C using a heating mantle, followed by a one-minute cooling phase before absorbance measurement. The tubing used has an internal diameter of 1.5 millimetres. The flow rate selected for the experiment is 0.77 millilitres per minute.

To verify the sufficiency of this design, the residence time was calculated using the standard formula (Equation (21)):

$$t = \frac{V}{Q} \tag{21}$$

t is the residence time in seconds, V is the volume of the tube in millilitres, and Q is the flow rate in millilitres per second.

The first step is to determine the cross-sectional area of the tube. Given that the internal diameter is 1.5 millimetres, the radius r is 0.75 millimetres, or 0.00075 metres. The cross-sectional area A is:

$$A = \pi r^2 = \pi * (0.00075)^2 = 1.767 \times 10^{-6}\ m^2 \tag{22}$$

For a tube length of 1.0 metre, the volume is.

$$V = A \times L = 1.767 \times 10^{-6}\ m^2\ \times 1\ m = 1.767 \times 10^{-6}\ m^3 = 1.767 mL \tag{23}$$

The flow rate is converted to seconds: *Q=0.77 mL/min=0.01283 mL/s*

Substituting values from the Equation (22) and Equation (23) into the residence time formula (Equation (21) gives

$$t = 1.767/0.01283 = 137.7\ s \tag{24}$$

This calculated residence time corresponds to approximately 2.3 minutes, which satisfies the reaction time requirement established in preliminary kinetic studies. The system, therefore, provides sufficient duration for complete reduction of nitrate under the specified thermal conditions.

The experimental setup for nitrate detection at 85°C was designed to ensure efficient mixing, precise heating, rapid cooling, and accurate absorbance measurements for reliable nitrate quantification. The setup followed a structured flow diagram, as depicted in Figure 38, in which distinct stages of the process were systematically integrated to optimise nitrate detection. The method involved the Vanadium Chloride Reduction Method, in which nitrate (NO_3^-) was reduced to nitrite (NO_2^-) under acidic conditions using vanadium chloride (VCl_3). The generated nitrite then reacted with the Griess reagents, namely sulphanilamide and N-(1-naphthyl)-ethylenediamine dihydrochloride (NED), to form a pink-coloured azo dye. The intensity of this dye was directly proportional to nitrate concentration. This colour development was quantified using UV-VIS spectrophotometry at 540 nm, and MATLAB software was used to interpolate concentration measurements from absorbance values. This approach ensured precise nitrate quantification.

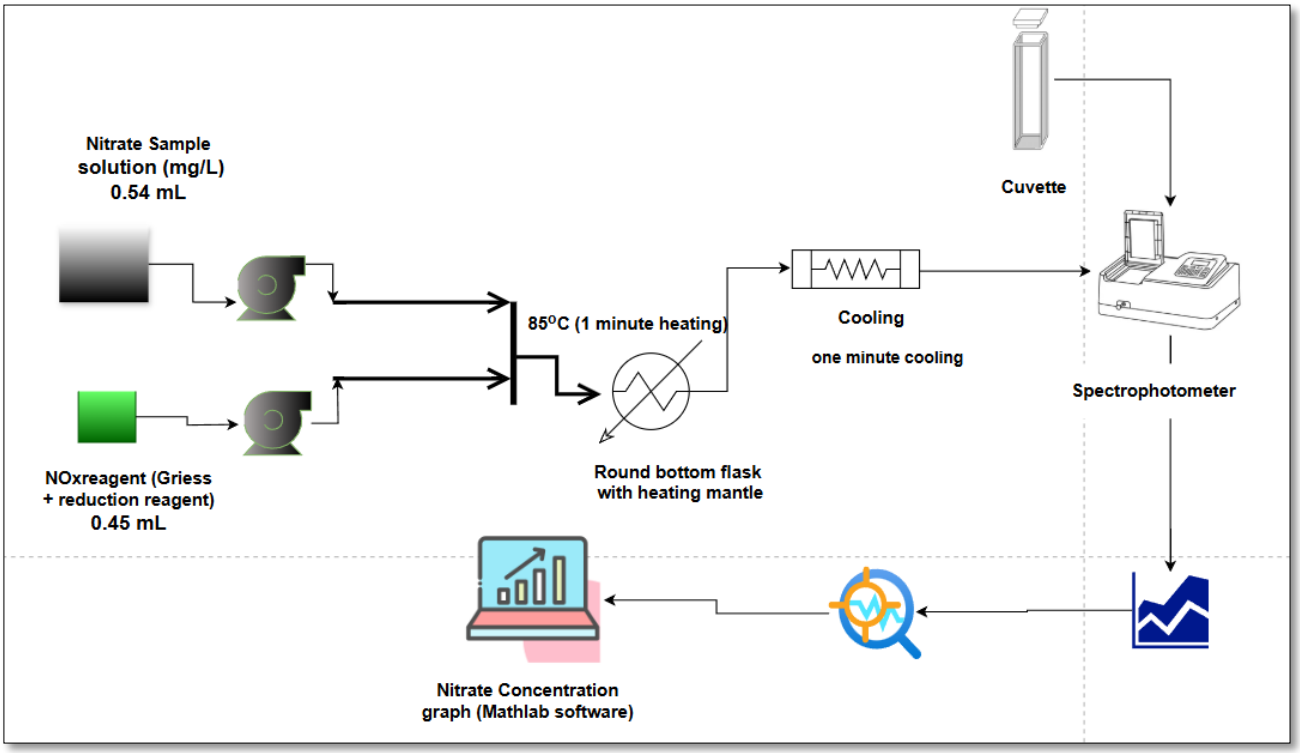

Figure 38 Flow Diagram of the Nitrate Detection Process at 85°C.

The experimental setup, as depicted in Figure 38, represented the workflow used for nitrate detection at 85°C. The process began with sample preparation, where a nitrate standard solution was prepared

by dissolving sodium nitrate in Milli-Q water, with added sodium chloride to maintain the ionic strength of the solution. This nitrate solution served as the calibration standard for determining unknown nitrate concentrations through spectrophotometric analysis.

In the reagent addition phase, the nitrate sample solution and NO_X reagent were pumped separately using peristaltic pumps to ensure a controlled and consistent flow rate. The nitrate sample solution, which was prepared using sodium nitrate and sodium chloride, was delivered using the Pharmacia Biotech Peristaltic Pump P-1. This pump ensured precise delivery of the nitrate sample and maintained consistent reaction conditions. Simultaneously, the NO_X reagent, a mixture of vanadium chloride, sulphanilamide, and N-(1-naphthyl)-ethylenediamine dihydrochloride (NED) was delivered using the Watson-Marlow 313V Pump. The NO_X reagent acted both as a reducing agent and as a colour-developing solution, facilitating the conversion of nitrate to nitrite and subsequently reacting with the Griess reagents to form the pink azo dye.

Both the nitrate sample solution and the NOx reagent were directed into the mixing unit, where static mixing beads were exclusively used to enhance effective mixing. Thermal beadings were employed to ensure homogeneous blending of the two solutions, which was essential for achieving accurate and consistent results. Proper mixing ensured that the reaction between nitrate and the NOx reagent proceeded efficiently, minimising variability in reaction kinetics and absorbance readings. This step was particularly critical, as incomplete mixing could have led to inaccuracies in the final measurement.

Once thoroughly mixed in the mixing unit, the reaction mixture flowed through glass tubing (1.5 mm diameter) into a round-bottom flask placed inside a water bath heated by a heating mantle (shown in Figure 39), maintained at 85°C with a residence time of 2.3 minutes. The glass tubing was submerged within the round-bottom flask, ensuring uniform heating of the reaction mixture. This controlled heating phase was crucial because it sustained the reaction rate for the reduction process, ensuring complete conversion of nitrate to nitrite within the designated residence time. The water bath served as a heat stabiliser, preventing overheating and ensuring consistent reaction conditions throughout the tube. The Vernier Go Direct® Wide-Range Temperature Probe continuously monitored the reaction temperature to verify that the setpoint of 85°C was maintained, thereby preventing thermal degradation of the reagents and ensuring consistency in reaction conditions.

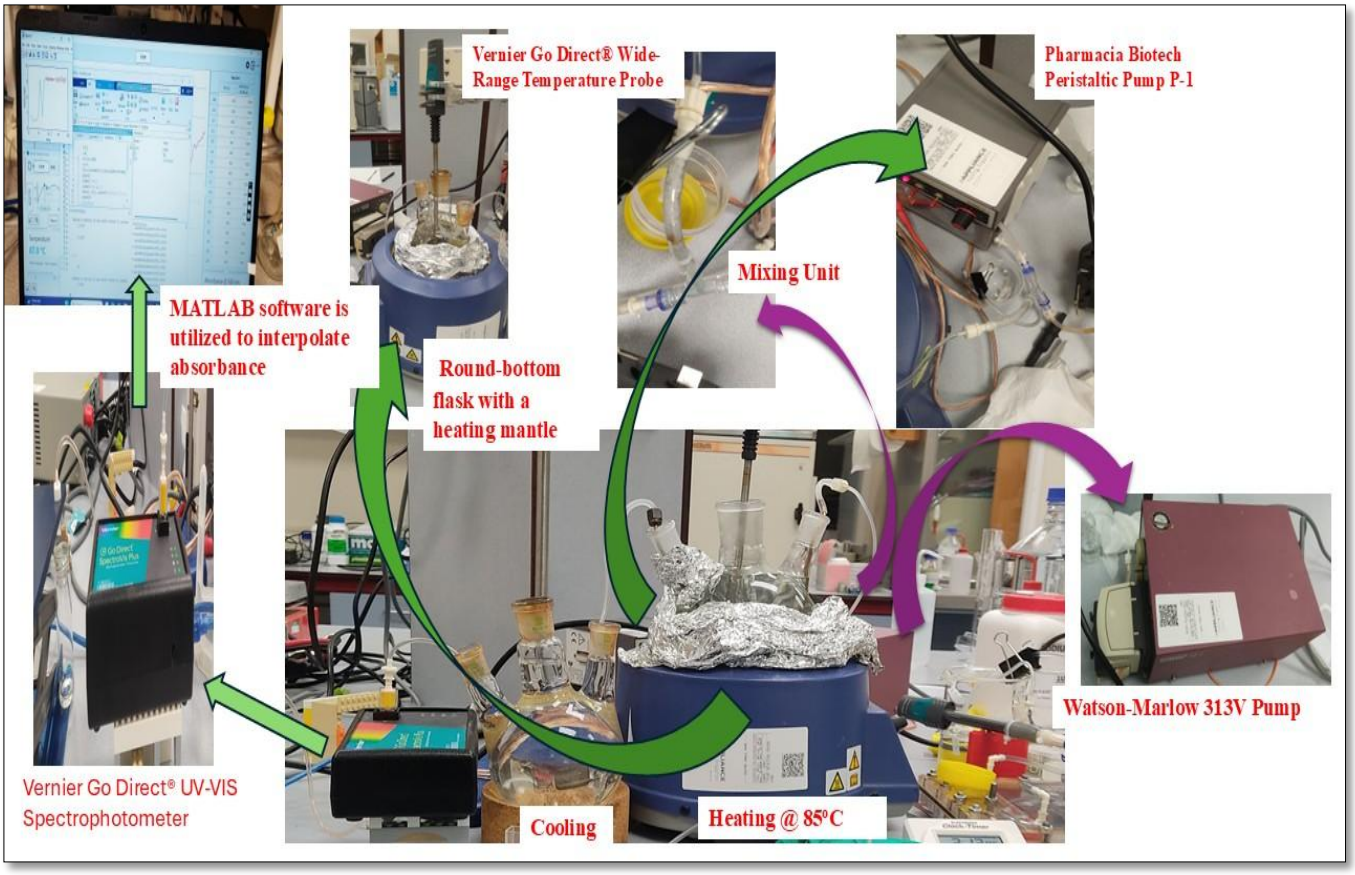

Figure 39 Experimental Setup for Nitrate Detection at 85°C: Integration of Peristaltic Pumps, Thermal Bead Mixing, Water Bath Heating, Cooling System, UV-VIS Spectrophotometry, and MATLAB-Based Data Analysis

After the heating phase, the reaction mixture was passed through a plastic tube (PVC) into the cooling phase, where the reaction was quenched by passing the tubing through cooling water contained in a round-bottom flask. This step ensured efficient heat exchange, bringing the reaction mixture to a stable temperature before spectrophotometric analysis. The cooling water in the round-bottom flask absorbed heat from the plastic tube, thereby preventing thermal degradation of the azo dye and ensuring that the sample remained stable. This cooling setup was effective because it provided a stable and controlled cooling environment, ensuring that all samples underwent consistent temperature reduction before analysis. Unlike air cooling, which could be inconsistent, water-based cooling provided rapid and uniform temperature stabilisation. This cooling phase was critical because any residual heat in the reaction mixture could have altered the absorbance readings, leading to inaccurate nitrate quantification.

Following the cooling phase, the stabilised reaction mixture flowed through PVC tubing into a flow-cell cuvette, which was then placed in a Vernier Go Direct® UV-VIS Spectrophotometer (shown in

Figure 39). This spectrophotometer was used to measure the absorbance of the sample at 540 nm, a wavelength corresponding to the peak absorbance of the pink azo dye. Since the intensity of this colour was directly proportional to the nitrate concentration, the absorbance values provided a quantitative measure of the nitrate levels present in the sample. Higher nitrate concentrations resulted in higher absorbance values, whereas lower concentrations produced lower absorbance readings. The Vernier Go Direct® UV-VIS Spectrophotometer was particularly well suited for this experiment due to its high sensitivity, precision, and real-time data acquisition capabilities, which enabled continuous monitoring and analysis.

The final step in the process involved MATLAB interpolation, where the recorded absorbance values were processed and analysed using MATLAB software (as illustrated in Figure 39). MATLAB was used to interpolate concentration measurements based on absorbance data obtained from UV-VIS spectroscopy, using a calibration curve generated from the original nitrate standards. The calibration curve had been established by measuring the absorbance values of standard nitrate solutions with known concentrations and applying linear regression analysis to derive a mathematical equation that related absorbance to concentration. By employing MATLAB for data interpolation, the accuracy and precision of nitrate quantification were significantly enhanced (Appendix 9.3). This approach reduced potential errors that could arise from manual calculations and improved overall reproducibility.

5.2 Theory of Non-Ideal Flow and the Application of the Dispersion Model to Flow Cell Reactor Design

Currently, the flow cell design consists of a series of tubes and discrete batches of volume such as the cuvette and conductivity cell. The use of a simple tube can be ordinarily thought of as a plug-flow reactor. In an ideal system, if a step change increase of dye is introduced at the inlet of a tube, the step will be reproduced at the outlet after the residence time has passed. This ideal condition relies on a key assumption, which is that there is no back mixing or diffusion (Figure 40) occurring during the passage of the material through the tube. This assumption produces reasonable results for short lengths of tube.

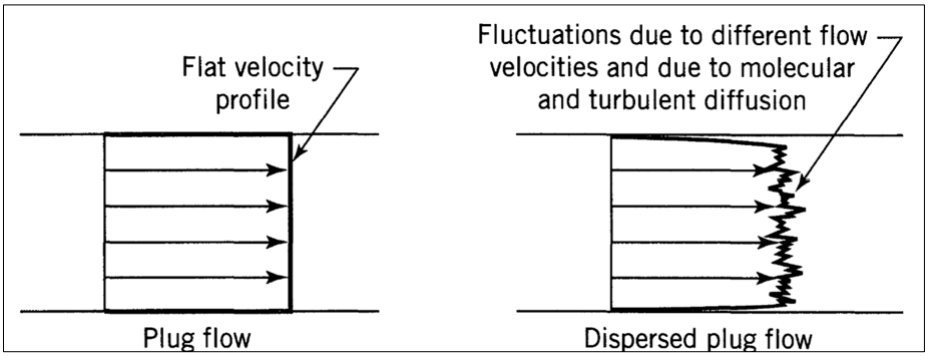

Figure 40 Comparison of ideal plug flow and dispersed plug flow profiles, illustrating the impact of axial mixing and diffusion on outlet concentration behaviour in tubular reactors.(Levenspiel, 1999)

Figure 55 illustrates the fundamental difference between ideal plug flow and dispersed plug flow, both of which are critical in understanding the behaviour of flow within the nitrate detection system. In ideal plug flow, fluid elements travel at uniform velocity without axial mixing, resulting in a sharp step response when a tracer or dye is introduced. This assumes negligible diffusion and turbulence, conditions that are only approximated in very short or narrow tubing.

However, in real systems, especially those involving longer tubing or laminar flow conditions, dispersion becomes significant. Axial mixing due to molecular diffusion and radial velocity gradients causes a spreading of the concentration front, resulting in a gradual rise and fall in outlet concentration. This behaviour is represented in the dispersed plug flow profile, where the response curve deviates from the ideal step function.

The extent of this deviation is characterised by Levenspiel's dispersion model using the dimensionless number D/UL, where D is the axial dispersion coefficient, U the superficial velocity, and L the reactor length (Levenspiel, 1999). Accurate interpretation of dispersion is essential for optimising the reactor design in nitrate detection, ensuring sample integrity and measurement precision.

5.2.1 Residence Time Distribution (RTD) Analysis

This RTD analysis was based on the earlier nitrate detection experiment using vanadium chloride under heated flow conditions. In that experiment, a reaction temperature of 65°C was selected to promote the rapid reduction of nitrate to nitrite, followed by colour development via the Griess reaction. To support this, the fluid was subjected to a 5-minute heating phase followed by a 5-minute cooling period, resulting in a total expected system delay of approximately 10 minutes before the

absorbance signal stabilised. The tubing used had a length of 1.944 metres, and the superficial velocity of the fluid, calculated from the known flow conditions, was 0.0027 m/s.

The residence time distribution (RTD) function, *E(t),* describes the probability that fluid elements spend a given amount of time in the reactor. The RTD curve provides critical insights into the system's flow behaviour.

Figure 42 illustrates the experimental RTD curve in comparison with an ideal plug flow profile. In ideal plug flow, all fluid elements have identical residence times, represented by a sharp peak. In contrast, the broader curve obtained experimentally suggests significant dispersion within the system, where fluid elements experience a range of residence times.

The RTD function is defined as shown in Equation (25) **:**

$$\mathrm{E(t)} = \frac{\text{Fraction of fluid leaving at time t}}{\text{Total residence time}\mathrm{E(t)}} \tag{25}$$

The broad nature of the RTD curve in the graph indicates significant deviations from ideal plug flow, where all fluid elements would have the same residence time. This non-uniform behaviour impacts the overall reaction efficiency and delays the time to maximum absorbance.

The RTD function is calculated using Equation (26):

$$\mathrm{E(t)} = \frac{\mathrm{C(t)}}{\int_0^\infty \mathrm{C(t)\,dt}} \tag{26}$$

Where:

C(t)- Concentration (or, in this case, absorbance) at time t

$\int_\infty^0 C(t)dt$- The total area under the absorbance curve, which normalizes *E(t)* so that the total probability equals 1.

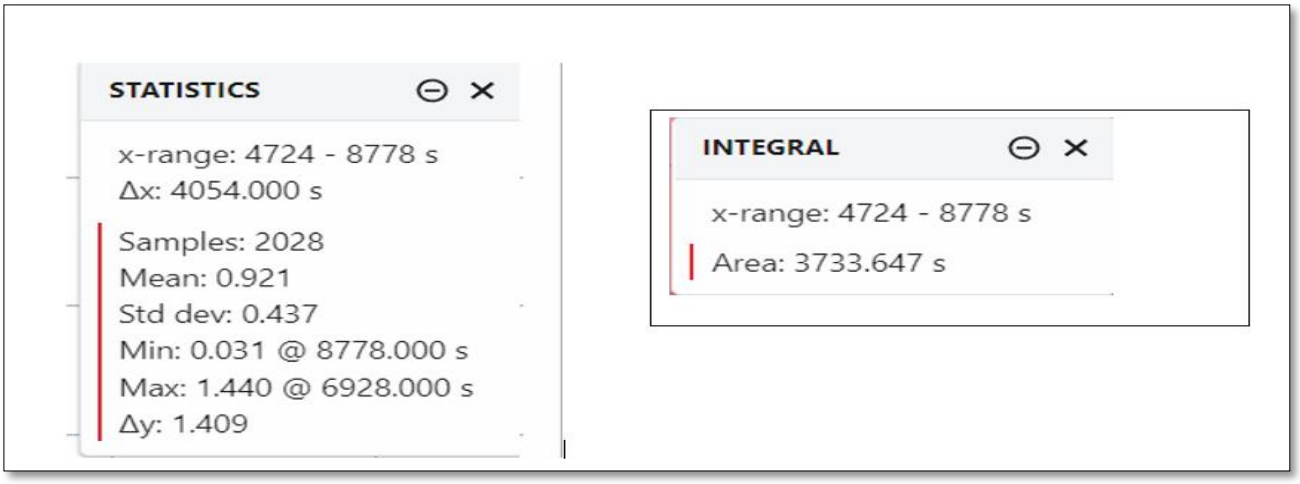

Figure 41 Statistical summary and integral area for absorbance at 540 nm during nitrate detection, showing a time range of 4724–8778 s, mean absorbance of 0.921, standard deviation of 0.437, and a total integrated area of 3733.647 s

From the graph:

$C(t)$ - Absorbance at time t (given on the graph).

$\int_{t2}^{t1} C(t)\,dt$ - Total area under the curve, which is $3733.6\,s$ (given as the integral (Figure 41)).

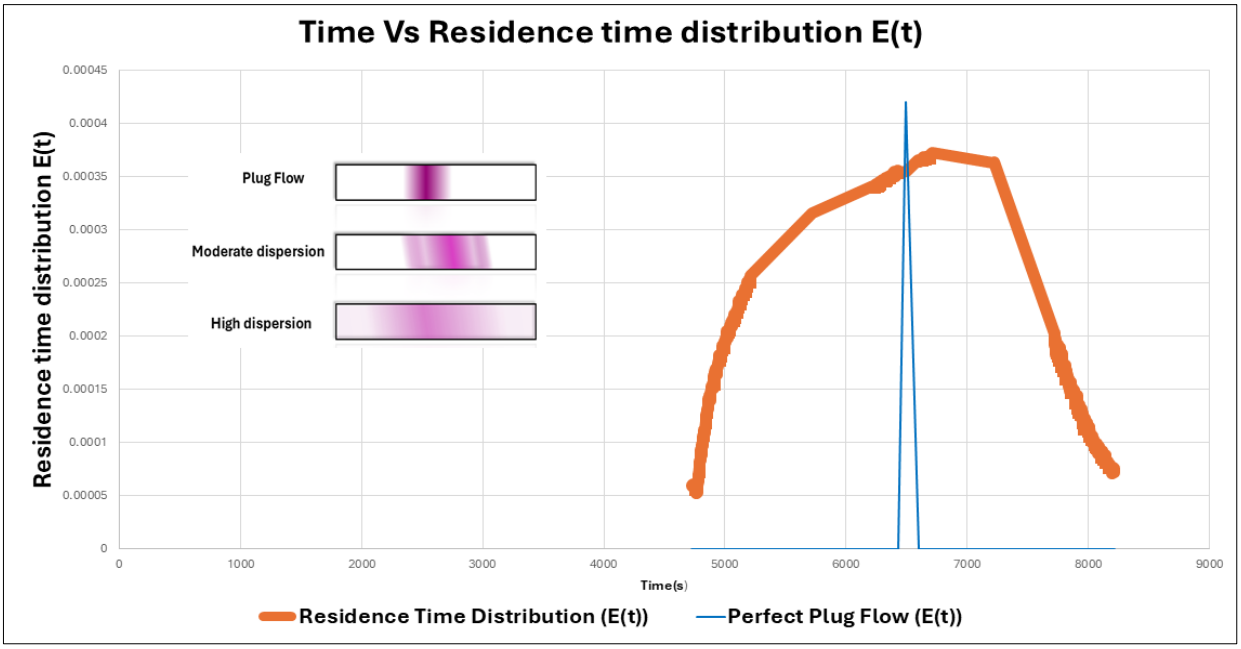

Figure 42 Residence time distribution curve with corresponding tracer profiles showing plug flow to high dispersion

Figure 42 shows the relationship between tracer dispersion and flow behaviour within the system using both a graphical RTD (residence time distribution) curve and visual tracer profiles. On the right,

the E(t) curve displays the normalised distribution of residence times for fluid elements, providing insight into how long different portions of the fluid remain in the reactor. The peak at t = 6928 s (E(t) = 0.0003) represents the most probable residence time, where most fluid elements exit the system. On the left, three gradient bars demonstrate how a tracer, such as a dye, disperses under varying flow conditions. The top bar shows ideal plug flow with a sharp, narrow band of colour, while the lower bars reflect increasing degrees of dispersion and mixing. Together, the graph and gradients allow for a clear visual interpretation of the extent of non-ideal flow in the system.

The RTD curve also reveals non-idealities in flow behaviour through its extended tail beyond 7000 seconds, indicating the presence of axial dispersion, back mixing, or stagnant regions within the reactor. These irregularities cause certain fluid elements to remain in the reactor longer than necessary, resulting in inefficient mixing and delayed reaction progress. The broadness of the E(t) curve deviates significantly from the sharp peak expected in an ideal plug flow system, highlighting uneven fluid distribution. Improving reactor design through enhanced mixing, reduced dead zones, or shorter flow paths could help reduce these non-ideal effects and bring system performance closer to ideal plug flow, ultimately increasing reaction efficiency and consistency.

5.2.2 Implications of RTD

The residence time distribution (RTD) curve provides essential insights into the internal flow behaviour of the reactor. In an ideal plug flow system, all fluid elements would spend the same amount of time in the reactor, resulting in consistent and efficient chemical reactions. However, the broad shape of the observed RTD curve and the presence of a long tail after the peak at 6928 seconds indicate significant deviations from ideal behaviour. These deviations suggest that some fluid elements experience shorter residence times and exit the reactor before completing the reaction, while others remain in the system longer due to factors such as axial dispersion, back mixing, or stagnant zones. This uneven distribution leads to incomplete mixing and delays in reaching peak absorbance, thereby reducing the accuracy and responsiveness of nitrate detection. The RTD analysis highlights the need for design improvements, such as reducing tubing length, increasing flow velocity, or incorporating better mixing elements, to improve uniformity in residence times and enhance detection performance.

5.2.3 Dispersion Model and Calculation

The dispersion model is a powerful framework in chemical reaction engineering used to quantify the effects of axial mixing in flow systems, particularly in tubular reactors. In an ideal plug flow reactor (PFR), all fluid elements travel at the same velocity and exit the reactor simultaneously, resulting in a uniform residence time distribution (RTD). However, in real systems, deviations from ideal plug flow often occur due to axial dispersion, where fluid elements mix along the direction of flow. These deviations lead to non-uniform residence times, impacting reaction efficiency, product quality, and system performance.

The dispersion model quantifies the effect of axial mixing on reactor performance. The dimensionless dispersion number, *D/uL*, measures the extent of deviation from plug flow.

The dispersion number is given by the Equation (27):

$$\frac{\mathrm{D}}{\mathrm{uL}} = \frac{\sigma_\theta^2}{2} \tag{27}$$

This equation is central to the dispersion model and allows us to calculate the dimensionless dispersion coefficient (*D/uL*), which characterises the extent of dispersion in a flow system relative to convection. To compute *D/uL*, the normalised variance (σ_θ^2) is required, which is derived from the variance (σ_t^2) and the mean residence time ($\bar{t}$)

The mean residence time ($\bar{t}$) represents the average time the tracer or substance spends in the system. It is calculated by weighting the time at each observation point (*ti*) by the corresponding concentration or absorbance (*Ci*) at that time. This gives an overall measure of how long, on average, the tracer remains in the system, as defined by Equation (28).

$$\bar{\mathrm{t}} = \frac{\sum(\mathrm{ti} * \mathrm{Ci})}{\sum \mathrm{Ci}} \tag{28}$$

In practice, the mean residence time is crucial for designing flow systems or reactors. For instance, in chemical processes, knowing the mean residence time helps ensure the reaction has enough time to complete before the fluid exits the system. In Appendix 9.1, the calculated mean residence time is 6505.98s.

The variance (σ_t^2) measures the spread of the residence time distribution (RTD) around the mean residence time. A low variance indicates that most of the tracer spends the same amount of time in the system, suggesting flow behaviour close to plug flow. A high variance suggests more dispersion, where some tracer particles spend significantly more or less time than the mean. The variance is mathematically defined in Equation (29) as:

$$\sigma t^2 = \frac{\sum((ti - \bar{t})^2 * C_i)}{\sum C_i} \tag{29}$$

The variance is determined by taking the weighted average of the squared deviations of t_i from $\bar{t}$, divided by C_i. This parameter is especially useful in identifying inefficiencies in the flow, such as back mixing or dead zones. From Appendix 9.1, the variance for this system is 815900 s^2.

The normalised variance (σ_θ^2) makes the variance dimensionless by dividing σ_t^2 by the square of the mean residence time $(\bar{t}^2)$. This normalisation enables variance comparisons across systems with different scales or operating conditions, as shown in Equation (30).

$$\sigma\theta^2 = \frac{\sigma_t^2}{(\bar{t})^2} \tag{30}$$

The normalised variance is particularly useful in characterising the degree of mixing in a system. Lower values of σ_θ^2 indicate behaviour closer to ideal plug flow, whereas higher values suggest greater dispersion or mixing. For the current system, the normalised variance is 0.0193, indicating minimal dispersion and a flow pattern close to plug flow.

The dimensionless dispersion coefficient (D/uL) is a critical parameter that quantifies the relative importance of dispersion compared to convective transport. It is related to the normalised variance by the Equation (31).

$$\frac{D}{uL} = \frac{\sigma_\theta^2}{2} \tag{31}$$

The value of D/uL helps classify flow behaviour:

$D/uL \ll 1$: The system approaches plug flow, with minimal mixing or dispersion.

$D/uL \gg 1$: The system behaves more like a well-mixed reactor, with significant dispersion.

For this system, the calculated value of D/uL is 0.00960, suggesting that the flow is close to ideal plug flow with little dispersion. This insight is critical in reactor design and flow system optimisation, ensuring the system achieves efficient mixing or maintains desired flow patterns.

The dispersion coefficient (D) is a crucial parameter in fluid flow systems, quantifying the degree of solute mixing or spreading due to velocity variations and molecular diffusion. Using the formula (Equation (32))

$$\mathrm{D} = 0.00960 \times \mathrm{u} \times \mathrm{L} \tag{32}$$

where $u = 0.0027\ m/$s, and L=1.944 m, the dispersion coefficient is calculated by substituting these values into the Equation (33):

$$\mathrm{D} = 5.05875 \times 10^{-5}\ \mathrm{m}^2/\mathrm{s} \tag{33}$$

This value represents the extent of dispersion within the system and highlights the limited mixing present. A small dispersion coefficient like this suggests the system is closer to plug flow behaviour, where fluid elements travel at the same velocity.

To eliminate the need for a sample-and-hold mechanism in our nitrate detection system, it was critical to determine the minimum dispersion coefficient D that ensures the dye concentration falls below 5% at the end of one internal volume of flow ($\theta=1$). This theoretical value was derived using a step-function response analysis, a method grounded in Levenspiel's chemical reaction engineering framework (Levenspiel, 1999). A step input of dye was introduced at 4724 seconds, and the system reached its maximum absorbance at 6928 seconds, indicating a response delay (Δt) of 2204 seconds due to dispersion. With a known mean residence time $\bar{t}$ of 6505.98 s, the variance was calculated as shown in Equation (34).

$$\sigma_t^2 = (2204)^2 = 4.859 \times 106\, s^2 \tag{34}$$

and the normalised variance was computed using Equation (35).

$$\sigma_\theta^2 = \frac{\sigma_t^2}{\bar{t}} = \frac{4.859 \times 10^6}{(6505.98)^2} = 0.114 \tag{35}$$

According to the dispersion model, the dimensionless dispersion number is related by.

$$\frac{D}{uL} = \frac{\sigma_\theta^2}{2} = 0.057 \tag{36}$$

By substituting the flow velocity (*u=0.0027 m/*s) and tube length (*L=1.944 m)* into the equation (36), Using equation (37), the dispersion coefficient D is calculated as.

$$D = \frac{D}{uL} \cdot u \cdot L = 0.0574 \times 0.0027 \times 1.944 = 2.44 \times 10^{-4} m^2/s \tag{37}$$

This theoretical value is approximately 4.8 times higher than the experimentally determined value of 5.06×10^{-5} m^2/s, which explains why dye persists in the system even after the full fluid volume has passed, thereby justifying the use of the sample-and-hold system. Increasing the dispersion to this target level would ensure that dye clearance is effectively achieved at *θ=1*, enabling accurate real-time detection without isolating and holding samples.

5.3 Experiment to Determine Non-Ideal Flow Characteristics of Reactor Design for Online Nitrate Measurement

This study evaluates the non-ideal flow characteristics, such as the delay in nitrate detection, based on the length of the tubing in the experimental setup. To study this, pulse and step function experiments were performed. The objective is to determine how flow path length influences the system's response time, mixing dynamics, and dispersion effects. By understanding these delays, the system can be designed for online nitrate monitoring. The Go Direct® Conductivity Probe is used for real-time conductivity measurement. The expected response times vary based on tubing length:

- For a 2-meter tube length, the system is expected to detect nitrate within 10 minutes.
- For a shorter tube length, the expected response time is 2 minutes.

This study provides a quantitative and theoretical analysis of these delays using mathematical modelling, experimental observations, and response time calculations.

5.3.1 Experimental Setup

The experimental setup consisted of a continuous flow reactor system designed to analyse NaCl detection using conductivity measurements. The system included a peristaltic pump, a reaction chamber, and a Go Direct® Conductivity Probe. The peristaltic pump continuously introduced the NaCl solution at a controlled flow rate through a plastic tube, and its conductivity was monitored throughout the experiment to track mixing efficiency and flow behaviour. The experimental conditions were carefully controlled to evaluate flow effects, dispersion characteristics, and detection delay at different tube lengths. The longer tubing (2 metres) introduced greater residence time and dispersion, whereas the shorter tubing resulted in faster response times.

5.3.2 Methodology

The step function and pulse function experiments were performed separately to determine the delay in nitrate detection. The step function experiment measured the time required for the system to reach 90% of the final steady-state conductivity. The system was initially filled with deionised water to establish a baseline conductivity, after which a 2 g/L NaCl solution (conductivity: 3503 μS/cm) was continuously introduced at a controlled flow rate of 0.0734 mL/s. Conductivity was measured over time until it reached equilibrium. The detection delay was defined as the time required for the conductivity to reach 90% of its final value.

The pulse function experiment focused on the transient response and dispersion effects in the system. The system began with deionised water, and at time zero, a 1 mL injection of a high-conductivity (72,290 μS/cm) NaCl solution was introduced using a 10 mL syringe. The conductivity probe recorded changes in conductivity over time, tracking the peak and subsequent decay. The delay in detection was assessed based on the time required to reach peak conductivity and then return to baseline. This experiment helped evaluate how quickly the system could detect sudden changes in ion concentration and how tubing length influenced signal dispersion.

5.3.3 Results and Discussion

5.3.3.1 Delay in Step Response for 2-Meter Tube Length

This experiment was designed similarly to the earlier nitrate detection work at 65°C, with the critical change being the replacement of nitrate with a sodium chloride (NaCl) solution to allow response analysis using a conductivity probe. The 2-meter tube length remained constant, ensuring a direct comparison of system behaviour between nitrate and NaCl solutions. The objective was to specifically analyse the time delay observed during nitrate detection under similar conditions.

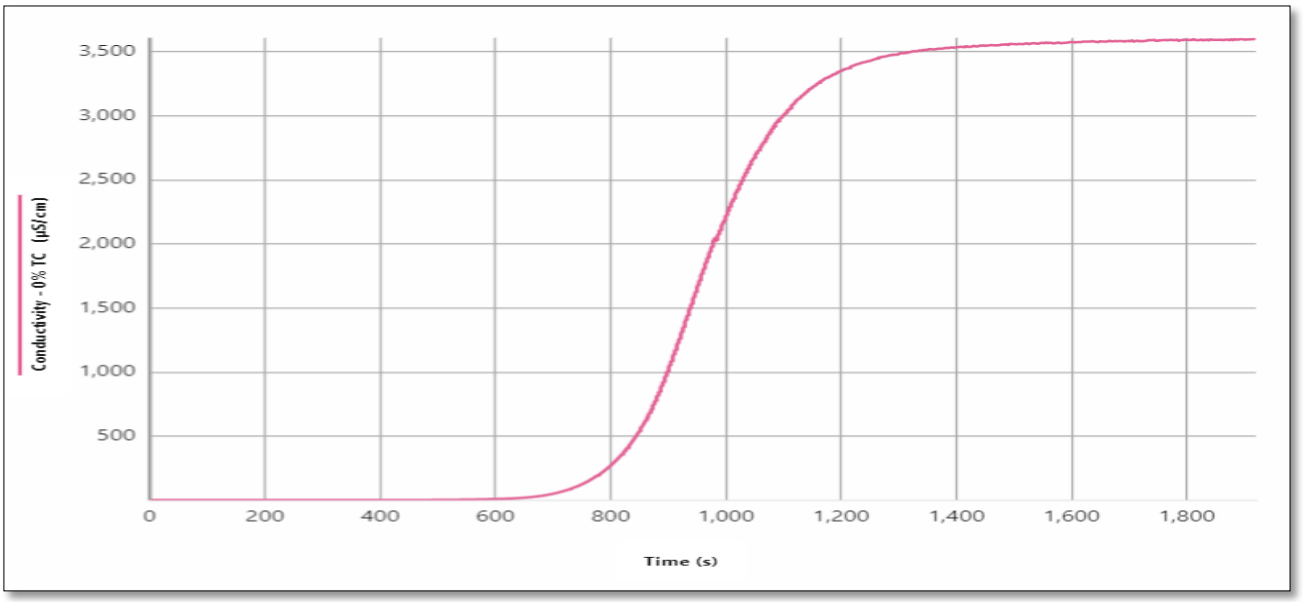

Figure 43 Step Response of 2 g/L NaCl Solution (3503 µS/cm) in a 2-Meter-long Tube. The system exhibits a delay of approximately 1000 seconds (16.7 minutes) before reaching steady state conductivity.

The step response graph (Figure 43) for NaCl detection exhibited a sigmoidal increase in conductivity, which was characteristic of a first-order system response. The observed detection delay (τ) was primarily due to residence time, axial dispersion, and flow resistance within the 2-metre tubing. This delay was quantitatively assessed using the following Equation (38):

$$\tau = \frac{Q}{V} \tag{38}$$

where:

V = system volume (m³)

Q = flow rate (m^3/s)

Using experimental data (Equation (39)),

$$\text{Delay time } \tau_2 \approx 1000\text{s (16.7 minutes)} \tag{39}$$

This delay was longer than the expected 10-minute benchmark. The extended response time suggested the presence of additional dispersion effects, dead volume, or tubing resistance that contributed to slower ion transport. Unlike an ideal step response, which is characterised by an instantaneous rise, the gradual increase observed in the experimental curve indicated substantial mixing inefficiencies along the flow path. Furthermore, diffusion-driven ion transport within the tubing exacerbated the detection delay, resulting in a slow progression toward steady-state conductivity. These results demonstrated that long tube lengths inherently introduced delays that could not be overcome simply by adjusting flow rates or tubing diameter.

Most importantly, the findings clearly showed that using a single continuous tube for real-time detection was fundamentally inadequate. Regardless of how well the tubing or flow conditions were optimised, inherent dispersion and dead volumes prevented rapid response. Therefore, this section strongly supported the development of a sample-and-hold system. By isolating discrete fluid samples rather than relying on continuous flow through extended tubing, much of the dispersion-related delay could be eliminated, thereby enabling faster and more accurate real-time nitrate detection.

5.3.3.2 Delay in Pulse Response for 2-Meter Tube Length

The pulse response experiment for the 2-metre tube length was conducted to analyse the transient behaviour resulting from a sudden injection of 1 mL of high-conductivity NaCl solution (72,290 µS/cm). The corresponding graph (Figure 44) exhibited a sharp conductivity peak (~16,000 µS/cm) at approximately 500 seconds, followed by an exponential decay back to baseline levels. The time to reach peak conductivity was measured at around 500 seconds (8.3 minutes), confirming a significant detection delay caused by the extended flow path length and dispersion effects.

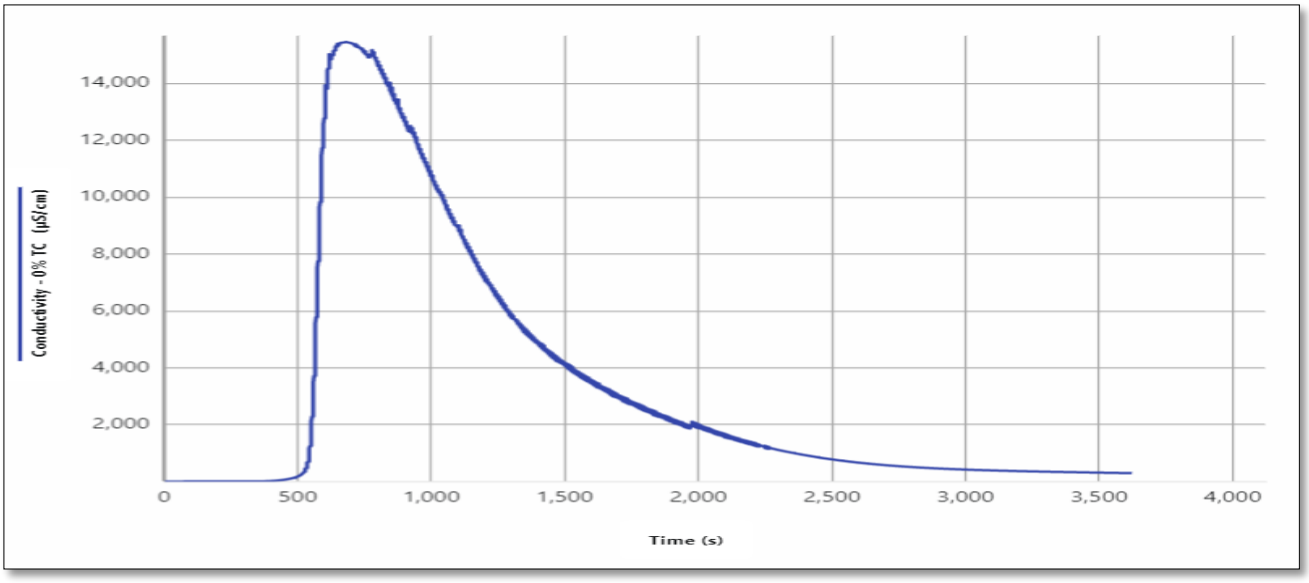

Figure 44 Pulse Response of 1 mL NaCl Injection (72,290 µS/cm) in a 2-Meter Tube. The system exhibits a peak conductivity of approximately 16,000 µS/cm at 500 seconds (8.3 minutes), with an expected delay of 10 minutes and a decay time exceeding 3500 seconds (58.3 minutes) due to dilution and dispersion effects.

The significant detection delay in reaching the peak and the prolonged decay phase (exceeding 3500 seconds or 58.3 minutes) once again highlighted the extensive influence of axial dispersion and flow path mixing. The initial sharpness of the pulse was rapidly lost as the injected solute spread over time and distance, resulting in diluted and smeared peaks.

This behaviour confirmed that, using long tubing, the system could not provide sharp, real-time detection under a continuous flow configuration. The extended dilution and dispersion effects introduced both temporal and concentration smearing, which degraded the fidelity of the measurements. Therefore, a strong conclusion was drawn that adopting a sample-and-hold system was essential. Such a system would eliminate the long path smearing by isolating samples at defined times and positions, thereby enabling more accurate concentration measurements and a faster system response.

Effect of Dilution on Peak Conductivity

Although the injected NaCl solution had an initial conductivity of 72,290 µS/cm, the maximum observed conductivity was only 16,000 µS/cm. This discrepancy was attributed to dilution and dispersion within the tubing. The effective volume of the system, including both the tubing and the associated dispersion effects, was estimated using the dilution Equation (40):

$$V_{total} = \frac{C_{injected} \times V_{injected}}{C_{final}} \quad (40)$$

where:

$C_{injected}$ = 72,290 µS/cm (initial solution conductivity)

C_{final} = 16,000 µS/cm (observed peak conductivity)

$V_{injected}$ = 1 mL (injected volume)

Substituting the values into the dilution Equation (41), the total volume was calculated as:

$$Vtotal = \frac{72{,}290 \times 1}{16{,}000} = 4.52 \text{ mL} \quad (41)$$

This calculation indicated that the 1 mL injection was effectively diluted across a system volume of approximately 4.5 mL by the time it reached the conductivity probe. Such dilution significantly affected both the sharpness and the magnitude of the detectable peak.

Although reducing tubing length or increasing flow rates might have partially mitigated this effect, these strategies could not fundamentally resolve the issue. When operated under continuous flow conditions, the system inherently suffered from axial dispersion and dead volumes. This finding further reinforced the conclusion that adopting a sample-and-hold method was the only truly effective solution. In such a configuration, a discrete and undispersed sample volume could be rapidly measured without the smearing effects associated with extended tube travel.

5.3.3.3 Delay in Step Response for Shorter Tube Length

This experiment was conducted to analyse the delay in nitrate detection using VCl_3 at 85°C. The same tubing configuration was used to compare the response time; however, instead of nitrate, a NaCl solution was evaluated under similar flow conditions. The flow rate applied in this experiment was 0.036 mL/s.

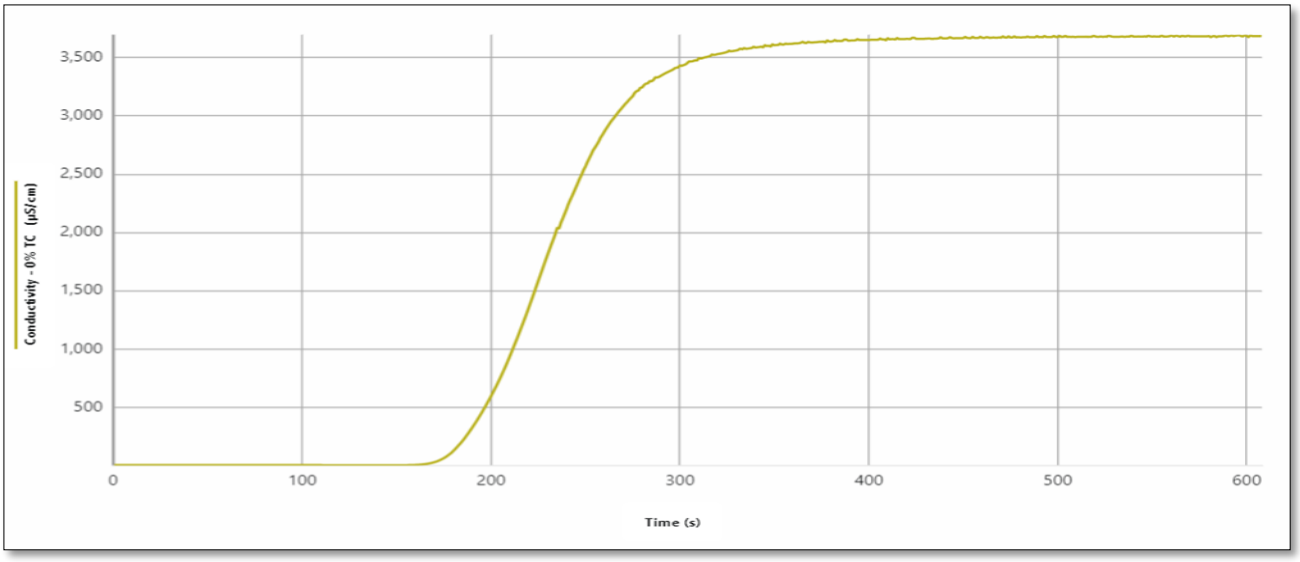

Figure 45 Step Response of 2 g/L NaCl Solution (3503 µS/cm) in a Shorter Tube Length. The system reaches steady-state conductivity at approximately 320 seconds, confirming a reduced detection delay compared to longer tubing.

The step response graph (Figure 45) demonstrated a much faster approach to steady-state conductivity than the 2-metre tube length experiment. This faster response was attributed to the shorter residence time, reduced axial dispersion, and decreased influence of dead volume effects. However, it was important to note that, although reduced, the delay remained longer than the ideal time constant predicted theoretically (120 seconds), suggesting that minor dispersion and flow resistance effects persisted even with the shortened path.

This finding underscored that reducing tube length was beneficial, but it could not fully eliminate delay and dispersion phenomena. Therefore, to achieve the sharp and rapid detection required for online nitrate monitoring, the system design must move beyond a reliance on tubing length alone. These results once again supported the essential transition towards a sample-and-hold approach to overcome the inherent limitations of tubing-based continuous flow systems.

5.3.3.4 Delay in Pulse Response for Shorter Tube Length

The pulse response experiment for the shorter tube length was conducted using a 2 g/L NaCl solution with an initial conductivity of 72,290 µS/cm. The objective was to analyse how quickly the system detected and responded to a sudden pulse input under reduced tubing length conditions. The graph in Figure 46 exhibited a sharp conductivity peak (~16,000 µS/cm) at approximately 100 seconds, followed by an exponential decay towards baseline levels.

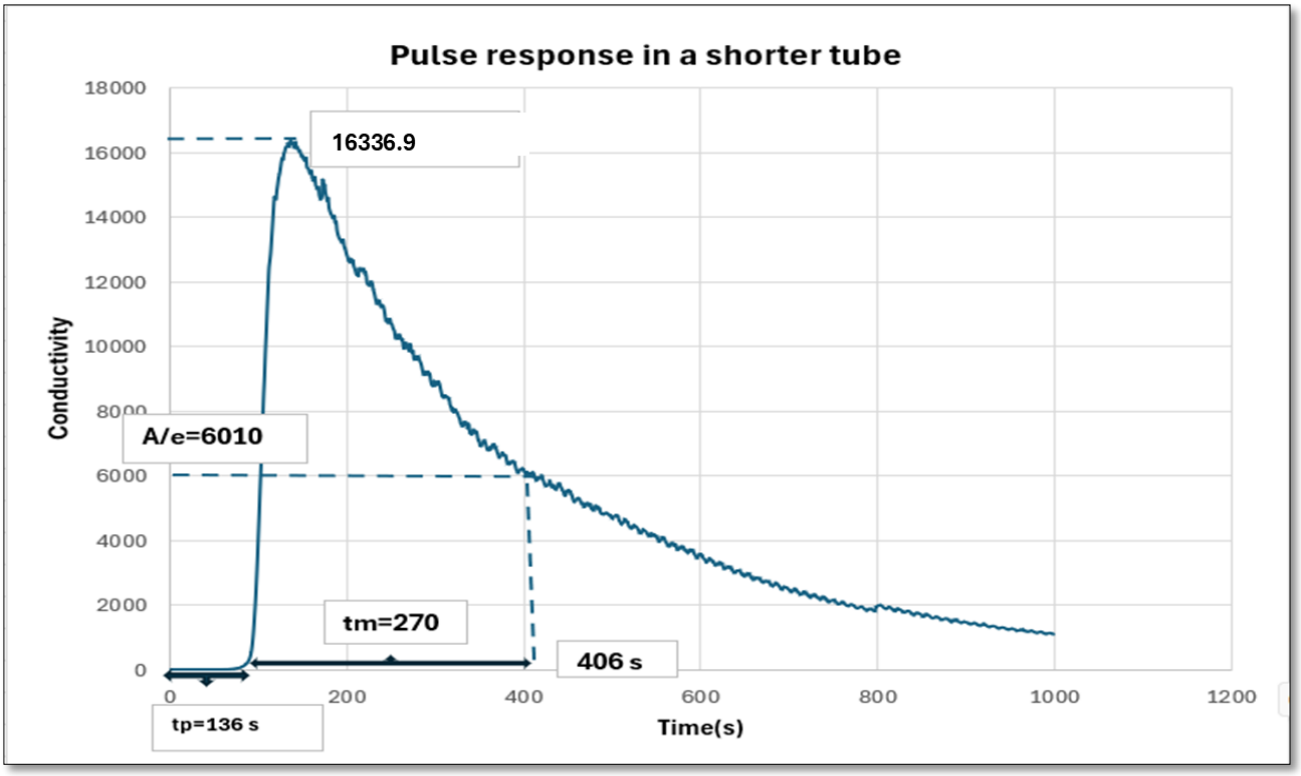

Figure 46 Pulse Response of 2 g/L NaCl Solution (72,290 µS/cm) in a Shorter Tube Length. The system exhibits a peak conductivity of approximately 16,000 µS/cm at ~100 seconds, with a decay phase extending beyond 1000 seconds due to dispersion and dilution effects.

The detection delay in this system was significantly lower than in the 2-metre tube setup, primarily due to reduced axial dispersion and faster ion transport. The time required to reach peak conductivity was approximately 100 seconds, and the system took around 1000 seconds (16.7 minutes) to return to baseline conductivity.

Figure 46 presented the pulse response of the short-tube system, where a 1 mL NaCl solution was injected over a period of 1.5 seconds. The x-axis showed time in seconds, while the y-axis represented conductivity, indicating the concentration response. The graph captured the system's behaviour from the moment of injection through to the conductivity peak and subsequent decay. The conductivity reached a maximum value of 16,336 µS/cm at approximately 136 seconds after injection, marking the time to peak (*tp*). The mean residence time (*tm*) was calculated as 270 seconds, representing the average time the tracer spent in the system. Additionally, the conductivity at the exponential decay level (*A/e*) was recorded as 6010 µS/cm, and the system response returned to near-baseline values after approximately 406 seconds.

This pulse response reflected the fluid transport and dispersion characteristics within the system. The steep initial rise to peak conductivity suggested a rapid transport phase, indicating minimal mixing or a short conduit between injection and detection. The time lag before the peak signified the travel time required for the fluid to move through the system. The gradual decline or long tail following the peak implied the presence of back-mixing or dispersion effects, which may have resulted from tubing coils, internal dead volumes, or minor system irregularities that caused the tracer to linger.

The dead volume of the system, a critical parameter in tracer analysis, was estimated based on the time to peak and the flow rate. In this experiment, the injection volume was 1 mL, delivered over 1.5 seconds, and the flow rate (Q) was maintained at 0.667 mL/s.

$$\tau = V/v = 1/0.667 = 1.499 \text{ s} \tag{42}$$

$$\text{But } \bar{t} \text{ active } = tp + tm = 406 \text{ s} \tag{43}$$

$$\text{Dead time } td = 270 - 136 = 134 \text{ s} \tag{44}$$

$$\text{Plug flow region } (Vp) = 0.667 * 136 = 90.71 \text{ mL} \tag{45}$$

$$\text{Mixed flow region } (Vm) = 0.667 * 270 = 180.0 \text{ mL} \tag{46}$$

$$\text{Dead or stagnant region } = 134 * 0.667 = 89.37 \text{ mL} \tag{47}$$

These results illustrated that significant internal dispersion still occurred, although transport was more rapid in shorter tubes. Thus, a tubing-based continuous flow system could not fully prevent signal smearing even under optimised conditions. These findings definitively confirmed the necessity of implementing a sample-and-hold system, which could rapidly isolate, retain, and analyse discrete fluid volumes without the adverse effects associated with continuous dispersion and dead volume, particularly in regions corresponding to the plug flow region (Equation (45)) and dead or stagnant region (Equation (47)).

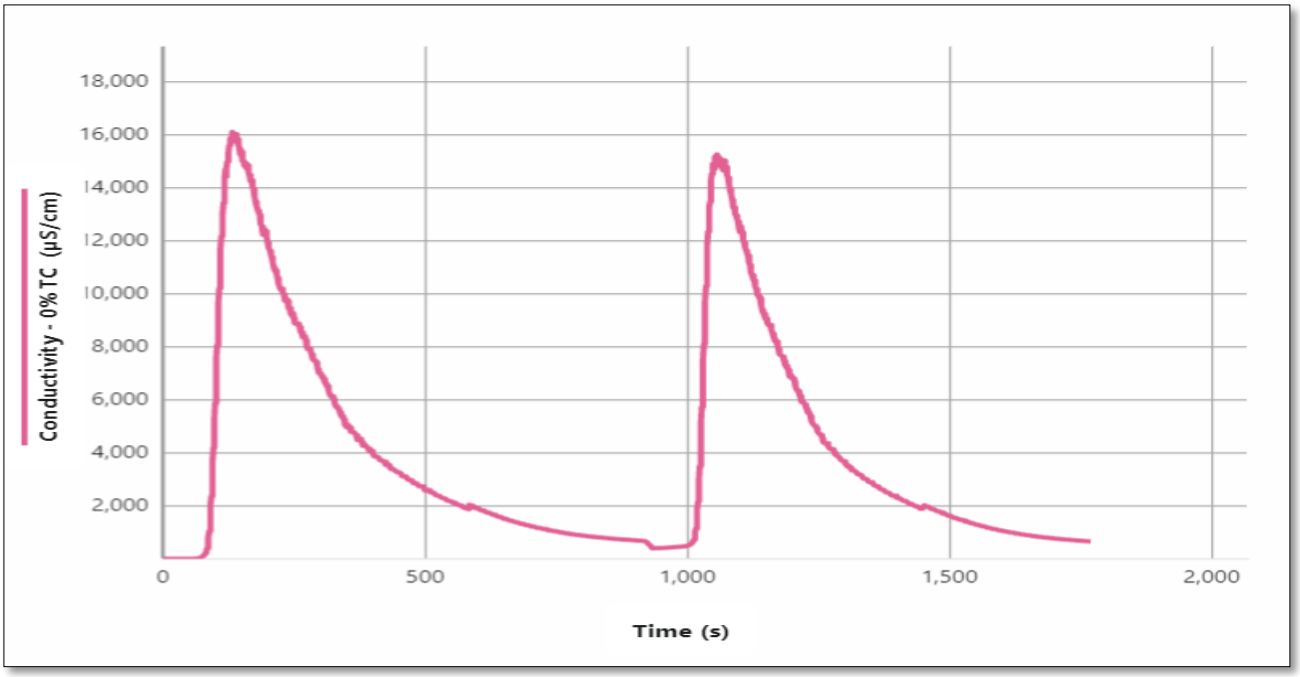

Figure 47 Pulse response for two consecutive injections, showing sharp peaks (plug flow behaviour) and long tails (mixed flow behaviour), indicating a dispersed flow regime.

The system's response to two consecutive tracer injections was evaluated to further assess the internal flow behaviour under reduced tubing conditions. As shown in Figure 47, each injection produced a distinct, sharp peak in conductivity, followed by an extended decay phase returning to baseline levels. The immediate rise in conductivity after each injection suggested a rapid initial transport phase resembling plug flow, whereas the prolonged decay tail reflected significant axial dispersion and back-mixing within the system.

The repetition of similar conductivity profiles for both injections, characterised by consistent peak heights and long decay tails of identical shape, further confirmed that dispersion and back-mixing were stable and intrinsic properties of the system's architecture. These effects reduced the temporal resolution of concentration detection and made it difficult to capture rapid changes in nitrate concentration during capacitive deionisation operation accurately.

Consequently, the use of a single straight tube for real-time monitoring was found to be fundamentally inadequate. Regardless of how much the tube length was reduced, dispersion effects arising from velocity gradients and molecular diffusion could not be eliminated. Therefore, it became necessary to transition towards a sample-and-hold system. This type of system allowed discrete fluid samples

to be isolated and rapidly analysed, bypassing the smearing and tailing effects inherent to continuous flow through both long and short tubing configurations.

Based on the residence time distribution characteristics observed through Levenspiel's tracer theory, the current study decisively demonstrated that a continuous tube-based detection method was unsuitable for rapid, high-fidelity nitrate monitoring. In response to these findings, the next chapter presents the theoretical design and practical implementation of a sample-and-hold system, developed to overcome the inherent limitations of continuous flow detection and to achieve true real-time monitoring performance.

5.4 Conclusion

This chapter demonstrated the practical implementation of the vanadium chloride-based method in a continuous flow cell system for real-time nitrate detection. Building upon the batch validation experiments previously described, the flow cell configuration was designed to operate at 85°C, optimising reaction kinetics for vanadium-mediated nitrate reduction. Through detailed residence time distribution (RTD) analysis and dispersion modelling, it was shown that non-ideal flow effects such as axial mixing significantly impact the accuracy and responsiveness of online measurement systems. To address these limitations, system parameters including tubing length, flow rate, and internal volume were optimised to improve detection resolution and reduce lag time. Experimental validation using step and pulse tracer injections confirmed the theoretical predictions, revealing dispersion coefficients and delay patterns critical to achieving high-fidelity nitrate concentration profiles.

The success of the flow cell design confirmed the feasibility of integrating vanadium chloride chemistry with UV-Vis absorbance-based detection in a continuous monitoring framework. However, limitations related to delayed signal response and the need for thermal equilibrium highlighted the necessity for an improved flow control architecture. These challenges led to developing a sample-and-hold design allowing for discrete sampling, thermal conditioning, and synchronised detection in a controlled sequence. The following chapter explores the design, fabrication, and evaluation of this sample-and-hold system, addressing the shortcomings of continuous flow by introducing parallel sampling strategies and valve-controlled measurement intervals to enhance temporal resolution and stability.

6 DESIGN OF VANADIUM CHLORIDE SAMPLE-AND-HOLD SYSTEM FOR CONTINUOUS NITRATE MEASUREMENT

This chapter details the design of a Sample-and-Hold system for continuous nitrate measurement based on the insight gained from the study of non-ideal flow characteristics within the flow cell reactor of the previous chapter.

The proposed system leverages real-time absorbance analysis and residence time control to address the inherent challenges of online nitrate measurement subject to the transient characteristics of CDI operation. These transient characteristics, detailed in Chapter 3, include the predicted nitrate concentration profile during repeated adsorption-desorption cycles and associated minimum/maximum concentration. These insights guided the design of the Sample-and-Hold system detailed in this chapter. Additional work covered in this chapter includes the design and validation of the interface to the real CDI process.

Following the details of the system's design, three sets of experiments were performed, including the analysis of tracer response using the dispersion model and tracer response from the sample-and-hold reactor operated under simulated process conditions.

6.1 Introduction- Sample-and-Hold Design as a Semi-Batch Reactor

The initial nitrate detection setup employed a continuous flow-through reactor comprising a long tube, which was designed to provide sufficient residence time for the vanadium chloride reaction to proceed at an elevated temperature of 85°C. Although this configuration enabled adequate colour development, it introduced significant delays in the detection response. The nitrate-containing solution required several minutes to pass through the heated segment of the tubing before reaching the UV-Vis spectrophotometer. Experimental observations revealed that the signal response was delayed and attenuated due to axial dispersion along the tube length. These limitations hindered the ability to synchronise nitrate concentration measurements with the rapid concentration fluctuations that characterised the adsorption and desorption cycles of the capacitive deionisation (CDI) system.

To overcome these challenges, a sample-and-hold system was introduced. This design functioned as a semi-batch reactor, in which discrete volumes of the effluent were collected in multiple isolated tubes rather than being continuously passed through a single channel. The key advantage of this

approach lies in its ability to preserve the concentration profile at a specific time point. Each tube effectively held a snapshot of the nitrate concentration from the CDI outlet, allowing the chemical reaction and spectrophotometric measurement to proceed under controlled and consistent conditions. This configuration mitigated the temporal smearing and response delay observed in the continuous flow system and enabled more accurate and timely data acquisition.

Initially, a design incorporating twenty sample tubes was considered. However, the construction of a twenty-port sample manifold proved to be impractical due to the complexity of fabrication, the increased potential for mechanical failure, and the difficulty of ensuring uniform flow distribution.

After evaluating the technical limitations, a revised design employing seven sample tubes was selected. This decision was supported by experimental optimisation of the reaction conditions. By increasing the reaction temperature to 85°C and fine-tuning the reagent ratios, the vanadium chloride reduction and colour development processes were successfully completed within a two-minute window. As a result, it became feasible to cycle through seven sample tubes in a rotating sequence, with each tube undergoing one minute of heating followed by one minute of cooling. This arrangement produced a functional sampling interval of approximately two minutes, which proved sufficient to capture the key features of the CDI effluent concentration profile.

The operating sequence of the seven-port sample-and-hold system followed a carousel-like rotation. When the first tube was filled with nitrate solution, it was immediately transferred to the heating zone, where it was maintained for one minute. During this heating period, the second tube began to fill. Once the heating of the first tube was complete, it was moved to the cooling zone for one minute, while the third tube entered the filling stage and the second tube progressed to the heating phase. When the second tube transitioned to the cooling phase, the first tube was directed to the UV-Vis spectrophotometer for nitrate detection. At that point, the third tube advanced to the heating stage, and the fourth tube began filling. This rotating cycle continued through all seven tubes, enabling a continuous and coordinated sampling regime. The system maintained a consistent flow pattern and ensured that each sample received equal and sufficient reaction time, thereby enabling reliable detection of nitrate concentration. Similar sequential sample-handling strategies were reported in automated nitrate monitoring systems employing rotary valves and integrated heating units for time-resolved concentration capture, demonstrating comparable cycle-driven designs (Fang et al., 2019).

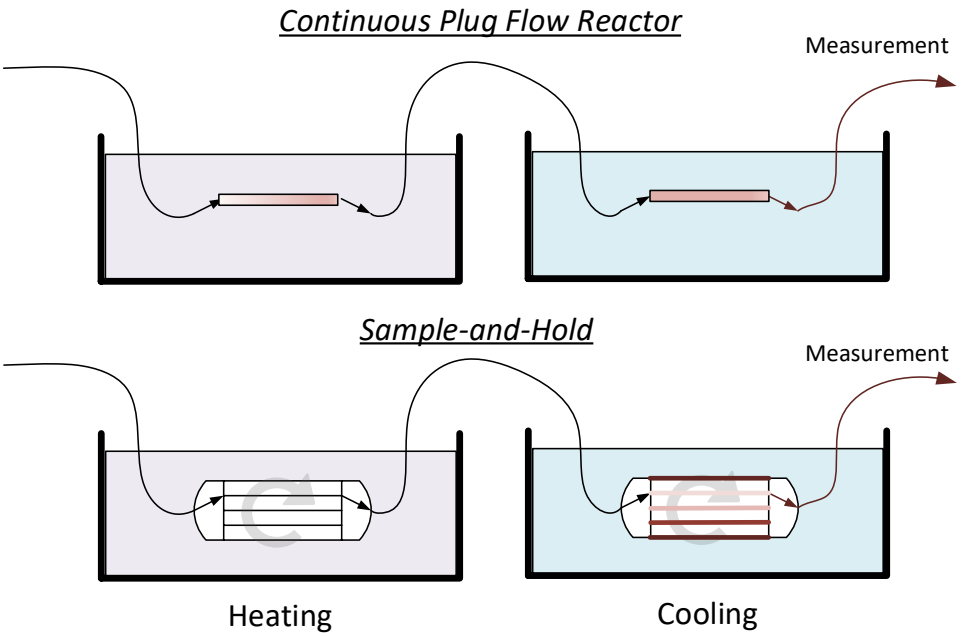

Figure 48 Schematic comparison of continuous plug flow and sample and hold systems for nitrate detection with heating, cooling, and measurement stages.

This sample-and-hold configuration achieved a significant improvement in measurement accuracy and responsiveness, as illustrated in Figure 48. It eliminated the temporal distortion associated with long tubular reactors and facilitated accurate, time-resolved concentration measurements that were aligned with the rapid kinetics of the CDI system. Recent studies highlighted the importance of real-time nitrate monitoring systems for tracking rapid nutrient fluctuations in aquatic environments, demonstrating the growing demand for high-frequency and field-deployable technologies (Mahmud et al., 2020; Pellerin et al., 2016). The decision to implement a seven-port rather than a twenty-port configuration reflected a deliberate balance between the desired temporal resolution and practical feasibility. This approach ensured the successful operation of a reliable and reproducible nitrate detection system while maintaining simplicity and robustness in the design.

6.2 Interfacing the VS3 CDI System to the Online Flow Cell System

6.2.1 Methodology

The experiment aimed to detect nitrate from a capacitive deionisation (CDI) system using the VS-3 module, which employed activated carbon electrodes integrated with anion and cation exchange membranes (mCDI). The key objective was to address the challenge of detecting nitrate at the CDI

outlet, which was complicated by the system's rapid adsorption and desorption cycles. The detection method utilised vanadium chloride reduction in conjunction with the Griess reaction, followed by nitrate concentration analysis using a MATLAB-based interpolation system. Figure 49 presents the complete experimental setup, including the CDI unit, the dilution section, and the nitrate detection system.

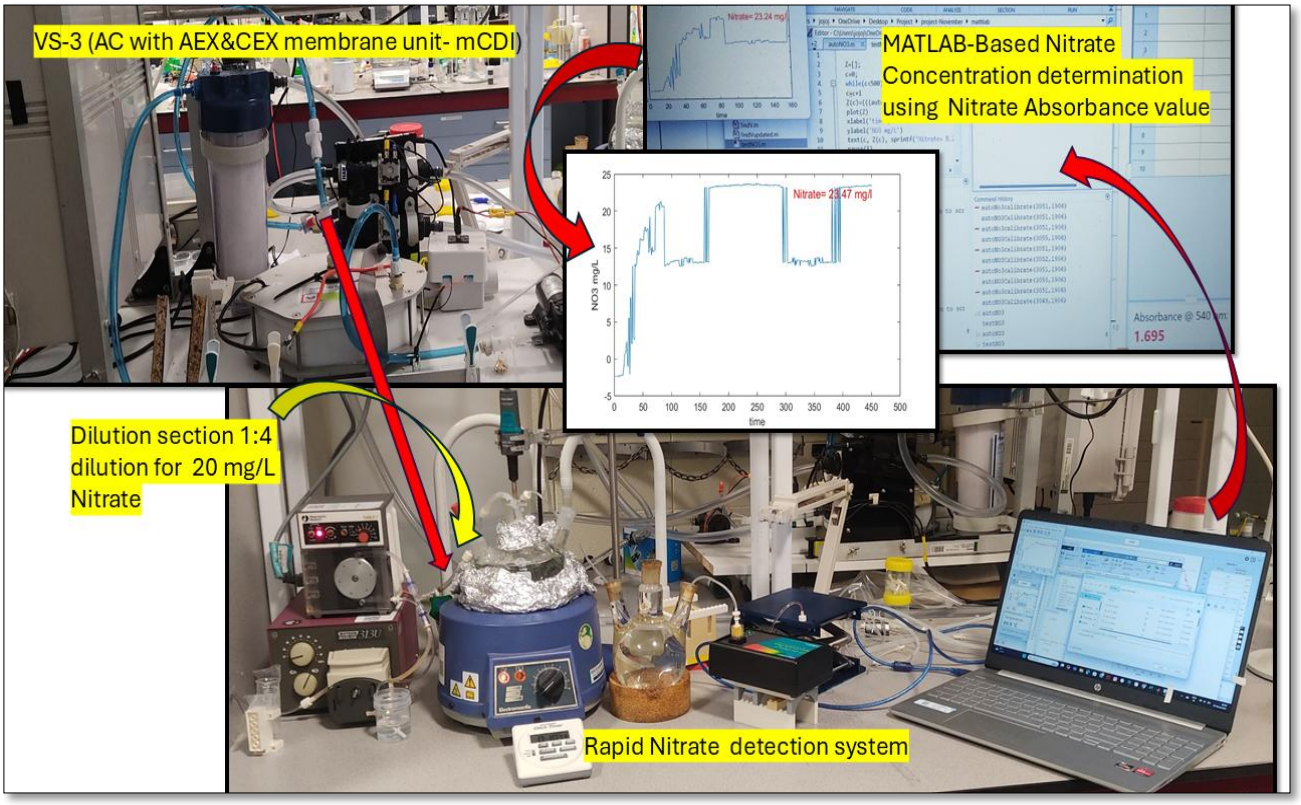

Figure 49 Experimental setup for nitrate detection from the VS-3 (AC with mCDI) unit, showing the dilution section (1:4 dilution for 20 mg/L nitrate), rapid nitrate detection system, and MATLAB-based nitrate concentration analysis using absorbance values

6.2.2 Experimental Setup

The experimental setup comprised the VS-3 mCDI unit, a dilution section, and a rapid nitrate detection system. As depicted in Figure 49, the CDI unit utilised anion exchange (AEX) and cation exchange (CEX) membranes to facilitate selective ion adsorption. To achieve a 1:4 dilution and reduce the 20 mg/L nitrate solution to 5 mg/L, the dilution section blended 0.198 mL/min of the VS-3 nitrate adsorption outlet with 0.577 mL/min of Milli-Q water, resulting in a total flow rate of 0.77 mL/min. To reach a conductivity of 2500 µS/cm, additional NaCl was added to the sodium nitrate and Milli-Q water mixture during the preparation of the 20 mg/L nitrate stock solution. This

adjustment simulated real water conditions and enhanced ion mobility, enabling more accurate analysis of CDI performance.

6.2.3 Results

The detection system used vanadium chloride (VCl_3) to reduce nitrate (NO_3^-) to nitrite (NO_2^-), which then reacted with sulphanilamide and NED to produce a pink-coloured azo dye. Absorbance at 540 nm was recorded by the UV-Vis spectrophotometer and analysed using MATLAB, as shown in the display in Figure 50.

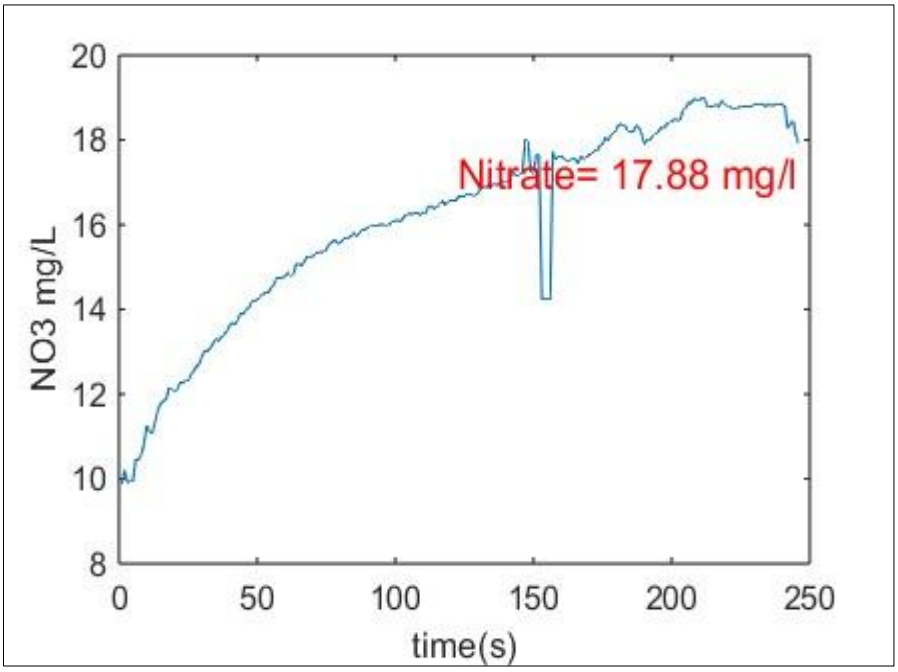

Figure 50 MATLAB-based interpretation of nitrate concentration over time(seconds) from the VS-3 (AC with mCDI) unit, showing a gradual increase to 17.88 mg/L with minor fluctuations during the detection process.

Flow rates were optimised to ensure measurement precision, with VCl_3 delivered at 0.64 mL/min and the nitrate sample at 0.77 mL/min. The spectrophotometric nitrate detection method, based on vanadium (III) chloride and Griess reagents, followed a well-established protocol that enabled sensitive, single-reagent colorimetric analysis of nitrate, even at low concentrations (Doane & and Horwáth, 2003).

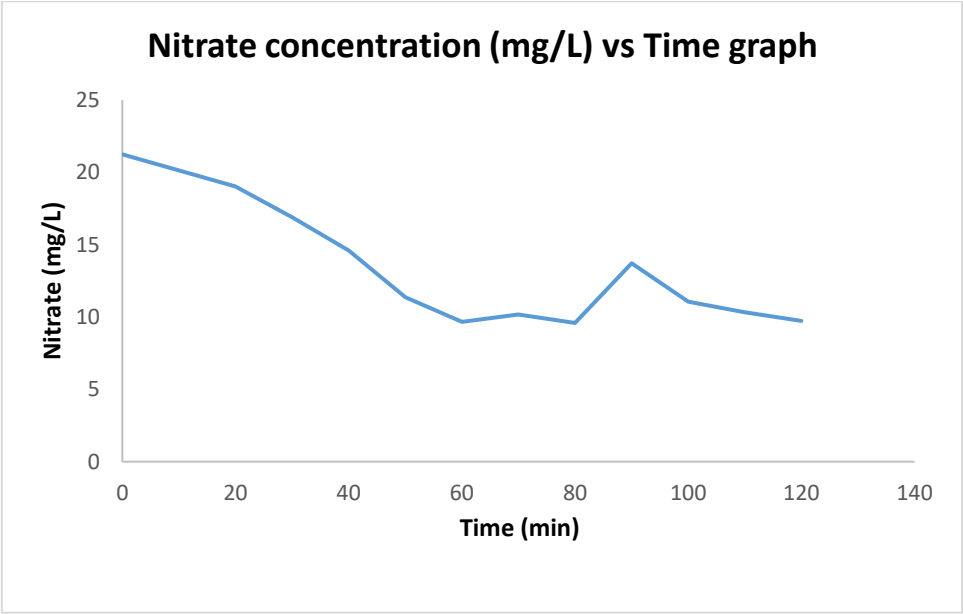

Figure 51 Nitrate concentration over time from the VS-3 mCDI unit, showing removal efficiency trends and operational fluctuations.

Figure 51 showed the nitrate concentration measured from samples collected at the storage tank associated with the VS-3 mCDI unit. At each time point, a sample was manually extracted and tested in the laboratory using a UV-Vis spectrophotometer. The graph illustrated a steady decline from approximately 21 mg/L at 0 minutes to 10 mg/L at 60 minutes, followed by a sharp spike around 90 minutes and gradual stabilisation near 10 mg/L. This pattern reflected the adsorption and desorption behaviour during CDI operation.

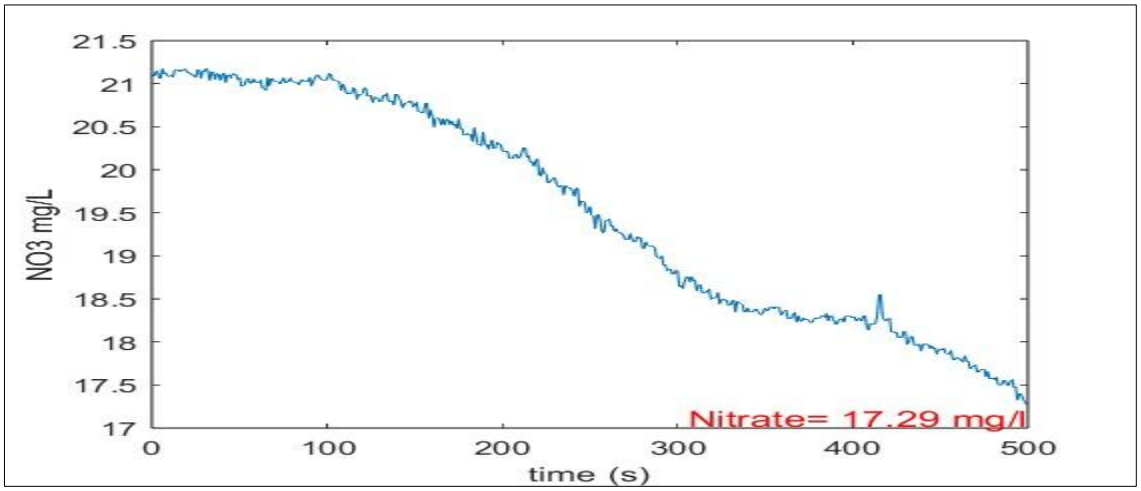

Figure 52 MATLAB-derived nitrate concentration profile showing a final reading of 17.29 mg/L, indicating potential carry-over effects.

Figure 52 presented MATLAB-derived nitrate concentrations, which recorded a final reading of 17.29 mg/L . This value was inconsistent with the measurements shown in Figure 51, indicating the presence of carry-over effects. These effects occur when residual nitrate from previous cycles influences subsequent measurements.

Carry-over refers to the unintended transfer of analytes or residues from one sample to the next within an analytical system. This can result in contamination and inaccurate readings. The phenomenon is particularly common in continuous flow analysis, where substances remaining from a prior sample may interfere with the analysis of the following sample. To quantify this effect, Zhang (1997) introduced the carry-over coefficient (k_o), which measures the extent of contamination between successive samples. Accurate determination of k_o is important for evaluating the reliability of an analytical method and for applying corrective strategies that minimise cross-sample interference (Zhang, 1997).

Calculation of the Carry-Over Coefficient

The carry-over coefficient (k_o) is calculated using the formula (Equation (48)):

$$k_o = (A_i - A_{i+1}) / A_{i-1} \quad (48)$$

Values from MATLAB Graph (300-400 seconds)

A_{i-1}- Previous sample absorbance=18.9 mg/L

A_i-Current sample absorbance=19.2 mg/L

A_{i+1}- Next sample absorbance=18.4 mg/L

$$Ko = (19.2 - 18.4) / 18.9 = 0.8 / 18.9 = 0.0423 \quad (49)$$

The calculated carry-over coefficient is 0.0423, indicating a 4.23% carry-over effect (Equation (49)). This residual contamination accounts for the slower decline and spike in MATLAB results compared to the expected trend. To mitigate carry-over, Zhang (1997) advises extending wash cycles, using air-segmentation to isolate samples, and adding debubblers to eliminate trapped gas. Implementing these

strategies will reduce cross-sample contamination and align MATLAB results with expected outputs, ensuring accurate nitrate detection (Zhang, 1997).

The study successfully demonstrates the effectiveness of capacitive deionisation (CDI) for rapid online nitrate detection and removal, supported by Stella model simulations and experimental analysis using the VS-3 mCDI system. The CDI system exhibited stable adsorption-desorption cycles, with consistent nitrate removal rates and efficient system operation. Additionally, the nitrate detection method using vanadium chloride reduction and MATLAB analysis highlighted the challenges of carry-over effects, which influenced measurement accuracy. Similar spectrophotometric systems have recently been developed for automated, low-cost continuous monitoring of nitrate concentrations in environmental waters, validating the feasibility and accuracy of such absorbance-based setups for field deployment (Bulusu et al., 2024). The carry-over coefficient calculation provided insight into cross-sample contamination, enabling recommendations for reducing interference. Overall, the findings confirm that CDI is a viable and efficient solution for nitrate detection and removal when optimised with proper flow rates, cycle timing, and wash protocols. This research contributes valuable knowledge for improving real-time water quality monitoring and advancing sustainable water treatment technologies.

6.3 Design and Fabrication of the 3D-Printed Sample Holder

A 3D-printed resin-based sample holder was designed to maintain sample integrity during controlled heating and cooling. The holder accommodated seven tubes, which allowed for the sequential injection of different solutions for nitrate detection. The heating and cooling sections were optimised to minimise temperature fluctuations and to ensure consistent reaction conditions. Resin was selected as the construction material due to its chemical resistance, providing durability when exposed to vanadium chloride and nitrate solutions. The precise alignment of the tubes ensured uniform flow distribution, while the modular structure of the holder allowed for easy adjustments and cleaning. A key feature of this design was its configuration with a single inlet and seven outlets, which enabled even sample distribution across separate paths for independent analysis.

The 3D-printed holder was fabricated using high-resolution stereolithography (SLA) printing, which ensured precision in tube alignment and minimised the risk of leakage. The ability to customise the tubes' length, diameter, and arrangement provided flexibility for a range of experimental conditions, allowing researchers to optimise both flow rates and sample retention times. The resin's chemical-

resistant properties contributed to the system's longevity and reliability in continuous monitoring applications, making the design suitable for extended operational use.

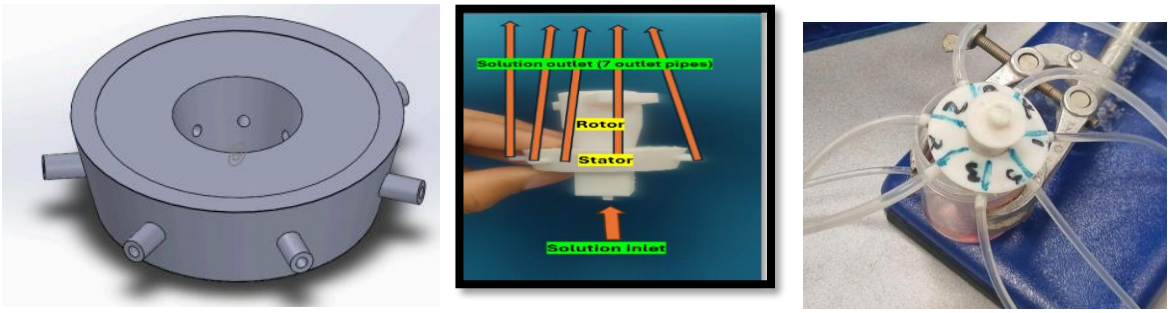

Figure 53 3D-printed sample holder (left) with a single solution inlet and seven outlet tubes (centre), the rotor aligns with the selected numbered outlet port thus connecting it to the solution inlet (right).

The sample holder (Figure 53) consisted of a rotor and stator assembly, which controlled the flow of the fluid. The solution entered through a single inlet, where the stator directed the flow towards the rotor mechanism. The rotor ensured even distribution of the sample into seven outlet tubes, allowing for controlled sample division. This mechanism prevented cross-contamination and maintained uniform reaction times across all outlets. Additionally, the controlled sample retention time in each tube enhanced measurement accuracy and consistency by reducing variations in flow rates and improving detection reliability.

The sample holder's modular structure played a critical role in maintaining consistent reaction conditions for nitrate detection. The design enabled independent or sequential processing of different solutions, making it an efficient system for real-time analysis. This adaptability made the system particularly suitable for high-precision environmental and industrial monitoring applications, where accurate nitrate detection was essential.

6.3.1 Performance Evaluation for Continuous Monitoring

The objective of this experiment was to evaluate the performance of an online nitrate detection system integrated with capacitive deionisation (CDI). The system was designed to provide accurate, continuous monitoring by incorporating a 3D-printed sample holder and a sample-and-hold method. This investigation aimed to assess the system’s efficiency in maintaining stable absorbance measurements over time, while minimising errors caused by the rapid nitrate removal cycles characteristic of CDI operation.

6.3.1.1 Materials and Equipment Used

The experiment utilised a 3D-printed resin-based sample holder, seven 1.5-metre-long tubes, a UV-VIS spectrometer, food dye solutions, syringes for injecting samples and a digital weigh balance. The sample holder (SH) was designed to provide precise control over sample flow, while the tubing ensured consistent retention times. The UV-VIS spectrometer was used to measure absorbance values, and the food dye solutions served as simulants for nitrate samples. Syringes were employed to deliver fixed injection volumes, and to ensure volume accuracy, each injection was verified using a digital weigh balance by measuring the mass of the solution dispensed. This approach enhanced the reproducibility and accuracy of the experiment by confirming that the correct millilitre amount was injected during each trial. Each component played a vital role in ensuring the overall experimental procedure's consistency, reliability, and accuracy.

6.3.1.2 Experimental Setup and Methodology

The purpose of this experiment was to simulate the transient nitrate concentration variations typically observed during a capacitive deionisation (CDI) cycle, particularly focusing on the desorption and adsorption phases. These dynamic characteristics are evidenced by an initial rise in nitrate concentration, followed by a controlled decline, as represented in the absorbance profile shown in Figure 56.

The experimental setup consisted of seven dye solutions, each prepared to mimic different nitrate concentrations by producing specific absorbance values. Each dye solution was loaded into a separate 1.5-metre-long tube, resulting in seven parallel paths for the sample flow. Using syringes, precise volumes of 3 mL, 4 mL, or 6 mL were manually injected into each tube within an 8–10 second window. This controlled injection duration allowed the flow rate (mL/s) calculation for each case, ensuring that the sample reached the detector under conditions that closely resemble real CDI desorption and adsorption transitions. To confirm volume accuracy, the mass of each injected sample was verified using a digital weigh balance connected at the outlet after the UV-Vis spectrophotometer.

Before beginning the experiment, the system was carefully primed. Priming involved filling all syringes with their respective dye solutions and pre-conditioning the flow paths with DI water to ensure baseline stability on the spectrophotometer. Special attention was given to minimising the internal volume of the 7-way inlet junction. A low internal volume was critical because excessive dead volume would cause sample mixing and dispersion before the spectrophotometer, thus blurring

the step changes between different dye concentrations. Minimising internal volume ensured sharp transitions in absorbance readings, closely resembling ideal plug flow conditions, which are necessary for validating the system's ability to accurately track rapid concentration fluctuations. Related studies have emphasised the importance of minimising dead volume and optimising fluid path architecture for maintaining absorbance fidelity in nitrate monitoring systems employing flow injection analysis with premixed Griess reagents (Pai et al., 2021).

The detailed step-by-step procedure for sample injection and switching is outlined in Table 7. Each step involved pushing a specific dye solution into the system, followed by systematically switching the valve position to connect the next tube. This rotation allowed each dye sample to pass sequentially through heating and cooling phases before reaching the UV-Vis spectrophotometer for absorbance measurement.

Table 7 Stepwise experimental procedure for sequential dye injection, valve switching, and absorbance measurement in the sample-and-hold nitrate detection system, simulating desorption, and adsorption cycles.

Step	Name	Function	State Change
1	Priming	Introducing DI-Water into reactor	Manual dispensing of syringe zero until baseline reading obtained on spectrophotometer
2	Push Solution 1	Introducing 0.5mg/L (Nitrate equivalent absorbance solution) solution into reactor	Manual dispensing "Push" of syringe 1 (Syr1) until 3,4 or 6 mL observed on digital weigh balance
3	Valve Change 1	Multiport selector set to reactor two	SH1 to position 2 (P2) and SH2 to position (P2)
4	Push Solution 2	Introducing 1.0mg/L solution (Nitrate equivalent absorbance solution)	Push Syr2 until 3,4 or 6mL observed
5	Valve Change 2	Multiport selector set to reactor three	SH1 to P3 and SH2 to P3
6	Push Solution 3	Introducing 1.6mg/L solution (Nitrate equivalent absorbance solution)	Push Syr3 until 3,4 or 6mL observed

7	Valve Change 3	Multiport selector set to reactor four	SH1 to P4 and SH2 to P4
8	Push Solution 4	Introduce 3.0mg/L solution (Nitrate equivalent absorbance solution)	Push Syr4 until 3,4 or 6mL observed
9	Valve Change 4	Multiport selector set to reactor five	SH1 to P5 and SH2 to P5
10	Push Solution 5	Introduce 3.5mg/L solution (Nitrate equivalent absorbance solution)	Push Syr5 until 3,4 or 6mL observed
11	Valve Change 5	Multiport selector set to reactor six	SH1 to P6 and SH2 to P6
12	Push Solution 6	Introduce 4.0mg/L solution (Nitrate equivalent absorbance solution)	Push Syr6 until 3,4 or 6mL observed
13	Valve Change 6	Multiport selector set to reactor seven	SH1 to P7 and SH2 to P7
14	Push Solution 7	Introduce 5.0mg/L solution (Nitrate equivalent absorbance solution)	Push Syr7 until 3,4 or 6mL observed
15	Valve Change 7	Multiport selector set to reactor six	SH1 to P6 and SH2 to P6
16	Push Solution 6	Introduce 4.0mg/L solution (Nitrate equivalent absorbance solution)	Push Syr6 until 3,4 or 6mL observed
17	Valve Change 6	Multiport selector set to reactor five	SH1 to P5 and SH2 to P5
18	Push Solution 5	Introduce 3.5mg/L solution (Nitrate equivalent absorbance solution)	Push Syr5 until 3,4 or 6mL observed
19	Valve Change 5	Multiport selector set to reactor four	SH1 to P4 and SH2 to P4

20	Push Solution 4	Introduce 3.0mg/L solution (Nitrate equivalent absorbance solution)	Push Syr4 until 3,4 or 6mL observed
21	Valve Change 4	Multiport selector set to reactor three	SH1 to P3 and SH2 to P3
22	Push Solution 3	Introducing 1.6mg/L solution (Nitrate equivalent absorbance solution)	Push Syr3 until 3,4 or 6mL observed
23	Valve Change 3	Multiport selector set to reactor two	SH1 to P2 and SH2 to P2
24	Push Solution 2	Introducing 1.0mg/L solution (Nitrate equivalent absorbance solution)	Push Syr2 until 3,4 or 6mL observed
25	Valve Change 2	Multiport selector set to reactor one	SH1 to P1 and SH2 to P1
26	Push Solution 1	Introducing 0.5mg/L solution (Nitrate equivalent absorbance solution) into reactor one	Manual dispensing of syringe one until 3,4 or 6mL observed on balance

In a representative example using 4 mL injection volume, the sequence proceeded as follows: a 4 mL sample was injected into *Tube 1*, where it underwent 1-minute heating. After heating, a second 4 mL sample was injected into *Tube 2*, and so forth until all seven tubes were filled. By the time the system completed one rotation, the first tube's sample had moved to the cooling phase for 1 minute. During cooling, another sample injection into *Tube 1* began the next cycle. After cooling, the sample was directed towards the UV-Vis spectrophotometer for absorbance measurement. This cyclic and structured operation ensured that every sample consistently underwent identical heating, cooling, and measurement steps, reducing experimental error and enhancing reproducibility.

Figure 54 shows the schematic diagram of the sample-and-hold system designed with seven parallel reactors for sequential dye injection through 1.5-metre tubes.

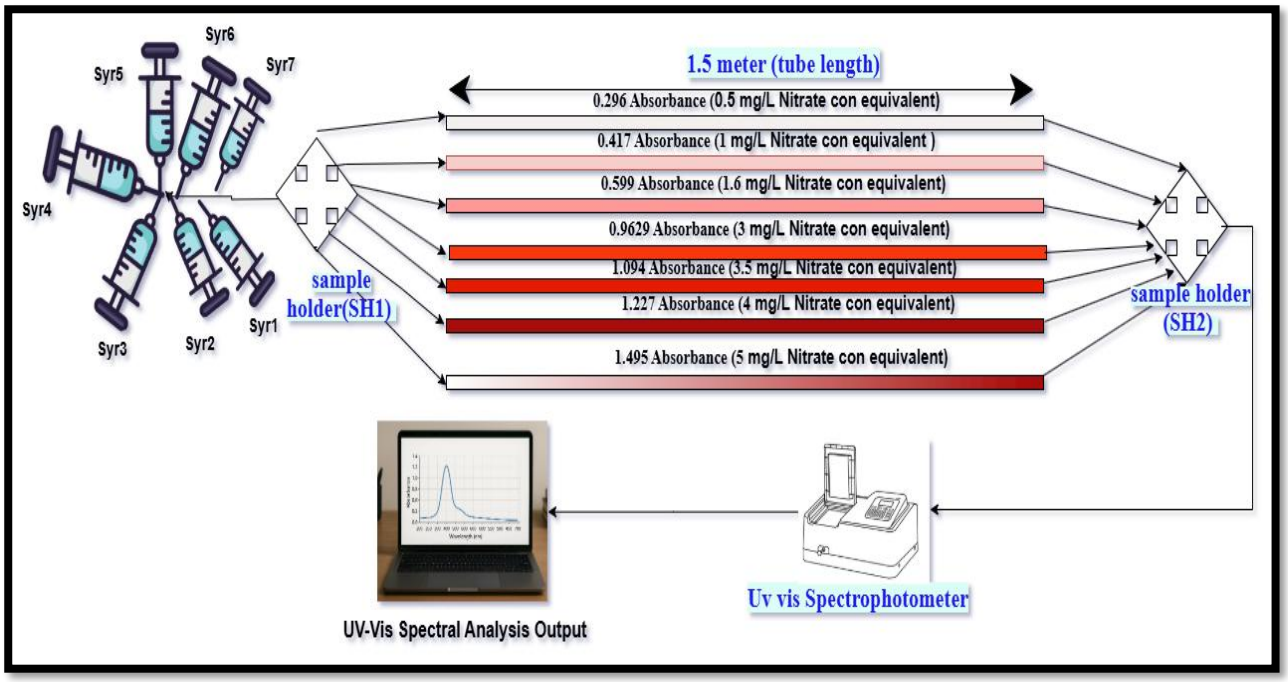

Figure 54 Schematic diagram illustrating the absorbance detection system using sequential dye injection through seven separate 1.5-metre tubes, leading to UV-Vis spectrophotometric analysis.

The experimental setup of the 3D-printed sample holder used in the lab is shown in Figure 55, demonstrating its role in enabling quick tube switching and maintaining consistent flow.

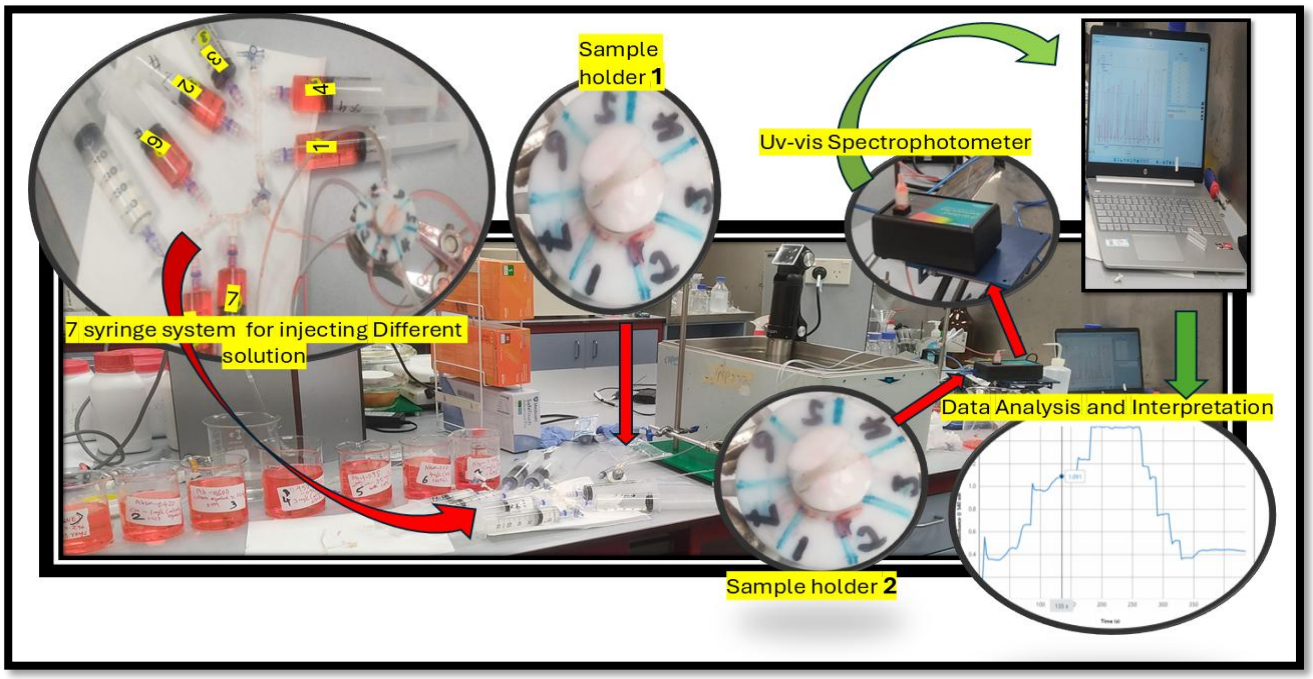

Figure 55 Photograph of the experimental setup showing the 3D-printed sample holder, syringe array, tubing connections, heating-cooling stages, and UV-Vis spectrometer interface used for nitrate detection

The measured absorbance values for each dye at 540 nm are summarised in Table 8, which correlates absorbance with nitrate-equivalent concentrations ranging from 0.5 mg/L to 5.0 mg/L. These values were carefully selected to represent a realistic range of nitrate concentrations encountered during CDI operation.

Table 8 Absorbance values of seven different dye solutions at 540 nm and their corresponding nitrate equivalent concentrations, used for reproducibility validation in the sample and hold method.

Dye Solution	Absorbance @ 540 nm	Nitrate Equivalent Concentration (mg/L)
Dye-1	0.296	0.5 mg/L
Dye-2	0.417	1 mg/L
Dye-3	0.599	1.6 mg/L
Dye-4	0.962	3 mg/L
Dye-5	1.094	3.5 mg/L
Dye-6	1.227	4 mg/L
Dye-7	1.495	5 mg/L

To validate system performance, the experimental absorbance versus time profile shown in Figure 56 was used to simulate the expected concentration dynamics. The absorbance graph exhibited a stepwise increase followed by a corresponding decrease, reflecting the sequence of dye injections. Each plateau on the graph represented a stable absorbance reading for a given nitrate-equivalent concentration. The sharp transitions between steps confirmed the system's ability to resolve sudden concentration changes with minimal dispersion.

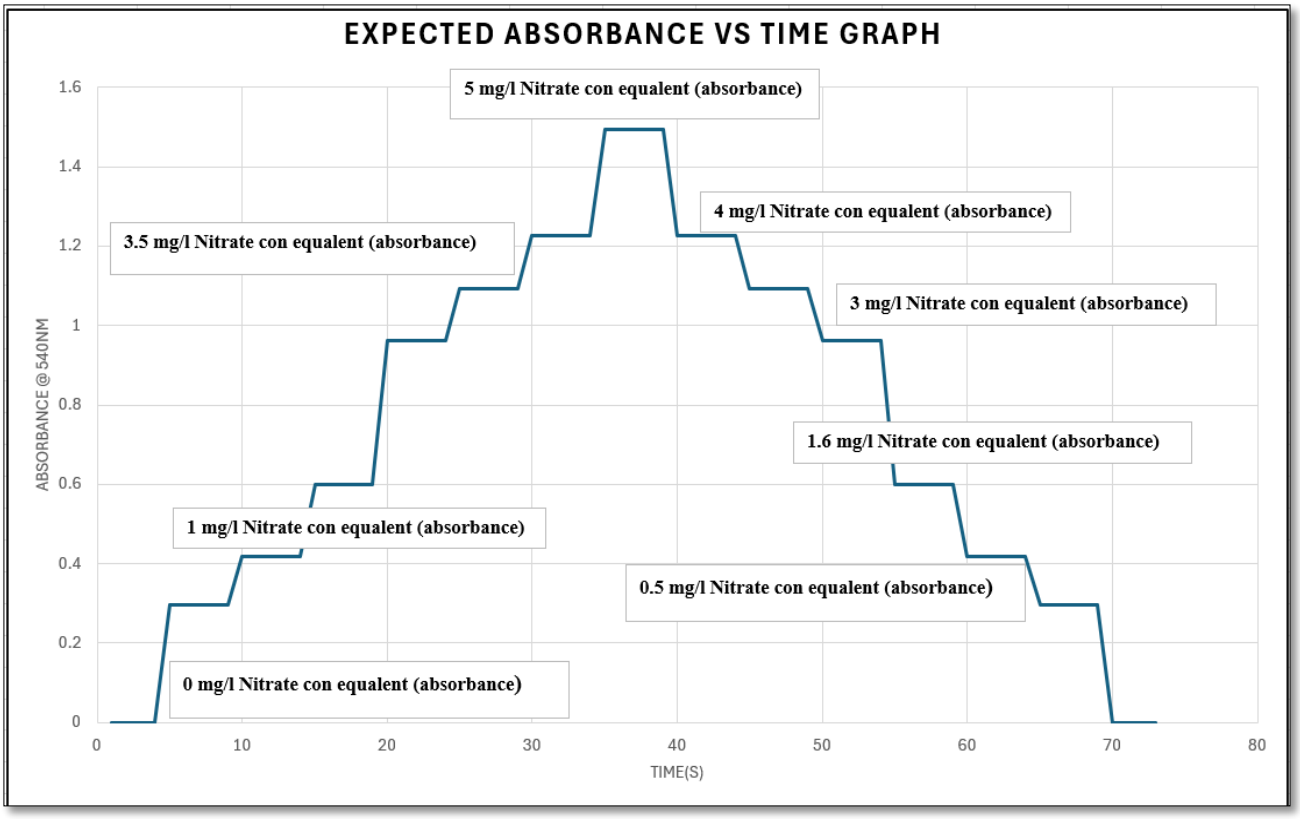

Figure 56 Expected absorbance vs. time graph during CDI desorption (increase in concentration) and adsorption (decrease in concentration), showing stepwise absorbance changes for different nitrate concentrations, attempting to validate system accuracy and stable measurement control.

This methodology demonstrated that the sample-and-hold system was capable of reliably producing sharp and stable absorbance signals, effectively validating its suitability for real-time nitrate detection in rapidly fluctuating environments such as those observed during CDI adsorption and desorption cycles. Overall, the careful design of injection protocols, priming procedures, low-dead-volume junctions, and coordinated heating and cooling scheduling provided a robust foundation for high-accuracy and reproducible online nitrate monitoring.

6.3.1.3 Data Analysis and Interpretation

The data analysis and interpretation for this experiment involved a detailed examination of absorbance values obtained from different sample injection volumes. Three methods were evaluated using 3 mL, 4 mL, and 6 mL injections, each presenting distinct advantages and limitations. The 6 mL method produced higher absorbance peaks but also exhibited greater fluctuations, suggesting that larger volumes introduced inconsistencies due to extended heating and cooling durations. In contrast, the 3 mL method yielded more stable initial readings but demonstrated signal decay over time,

indicating that smaller volumes might not sustain stability during prolonged cycling. The 4 mL injection method emerged as the optimal configuration, providing a balanced performance in terms of stability and accuracy. Absorbance values obtained from this method consistently aligned with expected nitrate concentrations, confirming its suitability for reliable and reproducible measurements in the sample-and-hold system.

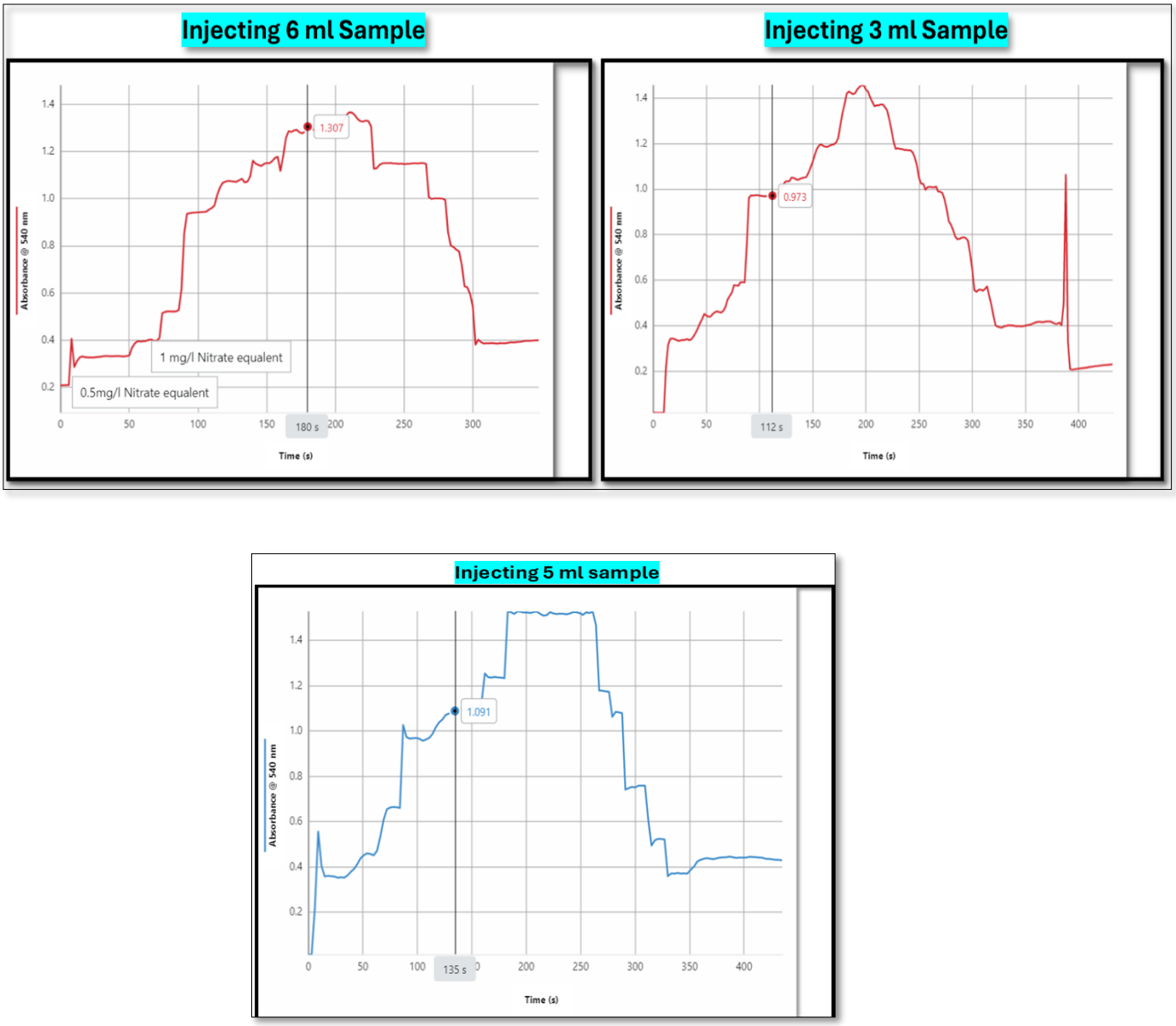

Figure 57 graph highlighting the comparison of 6 mL (a) ,3 mL (b) and 5 ml (c) sample injection methods in terms of stability and peak absorbance.

The comparison of Figure 57 and Figure 58 demonstrated that precise volume control was essential for accurate nitrate detection. Statistical tools, including standard deviation and coefficient of variation, were employed to assess the reproducibility of each injection method. The 4 mL method

exhibited the lowest standard deviation and the highest reproducibility, establishing it as the preferred choice for continuous monitoring in CDI systems. The data also revealed challenges such as minor signal noise and variations in heating efficiency. These issues were effectively mitigated through precise sample handling and consistent injection timing.

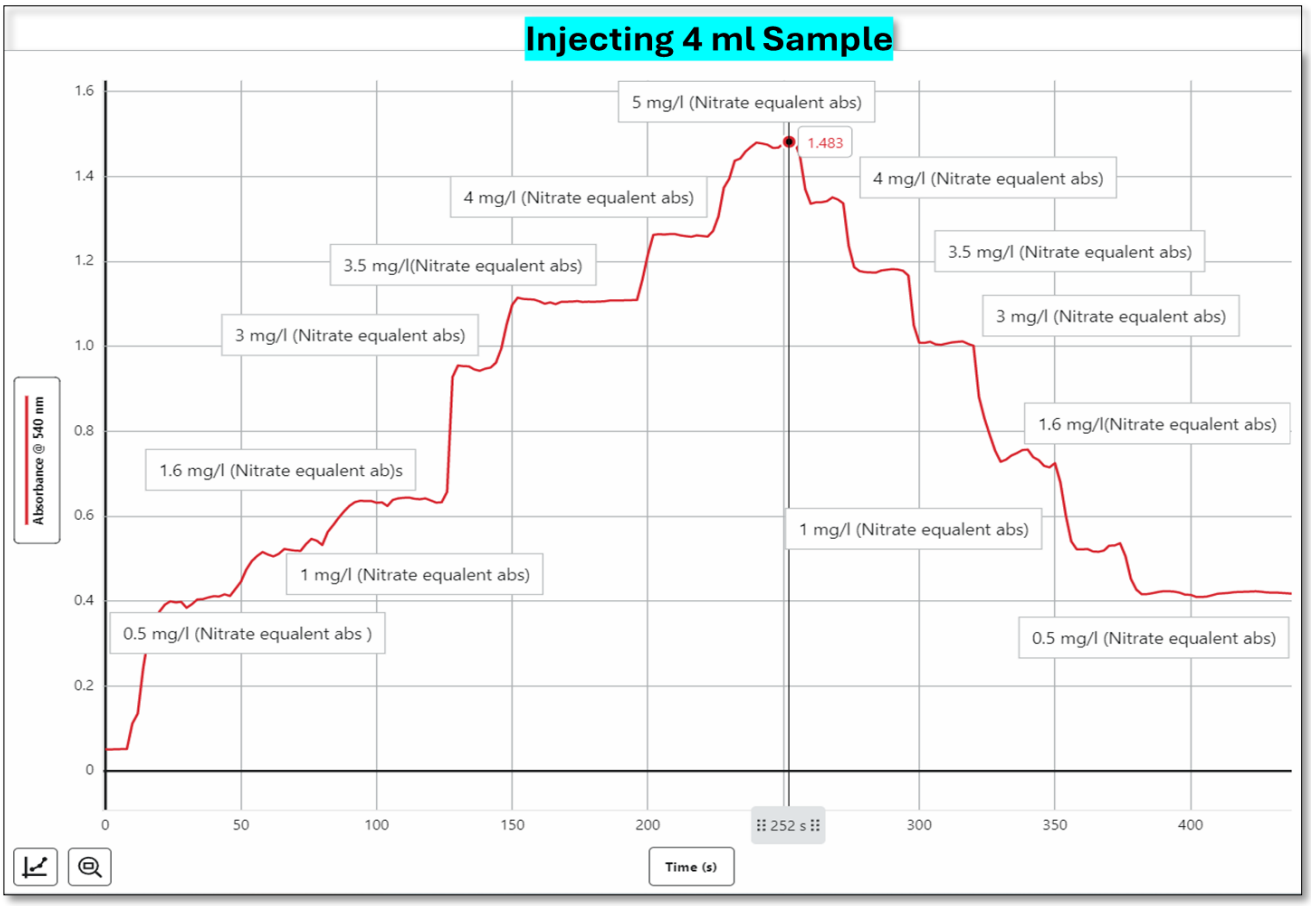

Figure 58 Absorbance vs. Time for 4 mL Sample Injection Method (Aligned with Expected Model)

Further analysis revealed that the 4 mL injection method maintained stable absorbance over multiple cycles, indicating its reliability for long-term monitoring applications. The absorbance values closely matched the expected nitrate concentrations, thereby validating the method's accuracy. Among the different injection volumes tested, the 4 mL injection delivered over 8 seconds provided the most consistent and precise results. This injection duration corresponded to an optimal flow rate, allowing uniform sample delivery and minimising dispersion effects. The study concluded that the 4 mL over 8 seconds injection protocol was best suited for nitrate detection in CDI systems, offering an ideal balance of accuracy, stability, and reproducibility.

6.4 Experiment - Analysis of Sample-and-Hold Design by Dispersion Model

To characterise the non-ideal flow behaviour of the sample-and-hold system, the dispersion model described by Levenspiel was applied. This model was used to analyse tracer response data obtained from step change experiments. In these experiments, a tracer was introduced into the system by creating a step change in concentration, and the tracer concentration at the outlet was measured over time. The resulting data produced a step response curve, from which the residence time distribution (RTD) was derived. The RTD curve revealed variations in fluid residence times and was used to identify deviations from ideal plug flow behaviour.

This approach was based on the foundational work of Danckwerts, who first formalised RTD theory as a method for characterising flow patterns in continuous systems (Danckwerts, 1953). The same RTD framework has been adopted in continuous nitrate detection systems, where flow and reaction are synchronised using automated microplate-based Griess protocols to achieve stable measurement under fluctuating nitrate input conditions (Miranda et al., 2001).

In the dispersion model, the dimensionless time variable, denoted as θ (equal to t/τ), represents the ratio of the actual time to the mean residence time. The cumulative distribution function, *F(θ),* indicates the fraction of tracer that has exited the system at a specific time. In an ideal plug flow reactor, the *F(θ)* curve rises steeply, reflecting uniform residence time for all fluid elements. In contrast, real systems often exhibit more gradual curves due to axial dispersion, which causes a distribution of residence times.

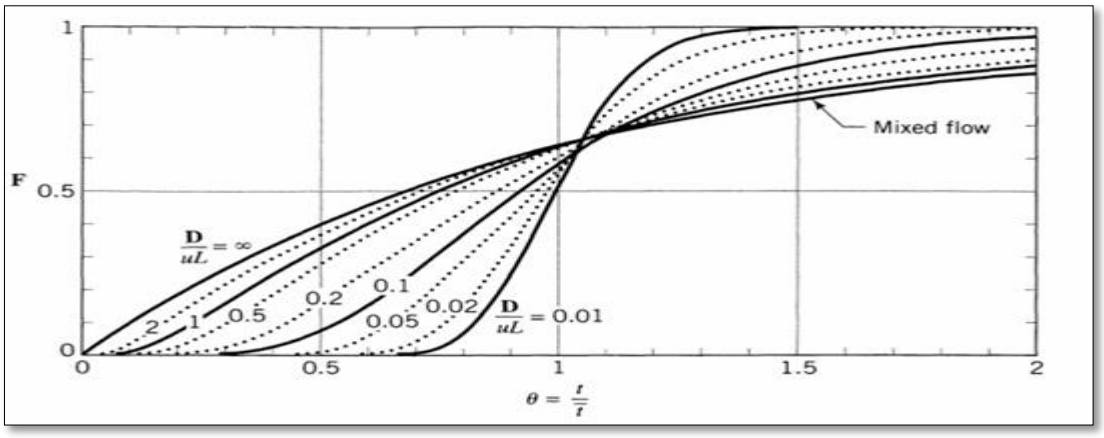

Figure 59 Step response curves from *Chemical Reaction Engineering* (Octave Levenspiel), illustrating deviations from ideal plug flow for various dispersion numbers (*D/UL*), transitioning from plug flow (*D/UL = 0.01*) to fully mixed flow (*D/UL = ∞)* in closed vessels (Levenspiel, 1999).

The dispersion model was essential for characterising deviations from ideal plug flow. It accounted for key parameters such as the diffusion coefficient (D), flow velocity (u), and reactor length (L). The dimensionless dispersion number (D/UL) quantified the extent of axial mixing within the system. Lower values *of* D/UL indicated behaviour approaching plug flow, while higher values were associated with more mixed flow conditions. Figure 59, adapted from *Chemical Reaction Engineering* by Levenspiel, visually demonstrated how different D/UL values influenced the cumulative distribution function $F(\theta)$, providing insight into the flow system's residence time characteristics.(Levenspiel, 1999)

In the nitrate detection system, accurate residence time distribution (RTD) analysis was critical to ensuring that nitrate samples remained in the detection zone for a sufficient duration to allow precise measurement. The system underwent progressive optimisation through adjustments in tube length, which effectively reduced dispersion and enhanced detection accuracy, as shown in Figure 60.

The initial experiment used a 1-metre tube and yielded a dispersion number of $D/UL = 0.051$. At a dimensionless time of $\theta = 1.5$, the corresponding $F(\theta)$ value was 0.8793, representing 87.93% detection accuracy. To improve performance, the tubing length was increased to 1.5 metres. This adjustment reduced the dispersion number to $D/UL = 0.03448$ and increased the $F(\theta)$ value to 0.9305, corresponding to 93.05% accuracy. Building upon these results, the optimised configuration incorporated a 1.847-metre tube, further reducing the dispersion number to $D/UL = 0.028$. This final setup achieved an $F(\theta)$ value of 0.9521 at $\theta = 1.5$, resulting in 95.21% detection accuracy.

This progression clearly highlighted the direct relationship between increased tube length, reduced dispersion, and improved measurement precision. These improvements aligned with the theoretical trends illustrated in Figure 59, confirming that minimising the dispersion number through tubing optimisation was essential for enhancing the accuracy and responsiveness of real-time nitrate monitoring.

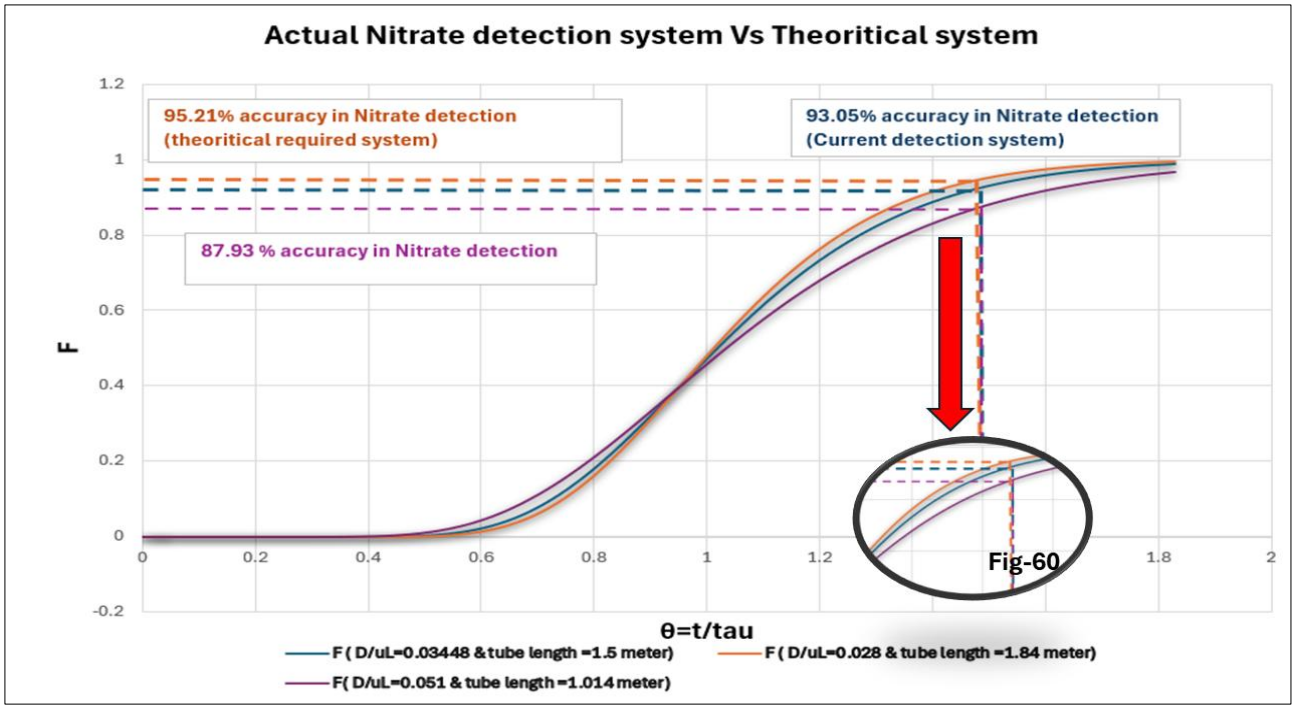

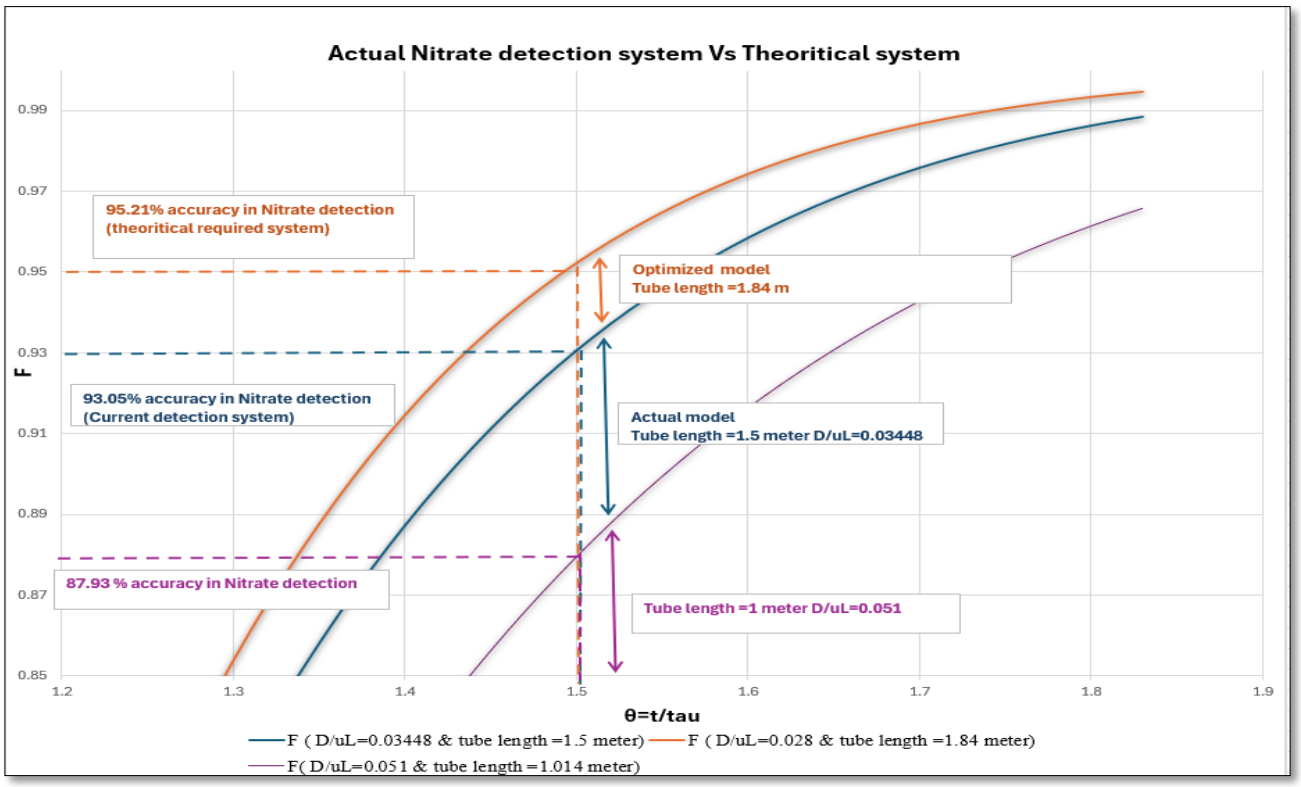

Figure 60 Progressive improvement of nitrate detection accuracy through tube length adjustments, showing increased F(θ) values from 0.8793 (87.93%) at 1 meter to 0.9305 (93.05%) at 1.5 meters, and 0.9521 (95.21%) at 1.847 meters, with corresponding reductions in D/UL values, highlighting the relationship between tube length, dispersion, and detection precision.

Figure 59 from Levenspiel's work highlighted the importance of minimising dispersion. It showed that lower D/uL values produced F(θ) curves closer to ideal plug flow, enhancing system accuracy. Figure 60 validated our design by comparing the current and proposed nitrate detection systems. The figure demonstrated that reducing dispersion through design modifications significantly improved accuracy, meeting the target of >95% accuracy in nitrate detection.

In conclusion, Levenspiel's tracer theory provided a solid foundation for designing nitrate detection systems. By optimising residence time, minimising dispersion, and carefully selecting system parameters, our CDI-based nitrate detection system achieved high accuracy. This design ensured reliable and rapid nitrate detection, essential for continuous water quality monitoring, with results aligning with theoretical predictions and experimental validation.

6.5 Experiment - Analysis of Nitrate detection using a long tube with 20 mL/min flow rate system.

This section presents a detailed analysis of the long-tube nitrate detection system, which was developed to enhance real-time nitrate monitoring through a high-flow-rate configuration. Unlike earlier dye-based tracer studies, this experiment employed nitrate solutions mixed with NOx reagent, consisting of vanadium (III) chloride and Griess reagent, to quantify nitrate concentrations directly rather than relying on a dye tracer. The flow rate was set to 4 mL over a 12-second interval, providing sufficient reaction time while maintaining high detection accuracy. This analysis aimed to compare the experimental outcomes with previous dye-based tracer results and evaluate the influence of flow rate and reaction conditions on nitrate detection efficiency. The study assessed dispersion characteristics, system response time, and measurement precision by applying Levenspiel's tracer theory and residence time distribution (RTD) analysis. These findings were important for optimising nitrate monitoring systems, ensuring rapid and accurate measurements with minimal dispersion effects.

6.5.1 Experimental Setup and Methodology

The experimental setup (Figure 61) was designed to ensure continuous real-time monitoring of nitrate concentration in a controlled environment. A peristaltic pump was used to regulate the flow rate at 4 mL in 12 seconds, ensuring a steady and consistent supply of nitrate solution. The system included an 8-meter-long reaction tube, which was crucial for providing adequate retention time for the

reaction between nitrate and Vanadium (III) chloride (VCl_3) before measurement. The reaction tube was maintained at a constant temperature using a water bath set at 85°C, ensuring the completion of the reduction process. A heated circulator was integrated to maintain a stable temperature environment, preventing any fluctuations that could impact reaction kinetics. The prepared nitrate solutions were introduced sequentially, with different concentrations (1 mg/L, 3.5 mg/L, and 5 mg/L) being tested to evaluate system response to varying levels of nitrate.

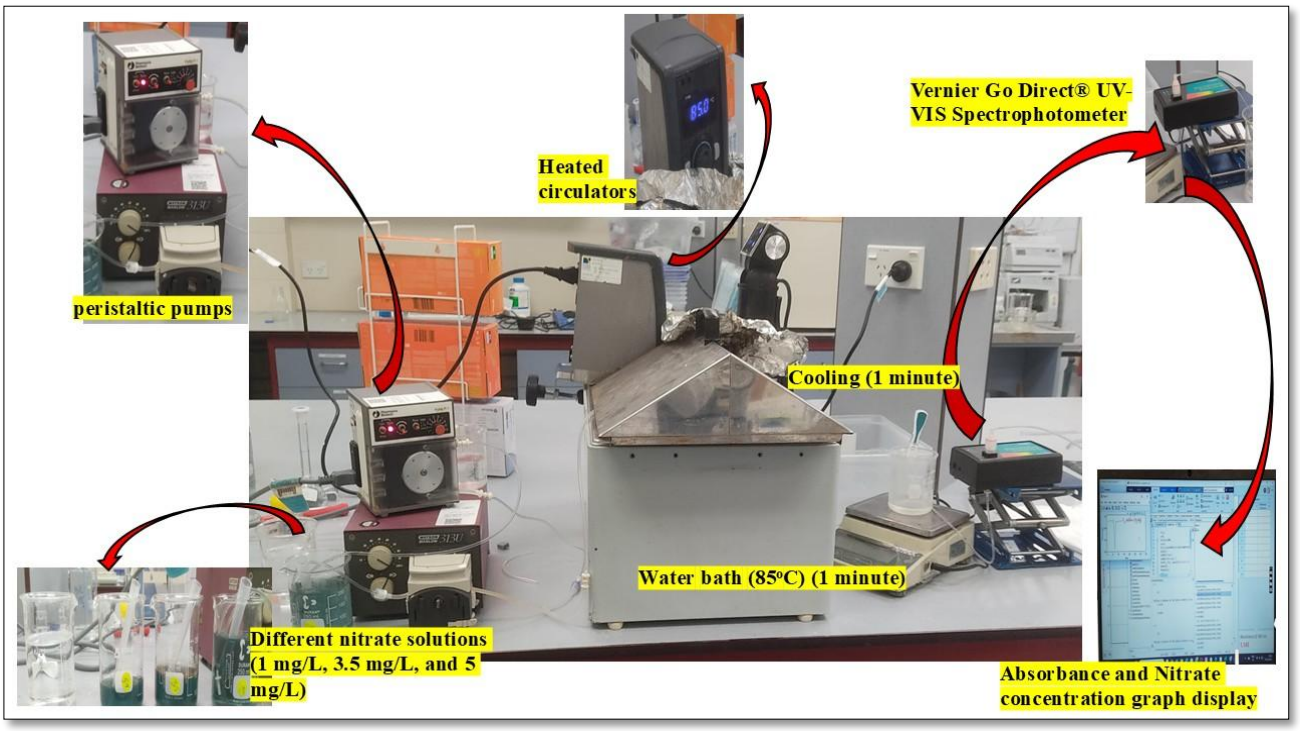

Figure 61 Experimental setup for nitrate detection, including peristaltic pumps, heated circulators, a water bath (85°C), a UV-VIS spectrophotometer, and an absorbance monitoring system.

The experimental procedure involved mixing the nitrate solutions with NOx reagent before being pumped into the system. The reaction took place in the heated water bath, where the mixture was held at 85°C for 1 minute to allow complete reduction of nitrate to nitrite. The solution was then cooled for 1 minute before being analysed using a Vernier Go Direct® UV-Vis Spectrophotometer, which measured absorbance at 540 nm to determine nitrate concentration. The system's ability to handle different retention times was tested by varying the pumping duration to 1 minute, 2 minutes, and 3 minutes per sample. This variation allowed for the assessment of how different residence times affect nitrate detection accuracy and response speed.

6.5.2 Results and discussion

The experimental results demonstrate the impact of varying retention times (1 minute, 2 minutes, and 3 minutes) on nitrate detection accuracy and response behaviour. In the 1-minute pumping case (Figure 62), absorbance peaks for 5 mg/L nitrate concentration reached 1.45 at 540 nm, but the response time was relatively short, around 200-250 seconds, with sharp signal decay observed. The carryover effect was significant, leading to some overlap in peak transitions. This suggests that a 1-minute retention time may not provide sufficient separation between concentration changes, impacting accuracy. This rapid transition between peaks is indicative of how a CDI system would behave in real-time nitrate removal, requiring an efficient detection mechanism that can adapt to fast concentration changes.

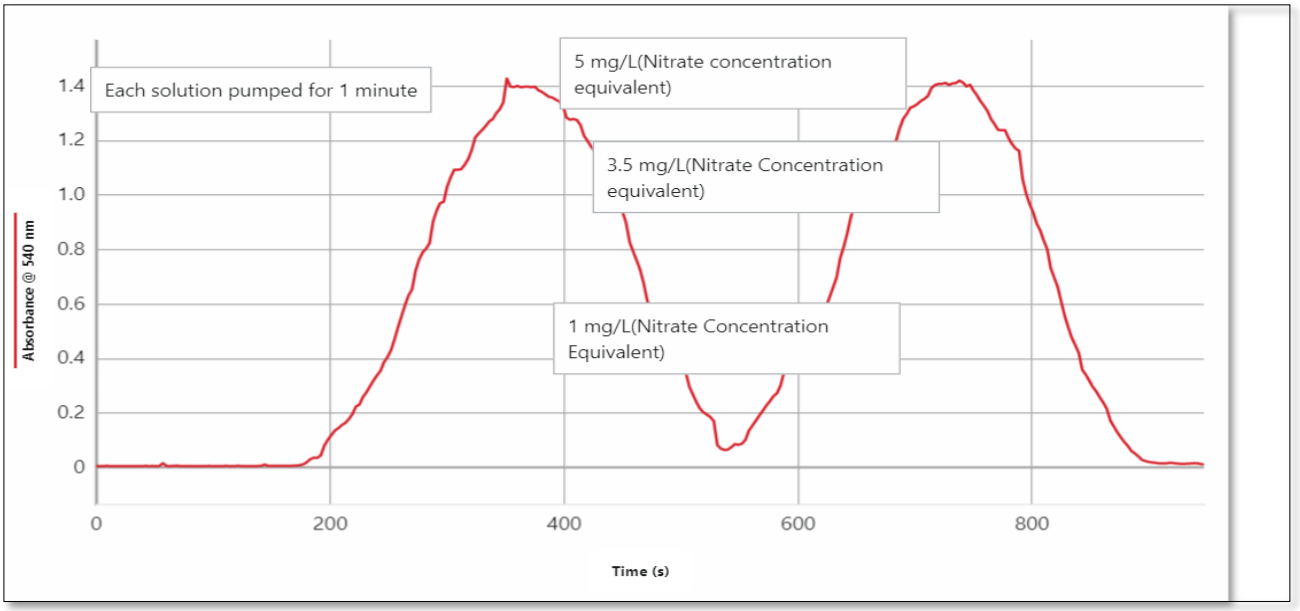

Figure 62 Absorbance response at 540 nm for nitrate detection with a 1-minute pumping cycle, showing distinct peaks for 1 mg/L, 3.5 mg/L, and 5 mg/L nitrate concentrations.

In contrast, the 2-minute pumping case (Figure 63) displayed more stable and well-defined absorbance peaks. The response time increased to 300-350 seconds, allowing for clearer transitions between 1 mg/L, 3.5 mg/L, and 5 mg/L nitrate concentrations. The carryover effects were reduced compared to the 1-minute case, confirming that longer retention times improve peak resolution. This suggests that a CDI system operating with this detection system would provide a clearer distinction between nitrate reduction cycles, improving overall monitoring efficiency. Field-based nitrate monitoring platforms using UV-Vis sensors, such as those developed by Luna Juncal, have

demonstrated the effectiveness of real-time detection strategies with comparable absorbance-based techniques.(Luna Juncal et al., 2020).

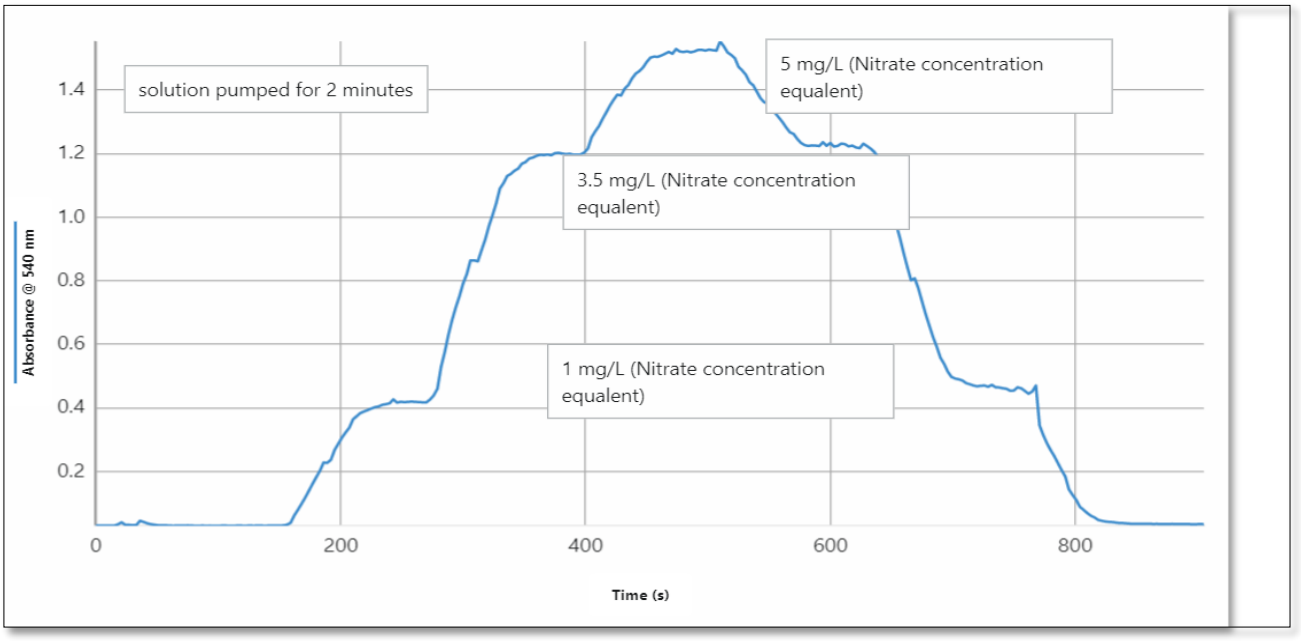

Figure 63 Absorbance response at 540 nm for nitrate detection with a 2-minute pumping cycle, showing improved peak stability and separation for 1 mg/L, 3.5 mg/L, and 5 mg/L nitrate concentrations.

The 3-minute pumping case (Figure 64) provided the most stable and clearly defined peaks, with response times extending to 400-450 seconds. This result suggests that a longer retention time leads to improved accuracy and minimal signal distortion. In the context of CDI systems, where nitrate is rapidly removed, a longer retention time ensures that the detection system accurately tracks concentration decreases with minimal signal interference, leading to better real-time analysis of nitrate reduction trends.

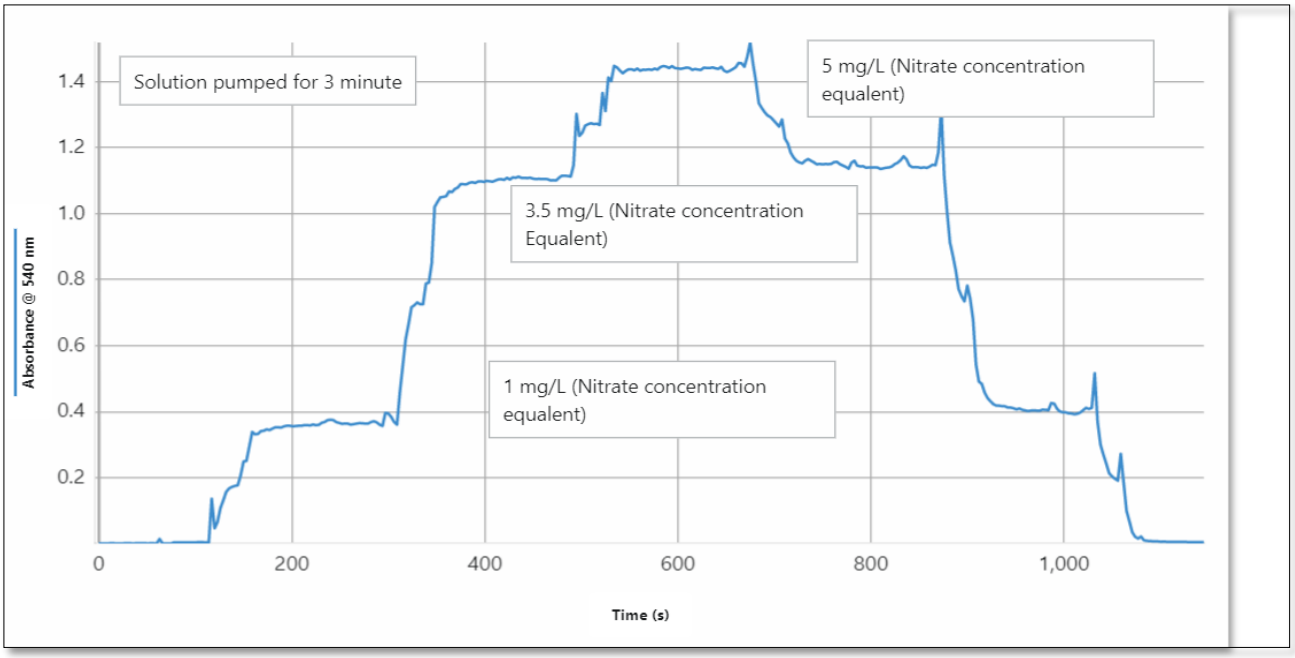

Figure 64 Absorbance response at 540 nm for nitrate detection with a 3-minute pumping cycle, showing the most stable and well-defined peaks for 1 mg/L, 3.5 mg/L, and 5 mg/L nitrate concentrations.

A quantitative comparison of absorbance measurements confirms that increasing retention time enhances concentration differentiation. The standard deviation in absorbance measurements was also analysed to assess accuracy:

- 1-minute pumping: 87.93% accuracy
- 2-minute pumping: 93.05% accuracy
- 3-minute pumping: 95.21% accuracy

These findings demonstrate that a 3-minute retention time provides the highest accuracy, with minimal carryover and mixing effects. The overall analysis suggests that increasing retention time significantly improves the precision of nitrate detection, making it an essential factor for optimising real-time monitoring systems in CDI applications. Since CDI systems remove nitrate rapidly, an accurate detection method is critical to avoid underestimating or overestimating nitrate removal efficiency. The results suggest that using a 3-minute retention time for CDI monitoring would provide the most accurate nitrate concentration readings while minimizing the risk of signal interference.

This analysis confirms that the long tube nitrate detection system at 4 mL in 12 seconds flow rate significantly enhances detection accuracy compared to dye-based tracer testing. The main

conclusions are that flow rate and residence time influence measurement precision, with slower flow improving peak clarity and reducing dispersion. To further enhance nitrate detection efficiency, a Multiple Sample and Hold System using 3D-Printed Resin Components was implemented with seven tubes. This system allows for parallel sample processing, making nitrate detection seven times faster. Rather than increasing tube length, increasing the number of tubes allows each tube to pass the solution and hold while rotating the sample holder, ensuring continuous and rapid nitrate detection. This system is highly suitable for CDI-based nitrate reduction applications, where rapid and accurate monitoring is required to optimise nitrate removal performance. Future recommendations include optimising sample rotation mechanisms for faster detection, enhancing mixing conditions to stabilize measurement signals. These optimisations will ensure that the nitrate detection system is highly accurate, fast, and suitable for industrial applications focused on real-time nitrate removal using CDI.

6.6 Experiment - Tracer Theory and Dye Testing for CDI Efficiency

Tracer theory, as introduced by Levenspiel, provides a robust framework for understanding fluid flow patterns and residence time distributions (RTD) within a system. In this experiment, red dye was employed as a tracer to evaluate nitrate concentration using absorbance curves generated by UV-Vis spectroscopy. This approach facilitated the detection of nitrate concentration from the CDI system during both adsorption and desorption cycles. The dye allowed for direct observation of flow behaviour, enabling the identification of any back-mixing or diffusion effects. Tracer studies help in understanding fluid flow patterns, RTD, and system efficiency, ensuring that nitrate removal processes are optimised, and real-time monitoring is achieved with high accuracy. The RTD function, E(t), was used to describe how long dye particles remained in the system, calculated using the formula (Equation (50)).

$$E(t) = \frac{C(t)}{\int_0^\infty C(t)\,dt} \tag{50}$$

where *C(t)* is the concentration at time *t*.

The mean residence time (MRT) was calculated using the formula (Equation (51)):

$$t_m = \frac{\int_0^\infty E(t)dt}{\int_0^\infty E(t)dt} \quad (51)$$

From the table (Appendix 9.2). MRT (mean residence time Value) is $t_m=10.94s$ representing the average time particles spent in the system.

The variance (σ^2) is calculated using the formula (Equation (52)):

$$\sigma^2 = \frac{\sum(t_i - t_m)^2 C(t_i)}{\sum C(t_i)} \quad (52)$$

where t_i represents the time at each interval, t_m is the mean residence time (10.94 s), and $C(t_i)$ is the concentration at each time point. Using the provided data from the table (Appendix 9.2, the final variance is found to be 8.255 s^2, reflecting a well-mixed system with minimal dispersion.

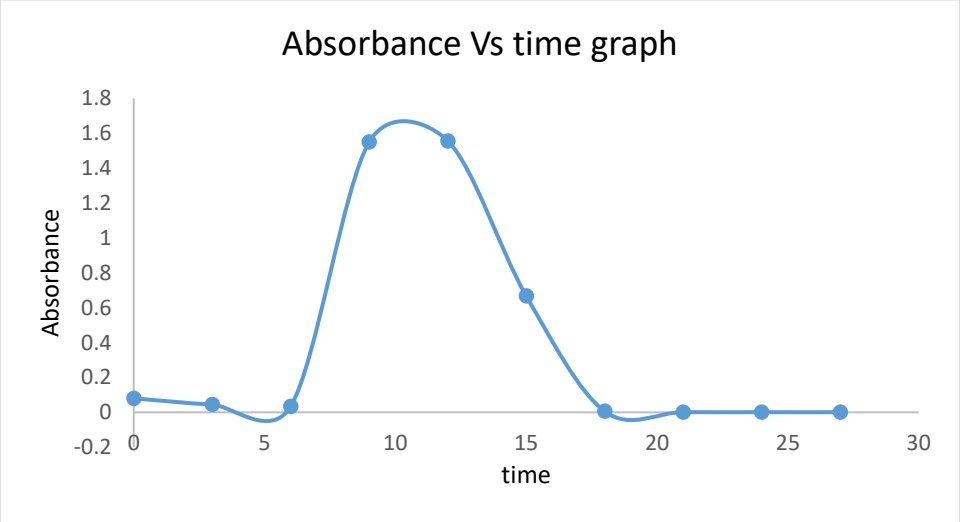

Figure 65 Absorbance vs. Time Graph for Red Dye Tracer Study

The absorbance vs. time graph (Figure 65) illustrates the absorbance readings at different time intervals, corresponding to table Appendix 9.2. The peak absorbance (~1.56) at 9-12 seconds aligns with the tracer injection period, followed by a gradual decline, representing the washout phase. This graph visually supports the calculated MRT (10.94 s) and variance (8.255 s^2), confirming minimal dispersion and efficient flow through the detection system.

The dispersion number ($D/(uL)$) helps determine the degree of dispersion in a flow system and assess if the flow approaches plug flow behaviour.

$$\frac{D}{uL} = \frac{\sigma^2}{2 * t_m^2} \quad (53)$$

where $\sigma^2 = 8.255\ s^2$, $t_m = 10.94$ s, $u = 0.667\ ml/s$, and $L = 1.5$ m, substituted in Equation (53).

$$D/uL = 0.03448 \quad (54)$$

$$D = 0.03450 \quad (55)$$

This value indicates moderate to high dispersion, deviating from ideal plug flow and suggesting that the system operates closer to mixed flow behaviour rather than a perfect plug flow system.

Analysing all calculated values, the mean residence time (10.94 s) and variance (8.255 s^2) indicate Nitrate detection system has moderate dispersion. The dispersion number *D/(uL),* calculated as 0.03448, suggests that while the system is not a perfect plug flow, it operates with low dispersion compared to mixed flow systems. The red dye tracer analysis, MRT, variance, and dispersion number collectively confirm that the syringe system with food dye used for testing nitrate detection from the CDI system during the adsorption and desorption stages provides efficient fluid flow with minimal back-mixing, making it suitable for nitrate removal applications.

6.6.1 Proposed Relationship Between Number of Parallel Reactors and System Design

The initial approach to continuous nitrate detection employed a single 2-metre-long tube designed to achieve a nominal residence time of 2 minutes. However, this setup resulted in considerable axial dispersion, which caused a broad and delayed step response. Therefore, the accuracy of the measurement dropped to less than 10%. Although the design theoretically allowed for the necessary residence time, the dispersion effect significantly distorted the output signal, making the system unsuitable for reliable online monitoring.

To address this problem, a sample-and-hold strategy was implemented. This approach allows the system to achieve the required residence time using a shorter tubing length by temporarily isolating the solution. In this method, the solution flows into a designated reactor tube for a short duration, after which the flow path is switched to a different tube. During this time, the first tube no longer

receives flow and holds the sample in a static condition to allow the reaction to proceed. After the measurement is completed, the system can cycle back to that tube or continue rotating through other available tubes. This design significantly reduces the impact of dispersion by limiting the solution movement during the reaction phase, which improves accuracy.

Using only one sample-and-hold tube limits the system to one measurement every two minutes, corresponding to the reaction cycle. To increase the frequency of data collection and provide near-continuous monitoring, multiple tubes can be connected in parallel. Each tube is operated with a time offset, allowing sequential sampling and holding cycles. This arrangement increases the system's responsiveness while still maintaining the required reaction time in each tube. The use of parallel reactors therefore offers a practical design solution to enhance temporal resolution and minimise the effects of dispersion in continuous nitrate detection systems.

To resolve the rapid transient features shown in the Stella simulation (Figure 66), it was necessary to introduce parallel reactors.

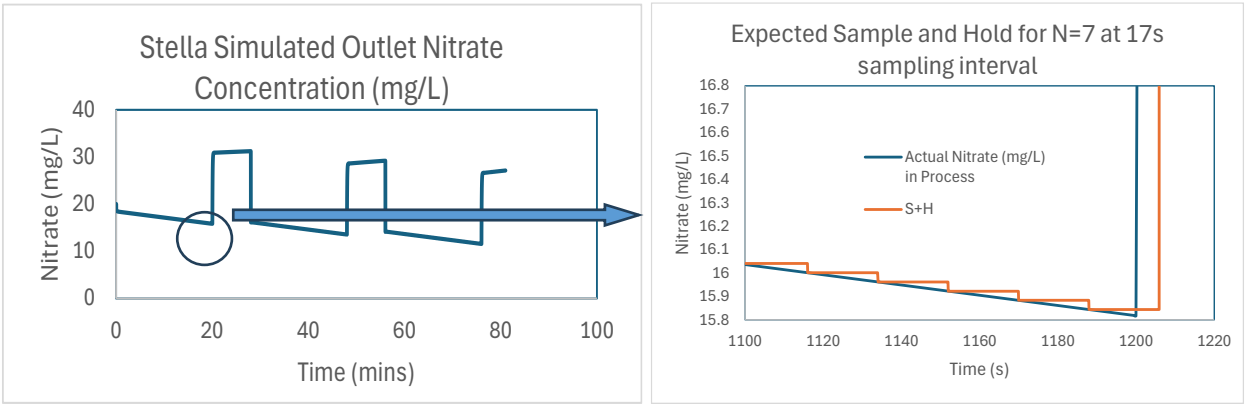

Figure 66 Simulated nitrate response using a seven-port sample-and-hold system with 17-second resolution to capture transient CDI dynamics.

Thus, for N parallel reactors, the effective sampling rate f_s is given by (Equation (56)),

$$f_s = \frac{\tau}{N} \tag{56}$$

For the design in this study, $N=7$ reactors were constructed with an effective sampling rate is 17s. In Figure 66, on the right, we can see the artifact introduced as steps by the technique. For most transient features in steady semi-batch operation of CDI at volumes of 10 to 20 L, a sampling rate of 17s would

reproduce the process data well. However, for short adsorb/desorb cycles such as in single pass CDI, where the cycle times are on the order of 1-2 minutes, 17s would be insufficient to resolve the transient information needed, such as maximum values in the desorb and minimum values in the adsorb. It is likely that the reading would become attenuated. A more suitable design would be, for example, *N=20* at a sampling rate of 6s.

Such a design would be challenging from a fabrication point of view given the challenges of fabricating a 7-reactor design and it would be advisable not to attempt a design any larger than 20. In such a case where finer resolution was required, developing an alternate method would be recommended.

6.7 Conclusion

This chapter presented the design and validation of a vanadium chloride-based sample-and-hold system for continuous nitrate detection, specifically developed to overcome the limitations of conventional continuous flow systems. The original 2-metre flow tube design, although capable of providing a two-minute residence time, exhibited excessive dispersion, which reduced detection accuracy to 10%. The sample-and-hold approach resolved this issue by isolating discrete sample volumes, enabling controlled thermal conditioning and consistent reaction time. The final design used seven parallel sampling channels, each operating with a 4-millilitre sample volume and a three-minute cycle, achieving nitrate detection accuracy greater than 93%. The highest accuracy recorded was 95.21%, demonstrating excellent stability and reproducibility under optimised flow and temperature conditions.

A key advancement of this system was its ability to improve temporal resolution through parallel sampling. With seven reactors operating sequentially, the system achieved an effective sampling interval of approximately 17 seconds. This resolution proved sufficient for monitoring nitrate concentration changes during adsorption and desorption cycles in capacitive deionisation systems handling batch volumes of ten to twenty litres. While this design meets the requirements for semi-batch processes, it may not capture rapid fluctuations in shorter single-pass CDI cycles, where even finer resolution would be necessary. Nevertheless, the sample-and-hold system developed in this study provides a robust, scalable, and high-fidelity solution for real-time nitrate detection.

7 CONCLUSION AND FUTURE WORK

7.1 Conclusion

This thesis described the development of a device that could continuously sample a process fluid and measure the nitrate concentration (NO_3^-) in the range of 0.1 to 5 mg/L (extendable up to 20 mg/L with inline dilution) at a sampling rate of 105 samples per CDI cycle. The implementation of the device closely corresponded with the sampling requirements of a Voltea VS3 membrane Capacitive Deionisation (mCDI) module operated in batch mode.

The VS3, representing the potential nitrate removal capacity of a commercially available disposable module, was the focus of the design constraints for the nitrate measurement device. The system was operated in a semi-batch mode, where a fixed volume of nitrate-containing water was repeatedly filled and recirculated through the CDI unit for adsorption, followed by desorption to release the stored ions. This setup allowed better control over the nitrate removal cycle and was suitable for modelling real-time fluctuations in concentration. In the Stella simulation, the system's behaviour was replicated using batch volumes of 10, 15, and 20 litres, with the best agreement between simulated and experimental data achieved at a nitrate removal rate (NRR) of 16 mg/min during the adsorption phase. This simulation outcome helped define the sampling interval and frequency required for accurately detecting nitrate concentration changes during CDI operation.

The VS3 was also simulated in Stella with closely corresponding TDS removal for three semi-batch designs of 10, 15 and 20L. These designs replicated the volume of systems expected to be encountered in residential “under-the-sink” systems and as such produced simulated nitrate removal (i.e., NO3- vs time). Having simulated transient data helped us inform the development of a suitable sampling protocol by highlighting the key points at which nitrate concentrations changed during CDI operation. This guided the configuration of the sample-and-hold detection system, particularly the measurement timing and frequency. However, the system was limited to spectrophotometric techniques, requiring controlled sample clarity, reagent stability, and consistent optical performance to ensure reliable and accurate detection.

The process of evaluating a suitable spectrophotometric nitrate method included “flow-cell” compatibility tests. These compatibility tests identified critical flaws with the Palintest kit and the zinc reduction method. In particular, the zinc reduction method exhibited issues such as over-

reduction of nitrite to ammonia, clogging caused by zinc oxidation, and inconsistent reaction performance.These drawbacks underscored the necessity of exploring alternative reductants that could perform reliably under dynamic conditions.

Vanadium chloride emerged as the preferred reductant for further investigation due to its rapid reaction kinetics, reproducibility, and compatibility with online monitoring systems. The methodology in this study followed the principle of reducing nitrate to nitrite using vanadium chloride in acidic conditions, followed by colorimetric detection through UV-Vis spectrophotometry. The absorbance at 540 nm, correlated to nitrate concentration via Beer-Lambert's Law, formed the core analytical signal. Careful calibration and optimisation of reagent ratios and temperature were essential to ensure accurate and repeatable measurements. The optimised condition of 85°C and a residence time of 2 minutes was selected for this system, which provided over 95% detection accuracy while maintaining molar absorptivity in line with published values (~50,000 M^{-1} cm^{-1}) (Pai et al., 2021). This result aligns with findings by Braman and Hendrix (1989), who reported rapid nitrate reduction above 80°C (Braman & Hendrix, 1989), and Fang (2021), who demonstrated that higher temperatures eliminated salinity-related interference in vanadium-based reductions (Fang et al., 2021). Comparatively, lower temperatures such as 45°C and 50°C required much longer reaction times of 25–60 minutes to achieve similar yield (Schnetger et al., 2014; Wang et al., 2016), highlighting the advantage of the optimised thermal conditions used in this thesis.

One of the early challenges encountered in this study was the dispersion effect observed in continuous plug flow systems. When a dye tracer was injected into a single long tube, the resulting signal became significantly distorted due to axial dispersion, making it unsuitable for real-time analysis. To address this limitation, the system was reconfigured using a sample-and-hold strategy. This new setup involved distributing water samples across seven parallel reactors, each designed with a fixed retention time to ensure complete reaction with the vanadium chloride reagent. The implementation of seven parallel sample-and-hold channels, with 17-second sampling intervals, enabled high temporal resolution suitable for capturing nitrate adsorption and desorption dynamics during CDI cycles, even when processing volumes of 10–20 litres.

The sample-and-hold nitrate detection system developed in this study achieved a sampling rate of 210 samples per hour (105 samples per CDI cycle), with a 17-second resolution between measurements. This performance reflects a significant improvement over existing vanadium chloride-based method. For instance, the iSEA analyser, designed by Fang for estuarine monitoring achieved

only 12 samples per hour due to syringe pump limitations and filtration delays (Fang et al., 2019). Similarly, Schnetger reported a throughput of 96 samples per hour using a microplate-based method requiring 60 minutes of incubation, while Wang recorded 20 samples per hour using a flow injection system (Schnetger et al., 2014; Jiapeng Wu et al., 2016). The improved throughput in this study was enabled by thermal optimisation at 85°C, rotary valve integration, and sequential injection control. This high-frequency capability is particularly valuable for capturing transient nitrate fluctuations during adsorption and desorption phases in CDI operation. Overall, the system offers a robust and scalable platform for real-time monitoring in decentralised water treatment applications.

The system was optimised for precise detection within the 0.1 to 5 mg/L range (higher concentrations accurately detected through appropriate dilution) based on vanadium chloride chemistry and UV-Vis absorbance at 540 nm. To accommodate higher concentrations encountered during CDI operation, a 1:4 dilution strategy was employed at the CDI outlet. This extended the effective detection range up to 20 mg/L without compromising sensitivity or accuracy. The resulting detection window of 0.1 to 20 mg/L nitrate enables the system to capture both low and high concentration transitions across dynamic adsorption-desorption cycles. This high-resolution, real-time performance, combined with affordability and scalability, positions the system as a practical tool for decentralised nitrate monitoring.The detection limit of 0.1 mg/L (1.6 μM) also aligns with environmental monitoring standards, including the WHO guideline of 10 mg/L NO_3-N

Although the results were promising, this study encountered certain limitations. All experiments were carried out using synthetic nitrate solutions with fixed ionic strength and pH.Real water samples, such as groundwater or wastewater, often contain interfering substances like phosphate, sulphate, and dissolved organic matter, which were not considered in this study. The vanadium chloride reagent has a limited shelf life, and its stability during long-term field applications needs further evaluation. While the sample-and-hold method simulates continuous monitoring, it does not provide second-by-second measurements. This may be a constraint for industrial processes that require continuous feedback control. The Stella model also assumes ideal system behaviour and needs further calibration based on extended real-world data.

Despite these constraints, the system successfully demonstrated the ability to perform rapid, automated, and accurate nitrate measurements in a compact format. This innovation could support decentralised water monitoring and enhance the reliability of nitrate removal verification in treatment systems.

7.2 Future Work

Future improvements to the nitrate detection system should focus on enhancing its automation, accuracy, and suitability for continuous field operation. Currently, manual switching between sampling channels introduces timing inconsistencies and limits practical use in real-time applications. To overcome this challenge, the system design will incorporate a motorised switching mechanism to ensure consistent and reliable channel transitions during automated operation.

A suitable upgrade would involve using a stepper motor linked to a rotating sample selector, managed by an Arduino microcontroller. This setup could automate the timing of sample collection, heating, and cooling. For precise alignment, the system should incorporate a position sensor that enables the rotor to consistently align with each sample inlet. This system would eliminate the need for manual control, thereby improving reproducibility and making the device viable for long-term use in automated environments.

In this study, a system using seven sampling channels with a 17-second interval was sufficient to monitor nitrate fluctuations during semi-batch CDI cycles involving 10 to 20 litres of water. However, for applications such as single-pass CDI, where adsorption and desorption events may occur within one to two minutes, a higher sampling resolution is necessary. A system with 20 parallel channels would allow sampling every 6 seconds while maintaining the required 2-minute residence time in each tube. This configuration would enable the system to achieve a maximum of 600 samples per hour (300 samples per CDI cycle), significantly improving its ability to resolve rapid transient changes in nitrate concentration.

Furthermore, experimental evidence in this work showed that a tube length of 1.847 metres provided the most accurate nitrate detection, achieving an $F(\theta)$ value of 0.9521, or 95.21 percent accuracy. This configuration exhibited minimal dispersion and defined the practical upper limit for tube length in future system designs. Tubes longer than this may result in signal distortion, reducing the system's reliability.

To achieve higher sampling resolution or accommodate more than 20 channels, the implementation of advanced techniques is recommended. Microfluidic switching systems, multiplexed flow injection, or inline optical sensors capable of simultaneous multi-point detection could offer next-level performance. These methods would allow the system to manage complex and rapid sampling demands without increasing physical bulk or mechanical complexity.

Additionally, incorporating wireless communication and cloud-based analytics will enable real-time data visualisation and remote monitoring. Features such as flow rate sensors, temperature feedback loops, and automated data logging would support fully autonomous operation. These enhancements are essential for deployment in decentralised and rural water monitoring systems.

8 References

Alahi, M. E. E., & Mukhopadhyay, S. C. (2018). Detection methods of nitrate in water: A review. *Sensors and Actuators A: Physical*, *280*, 210-221. https://doi.org/https://doi.org/10.1016/j.sna.2018.07.026

Anderson, M. A., Cudero, A. L., & Palma, J. (2010). Capacitive deionization as an electrochemical means of saving energy and delivering clean water. Comparison to present desalination practices: Will it compete? *Electrochimica Acta*, *55*(12), 3845-3856. https://doi.org/https://doi.org/10.1016/j.electacta.2010.02.012

APHA , S. M. (2000). 4500-NO₃[−] NITROGEN (NITRATE). In *Standard Methods For the Examination of Water and Wastewater*. https://doi.org/10.2105/smww.2882.089

Ayub, R., Messier, K. P., Serre, M. L., & Mahinthakumar, K. (2019). Non-point source evaluation of groundwater nitrate contamination from agriculture under geologic uncertainty. *Stochastic Environmental Research and Risk Assessment*, *33*(4), 939-956. https://doi.org/10.1007/s00477-019-01669-z

Azmi, A., Azman, A. A., Ibrahim, S., & Yunus, M. A. M. (2017). TECHNIQUES IN ADVANCING THE CAPABILITIES OF VARIOUS NITRATE DETECTION METHODS: A REVIEW. *International Journal on Smart Sensing and Intelligent Systems*, *10*(2), 1-39. https://doi.org/doi:10.21307/ijssis-2017-210

Bedwell, C. L., Hamar, D. W., Hoesterey, M. L., Sonderman, J. P., & Odde, K. G. (1995). Comparison of Four Methods for Forage Nitrate Analysis. *Journal of Veterinary Diagnostic Investigation*, *7*(4), 527-530. https://doi.org/10.1177/104063879500700418

Braman, R. S., & Hendrix, S. A. (1989). Nanogram nitrite and nitrate determination in environmental and biological materials by vanadium(III) reduction with chemiluminescence detection. *Analytical Chemistry*, *61*(24), 2715-2718. https://doi.org/10.1021/ac00199a007

Bulusu, S., Prieto García, C., Dahlke, H. E., & Levintal, E. (2024). Technical note: An open-source, low-cost system for continuous monitoring of low nitrate concentrations in soil and open water. *Biogeosciences*, *21*(12), 3007-3013. https://doi.org/10.5194/bg-21-3007-2024

Cadeado, A. N. S., Machado, C. C. S., Costa, M. Q., & Silva, S. G. (2022). A palm-sized wireless device for colorimetric nitrite determination in water. *Microchemical Journal*, *183*, 108138. https://doi.org/https://doi.org/10.1016/j.microc.2022.108138

Carroll, S. A., Keating, E., Mansoor, K., Dai, Z., Sun, Y., Trainor-Guitton, W., Brown, C., & Bacon, D. (2014). Key factors for determining groundwater impacts due to leakage from geologic carbon sequestration reservoirs. *International Journal of Greenhouse Gas Control*, *29*, 153-168. https://doi.org/https://doi.org/10.1016/j.ijggc.2014.07.007

da Ascenção, W. D., Augusto, C. C., de Melo, V. H. S., & Batista, B. L. (2024). A Simple, Ecofriendly, and Fast Method for Nitrate Quantification in Bottled Water Using Visible Spectrophotometry. *Toxics*, *12*(6), 383. https://www.mdpi.com/2305-6304/12/6/383

Danckwerts, P. V. (1953). Continuous flow systems: Distribution of residence times. *Chemical Engineering Science*, *2*(1), 1-13. https://doi.org/https://doi.org/10.1016/0009-2509(53)80001-1

Dench, W. E., & Morgan, L. K. (2021). Unintended consequences to groundwater from improved irrigation efficiency: Lessons from the Hinds-Rangitata Plain, New Zealand. *Agricultural Water Management*, *245*, 106530. https://doi.org/https://doi.org/10.1016/j.agwat.2020.106530

Doane, T. A., & and Horwáth, W. R. (2003). Spectrophotometric Determination of Nitrate with a Single Reagent. *Analytical Letters*, *36*(12), 2713-2722. https://doi.org/10.1081/AL-120024647

Epsztein, R., Nir, O., Lahav, O., & Green, M. (2015). Selective nitrate removal from groundwater using a hybrid nanofiltration–reverse osmosis filtration scheme. *Chemical Engineering Journal*, *279*, 372-378. https://doi.org/https://doi.org/10.1016/j.cej.2015.05.010

Fang, K., Gong, H., He, W., Peng, F., He, C., & Wang, K. (2018). Recovering ammonia from municipal wastewater by flow-electrode capacitive deionization. *Chemical Engineering Journal*, *348*, 301-309. https://doi.org/https://doi.org/10.1016/j.cej.2018.04.128

Fang, T., Li, H., Bo, G., Lin, K., Yuan, D., & Ma, J. (2021). On-site detection of nitrate plus nitrite in natural water samples using smartphone-based detection. *Microchemical Journal*, *165*, 106117. https://doi.org/https://doi.org/10.1016/j.microc.2021.106117

Fang, T., Li, P., Lin, K., Chen, N., Jiang, Y., Chen, J., Yuan, D., & Ma, J. (2019). Simultaneous underway analysis of nitrate and nitrite in estuarine and coastal waters using an automated integrated syringe-pump-based environmental-water analyzer. *Analytica Chimica Acta*, *1076*, 100-109. https://doi.org/https://doi.org/10.1016/j.aca.2019.05.036

Grout, L., Chambers, T., Hales, S., Prickett, M., Baker, M. G., & Wilson, N. (2023). The potential human health hazard of nitrates in drinking water: a media discourse analysis in a high-income country. *Environmental Health*, *22*(1), 9. https://doi.org/10.1186/s12940-023-00960-5

Guimarães, V., durão, H., & Azenha, M. (2014). Detailed Validation of a Method for the Determination of Nitrate in Water by UV/Vis Spectroscopy

Health, M. D. o. (2018). NITRATE IN WELL WATER AND METHEMOGLOBINEMIA.

Holm, T. R., Kelly, W. R., Sievers, L. F., & Webb, D. L. (1997). A comparison of ultraviolet spectrophotometry with other methods for the determination of nitrate in water. *Spectroscopy (Santa Monica)*, *12*(9), XI-45.

Jankovic, L. (2018). Visible Light Spectrum: From a Lighting Manufacturer's Perspective.

Jiwarungrueangkul, T., Kongpuen, O., Yucharoen, M., Sangmanee, C., Tipmanee, D., Areerob, T., & Sompongchiyakul, P. (2023). Modification and validation of an analytical method for the simple determination of nitrate in seawater by reduction to nitrite with zinc powder. *Marine Chemistry*, *251*, 104235. https://doi.org/https://doi.org/10.1016/j.marchem.2023.104235

Kazemzadeh, A., & Ensafi, A. A. (2001). Simultaneous determination of nitrite and nitrate in various samples using flow-injection spectrophotometric detection. *Microchemical Journal*, *69*(2), 61-68. https://doi.org/https://doi.org/10.1016/S0026-265X(01)00072-8

Kim-Shapiro, D. B., Gladwin, M. T., Patel, R. P., & Hogg, N. (2005). The reaction between nitrite and hemoglobin: the role of nitrite in hemoglobin-mediated hypoxic vasodilation. *Journal of Inorganic Biochemistry*, *99*(1), 237-246. https://doi.org/https://doi.org/10.1016/j.jinorgbio.2004.10.034

Kim, Y.-J., & Choi, J.-H. (2012). Selective removal of nitrate ion using a novel composite carbon electrode in capacitive deionization. *Water Research*, *46*(18), 6033-6039. https://doi.org/https://doi.org/10.1016/j.watres.2012.08.031

Kodamatani, H., Yamazaki, S., Saito, K., Tomiyasu, T., & Komatsu, Y. (2009). Selective determination method for measurement of nitrite and nitrate in water samples using high-performance liquid chromatography with post-column photochemical reaction and chemiluminescence detection. *Journal of Chromatography A*, *1216*(15), 3163-3167. https://doi.org/https://doi.org/10.1016/j.chroma.2009.01.096

Lacasa, E., Cañizares, P., Sáez, C., Fernández, F. J., & Rodrigo, M. A. (2011). Removal of nitrates from groundwater by electrocoagulation. *Chemical Engineering Journal*, *171*(3), 1012-1017. https://doi.org/https://doi.org/10.1016/j.cej.2011.04.053

Lado, J. J., Pérez-Roa, R. E., Wouters, J. J., Tejedor-Tejedor, M. I., Federspill, C., Ortiz, J. M., & Anderson, M. A. (2017). Removal of nitrate by asymmetric capacitive deionization. *Separation and Purification Technology*, *183*, 145-152. https://doi.org/https://doi.org/10.1016/j.seppur.2017.03.071

Lee, J.-H., & Choi, J.-H. (2012). The production of ultrapure water by membrane capacitive deionization (MCDI) technology. *Journal of Membrane Science*, *409-410*, 251-256. https://doi.org/https://doi.org/10.1016/j.memsci.2012.03.064

Levenspiel, O. (1999). *Chemical Reaction Engineering*. Wiley. https://books.google.co.nz/books?id=X4svAQAAIAAJ

Li, C., Fang, Z., Cen, B., Zhang, P., Li, F., Fang, D., He, M., Zhang, C., Liu, J., Mo, X., & Li, K. (2023). Efficient nitrate removal by nitrogen-doped carbon spheres electrodes with interconnected architecture in novel stirring capacitive deionization: Dual promoting effect of facile mass transfer and additional active centers. *Chemical Engineering Journal*, *474*, 145843. https://doi.org/https://doi.org/10.1016/j.cej.2023.145843

LibreTexts. (2020). 13.4: Flow Injection Analysis. Chemistry LibreTexts.

Lin, K., Wang, L., Xu, J., Huang, S., Guo, H., Huo, Y., & Zhang, Y. (2022). Reverse flow injection method for field determination of nitrate in estuarine and coastal waters using a custom-made linear light path flow cell and the vanadium reduction method. *Microchemical Journal*, *172*, 106901. https://doi.org/https://doi.org/10.1016/j.microc.2021.106901

Luna Juncal, M. J., Skinner, T., Bertone, E., & Stewart, R. A. (2020). Development of a Real-Time, Mobile Nitrate Monitoring Station for High-Frequency Data Collection. *Sustainability*, *12*(14), 5780. https://www.mdpi.com/2071-1050/12/14/5780

Mahmud, M. A. P., Ejeian, F., Azadi, S., Myers, M., Pejcic, B., Abbassi, R., Razmjou, A., & Asadnia, M. (2020). Recent progress in sensing nitrate, nitrite, phosphate, and ammonium in aquatic environment. *Chemosphere*, *259*, 127492. https://doi.org/https://doi.org/10.1016/j.chemosphere.2020.127492

Malone, & Newton. (2020). The Globalization of Cultural Eutrophication in the Coastal Ocean: Causes and Consequences. https://doi.org/10.3389/fmars.2020.00670

McDowell, R. W., Simpson, Z. P., Ausseil, A. G., Etheridge, Z., & Law, R. (2021). The implications of lag times between nitrate leaching losses and riverine loads for water quality policy. *Scientific Reports*, *11*(1), 16450. https://doi.org/10.1038/s41598-021-95302-1

Merino, L. (2009). Development and Validation of a Method for Determination of Residual Nitrite/Nitrate in Foodstuffs and Water After Zinc Reduction. *Food Analytical Methods*, *2*(3), 212-220. https://doi.org/10.1007/s12161-008-9052-1

Miranda, K. M., Espey, M. G., & Wink, D. A. (2001). A Rapid, Simple Spectrophotometric Method for Simultaneous Detection of Nitrate and Nitrite. *Nitric Oxide*, *5*(1), 62-71. https://doi.org/https://doi.org/10.1006/niox.2000.0319

Nelson, J. L., Kurtz, L. T., & Bray, R. H. (1954). Rapid Determination of Nitrates and Nitrites. *Analytical Chemistry*, *26*, 1081-1082.

Norman, R. J., & Stucki, J. W. (1981). The Determination of Nitrate and Nitrite in Soil Extracts by Ultraviolet Spectrophotometry. . . *Soil Science Society of America Journal, 45(2), 347-353*. https://doi.org/10.2136/sssaj1981.03615995004500020024x

Oladosu, N. O., Abayomi, A. A., Zhang, X., Olayinka, K. O., Alo, B. I., & Deng, A. (2017). Online zinc reduction-sequential injection analysis for the determination of nitrogen species in extracts of riverine sediment. *Journal of Analytical Science and Technology*, *8*(1), 5. https://doi.org/10.1186/s40543-017-0116-y

Ortiz, J. M., Expósito, E., Gallud, F., García-García, V., Montiel, V., & Aldaz, A. (2008). Desalination of underground brackish waters using an electrodialysis system powered directly by photovoltaic energy. *Solar Energy Materials and Solar Cells*, *92*(12), 1677-1688. https://doi.org/https://doi.org/10.1016/j.solmat.2008.07.020

Pai, S.-C., Su, Y.-T., Lu, M.-C., Chou, Y., & Ho, T.-Y. (2021). Determination of Nitrate in Natural Waters by Vanadium Reduction and the Griess Assay: Reassessment and Optimization. *ACS ES&T Water*, *1*(6), 1524-1532. https://doi.org/10.1021/acsestwater.1c00065

Pellerin, B., Stauffer, B., Young, D., Sullivan, D., Bricker, S., Walbridge, M., Clyde, G., & Shaw, D. (2016). Emerging Tools for Continuous Nutrient Monitoring Networks: Sensors Advancing Science and Water Resources Protection. *JAWRA Journal of the American Water Resources Association*, *52*, n/a-n/a. https://doi.org/10.1111/1752-1688.12386

Porada, S., Zhao, R., van der Wal, A., Presser, V., & Biesheuvel, P. M. (2013). Review on the science and technology of water desalination by capacitive deionization. *Progress in Materials Science*, *58*(8), 1388-1442. https://doi.org/https://doi.org/10.1016/j.pmatsci.2013.03.005

Prickett, M., Chambers, T., & Hales, S. (2024). When the first barrier fails: public health and policy implications of nitrate contamination of a municipal drinking water source in Aotearoa New Zealand. *Australasian Journal of Water Resources*, *28*(1), 64-73. https://doi.org/10.1080/13241583.2023.2272324

Richards, J., Chambers, T., Hales, S., Joy, M., Radu, T., Woodward, A., Humphrey, A., Randal, E., & Baker, M. G. (2022). Nitrate contamination in drinking water and colorectal cancer: Exposure assessment and estimated health burden in New Zealand. *Environmental Research*, *204*, 112322. https://doi.org/https://doi.org/10.1016/j.envres.2021.112322

Rizeei, H. M., Azeez, O. S., Pradhan, B., & Khamees, H. H. (2018). Assessment of groundwater nitrate contamination hazard in a semi-arid region by using integrated parametric IPNOA and data-driven logistic regression models. *Environ Monit Assess*, *190*(11), 633. https://doi.org/10.1007/s10661-018-7013-8

Rogers, K. M., van der Raaij, R., Phillips, A., & Stewart, M. (2023). A national isotope survey to define the sources of nitrate contamination in New Zealand freshwaters. *Journal of Hydrology*, *617*, 129131. https://doi.org/https://doi.org/10.1016/j.jhydrol.2023.129131

Schnetger, Bernhard, Lehners, & Carola. (2014). Determination of nitrate plus nitrite in small volume marine water samples using vanadium(III)chloride as a reduction agent. *Marine Chemistry*, *160*, 91-98. https://doi.org/https://doi.org/10.1016/j.marchem.2014.01.010

Schullehner, J., Hansen, B., Thygesen, M., Pedersen, C. B., & Sigsgaard, T. (2018). Nitrate in drinking water and colorectal cancer risk: A nationwide population-based cohort study. *Int J Cancer*, *143*(1), 73-79. https://doi.org/10.1002/ijc.31306

Sebilo, M., Mayer, B., Nicolardot, B., Pinay, G., & Mariotti, A. (2013). Long-term fate of nitrate fertilizer in agricultural soils. *Proceedings of the National Academy of Sciences*, *110*(45), 18185-18189. https://doi.org/doi:10.1073/pnas.1305372110

Serio, F., Miglietta, P. P., Lamastra, L., Ficocelli, S., Intini, F., De Leo, F., & De Donno, A. (2018). Groundwater nitrate contamination and agricultural land use: A grey water footprint perspective in Southern Apulia Region (Italy). *Sci Total Environ*, *645*, 1425-1431. https://doi.org/10.1016/j.scitotenv.2018.07.241

Sharma, V., Tiwari, P., Kaur, N., & Mobin, S. M. (2021). Optical nanosensors based on fluorescent carbon dots for the detection of water contaminants: a review. *Environmental Chemistry Letters*, *19*(4), 3229-3241. https://doi.org/10.1007/s10311-021-01241-8

Shim, H. (2020). Basic structure of spectrophotometers [Diagram]. In LibreTexts Chemistry. University of California Davis.

Shukla, S., & Saxena, A. (2018). Global Status of Nitrate Contamination in Groundwater: Its Occurrence, Health Impacts, and Mitigation Measures. In C. M. Hussain (Ed.), *Handbook of Environmental Materials Management* (pp. 1-21). Springer International Publishing. https://doi.org/10.1007/978-3-319-58538-3_20-1

Singh, P., Singh, M. K., Beg, Y. R., & Nishad, G. R. (2019). A review on spectroscopic methods for determination of nitrite and nitrate in environmental samples. *Talanta*, *191*, 364-381. https://doi.org/https://doi.org/10.1016/j.talanta.2018.08.028

Singh, S., Anil, A. G., Kumar, V., Kapoor, D., Subramanian, S., Singh, J., & Ramamurthy, P. C. (2022). Nitrates in the environment: A critical review of their distribution, sensing techniques, ecological effects and remediation. *Chemosphere*, *287*, 131996. https://doi.org/https://doi.org/10.1016/j.chemosphere.2021.131996

Stayner, L. T., Jensen, A. S., Schullehner, J., Coffman, V. R., Trabjerg, B. B., Olsen, J., Hansen, B., Pedersen, M., Pedersen, C. B., & Sigsgaard, T. (2022). Nitrate in drinking water and risk of birth defects: Findings from a cohort study of over one million births in Denmark. *The Lancet Regional Health - Europe*, *14*, 100286. https://doi.org/https://doi.org/10.1016/j.lanepe.2021.100286

Stuart, M. E., Gooddy, D. C., Bloomfield, J. P., & Williams, A. T. (2011). A review of the impact of climate change on future nitrate concentrations in groundwater of the UK. *Science of The Total Environment*, *409*(15), 2859-2873. https://doi.org/https://doi.org/10.1016/j.scitotenv.2011.04.016

Tang, W., Kovalsky, P., He, D., & Waite, T. D. (2015). Fluoride and nitrate removal from brackish groundwaters by batch-mode capacitive deionization. *Water Research*, *84*, 342-349. https://doi.org/https://doi.org/10.1016/j.watres.2015.08.012

Temkin, A., Evans, S., Manidis, T., Campbell, C., & Naidenko, O. V. (2019). Exposure-based assessment and economic valuation of adverse birth outcomes and cancer risk due to nitrate in United States drinking water. *Environmental Research*, *176*, 108442. https://doi.org/https://doi.org/10.1016/j.envres.2019.04.009

Tsikas, D. (2007). Analysis of nitrite and nitrate in biological fluids by assays based on the Griess reaction: Appraisal of the Griess reaction in the l-arginine/nitric oxide area of research. *Journal of Chromatography B*, *851*(1), 51-70. https://doi.org/https://doi.org/10.1016/j.jchromb.2006.07.054

Verma, A., Sharma, A., Kumar, R., & Sharma, P. (2023). Nitrate contamination in groundwater and associated health risk assessment for Indo-Gangetic Plain, India. *Groundwater for Sustainable Development*, *23*, 100978. https://doi.org/https://doi.org/10.1016/j.gsd.2023.100978

Vernier. (2021). Vernier Go Direct® SpectroVis® Plus Spectrophotometer: A picture is worth 570 wavelengths (Part 1).

Wang, Q.-H., Yu, L.-J., Liu, Y., Lin, L., Lu, R.-g., Zhu, J.-p., He, L., & Lu, Z.-L. (2017). Methods for the detection and determination of nitrite and nitrate: A review. *Talanta*, *165*, 709-720. https://doi.org/https://doi.org/10.1016/j.talanta.2016.12.044

Wang, S., Lin, K., Chen, N., Yuan, D., & Ma, J. (2016). Automated determination of nitrate plus nitrite in aqueous samples with flow injection analysis using vanadium (III) chloride as reductant. *Talanta*, *146*, 744-748. https://doi.org/https://doi.org/10.1016/j.talanta.2015.06.031

Ward, M. H., deKok, T. M., Levallois, P., Brender, J., Gulis, G., Nolan, B. T., & VanDerslice, J. (2005). Workgroup report: Drinking-water nitrate and health-recent findings and research needs. *Environ. Health Perspect.*, *113*(11), 1607.

Ward, M. H., Jones, R. R., Brender, J. D., de Kok, T. M., Weyer, P. J., Nolan, B. T., Villanueva, C. M., & van Breda, S. G. (2018). Drinking Water Nitrate and Human Health: An Updated Review. *Int J Environ Res Public Health*, *15*(7). https://doi.org/10.3390/ijerph15071557

Wu, J., Hong, Y., Guan, F., Wang, Y., Tan, Y., Yue, W., Wu, M., Bin, L., Wang, J., & Wen, J. (2016). A rapid and high-throughput microplate spectrophotometric method for field measurement of nitrate in seawater and freshwater. *Sci Rep*, *6*, 20165. https://doi.org/10.1038/srep20165

Wu, J., Hong, Y., Guan, F., Wang, Y., Tan, Y., Yue, W., Wu, M., Bin, L., Wang, J., & Wen, J. (2016). A rapid and high-throughput microplate spectrophotometric method for field measurement of nitrate in seawater and freshwater. *Scientific Reports*, *6*(1), 20165. https://doi.org/10.1038/srep20165

Yasir, M., & Dadi, M. (2022). Spectroscopy and Spectrophotometry: Principles and Applications for Colorimetric and Related Other Analysis. In A. K. Samanta (Ed.), *Colorimetry*. IntechOpen. https://doi.org/10.5772/intechopen.101106

Zhang, J.-Z. (1997). Distinction and quantification of carry-over and sample interaction in gas segmented continuous flow analysis. *J Automat Chem*, *19*(6), 205-212. https://doi.org/10.1155/s1463924697000254

9 Appendices

9.1 The computed values for residence time, variance, normalised variance, and dispersion coefficient

Time(s)	Absorbance (C_i)	t_i*Ci	$((t_i-\bar{t})^2 \cdot Ci)$
4724	0.220847573	1043.283935	6505.980648
4726	0.223673365	1057.080323	701291.5363
4728	0.224616718	1061.987843	708671.2799
4730	0.2241812	1060.377076	710061.7794
4732	0.225528389	1067.200337	707091.5507
4734	0.229062646	1084.382566	709739.4952
4736	0.221639213	1049.683313	719237.3334
4738	0.219036389	1037.794411	694358.3066
4740	0.215957731	1023.639645	684654.2131
4742	0.221865381	1052.085637	673504.7082
4744	0.223445828	1060.027008	690362.4708
4746	0.226441682	1074.692223	693704.5108

9.2 Experimental Data of Time and Absorbance at 540 nm.

Time(s)	Absorbance @540 nm	E(t)	t(E(t))	Variance (σ^2)
0	0.080020679	0.020299145	0	9.590584111
3	0.044613147	0.011317184	0.033951551	2.81800476
6	0.03433997	0.008711148	0.05226689	0.840620732
9	1.55	0.393194288	3.538748593	5.879755068
12	1.556733602	0.394902426	4.738829113	1.723947948

15	0.66767073	0.169370527	2.540557909	10.9641127
18	0.006062303	0.001537847	0.027681248	0.301511444
21	0.001109803	0.000281528	0.005912087	0.112145056
24	0.000925181	0.000234694	0.005632662	0.157617158
27	0.000596091	0.000151213	0.004082743	0.15359933

9.3 MATLAB Scripts for Nitrate detection

9.3.1 Automated Calibration of Absorbance Values from UV-Vis Spectrophotometer Display

```
function [NO3]=autoNO3Calibrate(XSTART,YSTART)

W=35;
X1=9;
Xo=63;
%XSTART=3290; %Change This
%YSTART=1892; %Change This

!screenCapture screen2.png
A2=imread('screen2.png');
A=imresize(A2,[2160 3840]);
S=size(A);
B=A(YSTART:(YSTART+50),XSTART:(XSTART+174),:);
B2=A(YSTART:(YSTART+61),XSTART:(XSTART+220),:);
B=imresize(B2,[51 175]);
image(B);
NO3=0;
pause(2)

%Extract digits
D=B(:,X1:(X1+W+15),:);
%D1=B(:,X1:(X1+W),:);

open D0.mat;
D0=ans.D0;
R3 = imabsdiff(rgb2gray(D),rgb2gray(D0));
NO3=sum(sum(R3));

image(R3)

disp(NO3)
```

9.3.2 MATLAB Script for Digit-Wise Extraction and Reconstruction of Nitrate Absorbance from UV-Vis Display

```
function [NO3]=autoNO3(XSTART,YSTART)

W=35;
X1=9;
Xo=63;
XSTART=3051; %Change This
YSTART=1906; %Change This

!screenCapture screen2.png
A2=imread('screen2.png');
A=imresize(A2,[2160 3840]);
S=size(A);
B=A(YSTART:(YSTART+50),XSTART:(XSTART+174),:);
B2=A(YSTART:(YSTART+61),XSTART:(XSTART+220),:);
B=imresize(B2,[51 175]);
image(B);
NO3=0;


%Extract digits
D0=B(:,X1:(X1+W+15),:);
D1=B(:,X1:(X1+W),:);
D2=B(:,Xo:(Xo+W),:);
D3=B(:,(Xo+W+1):(Xo+2*W+1),:);
D4=B(:,(Xo+2*W+2):(Xo+3*W+2),:);

NO3=1*findV(D1);
NO3=NO3+0.1*findV(D2);
NO3=NO3+0.01*findV(D3);
NO3=NO3+0.001*findV(D4);

disp(NO3)
```

9.3.3 MATLAB Script for Continuous Real-Time Plotting of Nitrate Concentration (mg/L) from UV-Vis Absorbance

```
Z=[];
c=0;
while(c<1000)
c=c+1
Z(c)=(((autoNO3()-0.169)/16409)*62*1000);
plot(Z)
xlabel('time')
ylabel('NO3 mg/L')
text(c, Z(c), sprintf('Nitrate= %.2f mg/l', Z(c)), 'FontSize', 12, 'Color',
'red','HorizontalAlignment', 'right', 'VerticalAlignment', 'top').
pause(1)
disp(Z(c))
end
```

9.3.4 MATLAB-Based Interpolation of Nitrate Concentration from UV-VIS Spectrophotometric Absorbance Data